EFFECT OF RELATIVE HUMIDITY OF REACTANT GASES ON PROTON EXCHANGE MEMBRANE FUEL CELL PERFORMANCE

A THESIS SUBMITTED TO
THE GRADUATE SCHOOL OF NATURAL AND APPLIED SCIENCES
OF
MIDDLE EAST TECHNICAL UNIVERSITY

BY

BURCU ÖZSAN

IN PARTIAL FULFILLMENTS OF THE REQUIREMENTS
FOR
THE DEGREE OF MASTER OF SCIENCE
IN
CHEMICAL ENGINEERING

MAY 2012

Approval of the thesis

EFFECT OF RELATIVE HUMIDITY OF REACTANT GASES ON PROTON EXCHANGE MEMBRANE FUEL CELL PERFORMANCE

Submitted by **BURCU ÖZSAN** in partial fulfillment of the requirements for the degree of **Master of Science in Chemical Engineering Department, Middle East Technical University by,**

Prof. Dr. Canan Özgen
Dean, Graduate School of **Natural and Applied Sciences** _____

Prof. Dr. Deniz Üner
Head of Department, **Chemical Engineering Dept.** _____

Prof. Dr. İnci Eroğlu
Supervisor, **Chemical Engineering Dept., METU** _____

Examining Committee Members:

Prof. Dr. Saim Özkar
Chemistry Dept., METU _____

Prof. Dr. İnci Eroğlu
Chemical Engineering Dept., METU _____

Prof. Dr. Gülsün Gökağaç
Chemistry Dept., METU _____

Prof.Dr. Gürkan Karakaş
Chemical Engineering Dept., METU _____

Assistant Prof. Dr. Serkan Kıncal
Chemical Engineering Dept., METU _____

Date: 22.05.2012

I hereby declare that all information in this document has been obtained and presented in accordance with academic rules and ethical conduct. I also declare that, as required by these rules and conduct, I have fully cited and referenced all material and results that are not original to this work.

Name, Last Name : Burcu ÖZSAN

Signature :

ABSTRACT

EFFECT OF RELATIVE HUMIDITY OF REACTANT GASES ON PROTON EXCHANGE MEMBRANE FUEL CELL PERFORMANCE

Özsan, Burcu
M.Sc., Department of Chemical Engineering
Supervisor: Prof. Dr. İnci Eroğlu
May 2012, 119 pages

Fuel cells are expected to play a major role in the economy of this century and for the foreseeable future. The use of hydrogen and fuel cells can address critical challenges in all energy sectors like commercial, residential, industrial, and transportation. Fuel cells are electrochemical devices that convert energy of a chemical reaction directly into electrical energy by combining hydrogen fuel with oxygen from air. If hydrogen is used as fuel, only byproducts are heat and water.

The objective of this thesis is to investigate the effect of operating temperature and relative humidity (RH) of reactant gases on proton exchange membrane (PEM) fuel cell performance by adjusting the operation temperature of the fuel cell and humidification temperature of the reactant gases.

In this study, the effect of the different operating parameters on the performance of single proton exchange membrane (PEM) fuel cell have been studied experimentally using pure hydrogen on the anode side and air on the cathode side. Experiments with different fuel cell operating temperatures, different air and hydrogen humidification temperatures have been carried out. The experimental results are presented in the form of polarization curves, which show the effects of the various operating parameters on the performance of the PEM fuel cell. The polarization curves data have been fit to a zero dimensional model, and the effect

of the fuel cell operation and humidification temperatures on the kinetic parameters and the cell resistance have been determined.

The fuel cell has been operated with 1.2 and 2 stoichiometry ratio for hydrogen and air, respectively. Fuel cell performance was detected at different fuel cell operation temperatures changing from 60 to 80 ºC, and relative humidity of the entering gases changing from 20 to 100 % for air and 50 % and 100 % for hydrogen. Tests were performed in a PEM fuel cell test station.

The highest performance of 275 mA/cm^2 at 0.6 V and 650 mA/cm^2 at 0.4 V was obtained for 50 % RH air with a constant 100 % relative humidity of hydrogen for working at atmospheric pressure and 60 ^{o}C fuel cell temperature. However, the highest performance of 230 mA/cm^2 at 0.6 V for 50 % RH of air with a constant 100 % relative humidity of hydrogen and the highest performance of 530 mA/cm^2 at 0.4 V for both 70 % RH and 100% RH air with a constant 100 % relative humidity of hydrogen was obtained for working at atmospheric pressure and 70 ^{o}C fuel cell temperature. Besides, the highest performance of 200 mA/cm^2 at 0.6 V and 530 mA/cm^2 at 0.4 V was obtained for 100 % RH air with a constant 100 % RH of hydrogen for working at atmospheric pressure and 80 ^{o}C fuel cell temperature.

Keywords: Proton exchange membrane, fuel cell, zero-D model, polarization curve, water management, membrane electrode assembly

ÖZ

REAKTANT GAZLARIN BAĞIL NEMİNİN PROTON DEĞİŞİM ZARLI YAKIT PİLİ PERFORMANSI ÜZERİNDEKİ ETKİSİ

Özsan, Burcu

Yüksek Lisans., Kimya Mühendisliği Bölümü

Tez Yöneticisi: Prof. Dr. İnci Eroğlu

Mayıs 2012, 119 sayfa

Yakıt hücrelerinin bu yüzyılın ekonomisinde ve öngörülebilir gelecekte önemli bir rol oynaması beklenmektedir. Hidrojen ve yakıt pillerinin kullanımı ticari, konut, sanayi ve ulaşım gibi tüm enerji sektörlerinde kritik sorunların çözümünde alternatif olarak düşünülebilir. Yakıt hücreleri, havadaki oksijen ile hidrojen yakıtını birleştirerek kimyasal enerjiyi doğrudan elektrik enerjisine dönüştüren elektrokimyasal cihazlardır. Hidrojen yakıt olarak kullanılır ise, tek yan ürün olarak ısı ve su açığa çıkmaktadır.

Bu tezin amacı, yakıt pili işletim sıcaklığı ve reactant gazların bağıl neminin yakıt pili performansı üzerindeki etkilerini, yakıt pili ve reaktant gazların nemlendirilme sıcaklıklarını ayarlayarak incelemektir.

Bu çalışmada, tek hücreli proton değişim zarlı (PEM) yakıt hücresinde, anot tarafında yakıt olarak hidrojen, katot tarafında ise hava kullanılarak farklı işletim parametrelerinin etkisinin hücre performansı üzerindeki etkisi deneysel olarak incelenmiştir. Farklı hücre işletim sıcaklığı, farklı anot ve katot nemlendirme sıcaklıkları denemeleri gerçekleşirilmiştir. Deneysel sonuçlar, farklı işletim parametrelerinin etkisini gösterebilmek adına polarizasyon eğrileri şeklinde gösterilmiştir. Polarizasyon eğrisi verileri sıfırıncı dereceden bir modele

uydurulmuş ve yakıt hücresi işletim ve nemlendirme sıcaklıklarının, kinetik parametreler ve hücre direnci üzerindeki etkisi belirlenmiştir.

Yakıt hücresinde sırasıyla hidrojen için 1.2 ve hava için 2 stokiyometrik oranı kullanılmıştır. Yakıt hücresi performansı 60 ile 80 ºC arasında değişen hücre işletim sıcaklıklarında ve hava tarafı için 20 ile 100 % arasında değişen ve hidrojen tarafı için ise % 50 ve % 100 nemlilik derecelerinde yakıt hücresi test istasyonunda deneyler gerçekleştirilmiştir.

60 ^{o}C hücre işetim sıcaklığı ve atmosferik basınçta en yüksek performans hidrojen tarafı % 100 bağıl nemlilik derecesinde iken, akım yoğunluğu 0.6 V'da 275 mA/cm2 ve 0.4 V'da 650 mA/cm^2 olarak % 50 hava bağıl nemlilik dercesinde elde edilmiştir. Bunun yanında, en yüksek performans hidrojen tarafı yine % 100 bağıl nemlilik derecesinde iken, akım yoğunluğu 0.6 V'da 230 mA/cm^2 olarak % 50 hava bağıl nem oranında, 0.4 V'da ise 530 mA/cm^2 olarak hem % 70 hemde % 100 hava nemlilik derecelerinde elde edilmiştir. 80 ^{o}C hücre işletim sıcaklığında ise en yüksek performans % 100 hidrojen nemlilik derecesinde, akım yoğunluğu 0.6 V' da 200 mA/cm^2 ve 0.4 V'da 530 mA/cm^2 olarak % 100 hava nemlilik derecesinde elde edilmiştir.

Anahtar Kelimeler: Proton değişimli membran, yakıt pili, 0-D model, polarizasyon eğrisi, su yönetimi, membran elektrot grubu

To my family

ACKNOWLEDGMENTS

I would like to express my sincere gratitude to my supervisor Prof. Dr. İnci Eroğlu for her guidance, criticism, encouragements and also sharing her immense knowledge with me throughout the research. Also, I'm grateful for her support in completing my study.

I thank Dr. Berker Fıçıcılar for helping me to gain abilities on fuel cell testing, emphasizing very strong discussions on fuel cell engineering approaches and guiding on problem solving. Also, I'm grateful for his encouragements even in my hard times.

This study was supported by TR Teknoloji. I would like to thank for their financial support. I would like to express thanks to friends, and colleagues for their understanding and support.

Many thanks to Şefika Can for her support and encouragement.

I am very grateful to my family for their infinite support and help. I am forever grateful for the support and motivation from my family. I owe it all to my mother Fatma, my father İsmail and my brother Utku for inspiring me to get to where I am today.

TABLE OF CONTENTS

LIST OF TABLES

TABLES

LIST OF FIGURES

FIGURES

LIST OF SYMBOLS

Latin Letters

C_B	: Bulk concentration of reactant	mol/cm^3
C_{ox}	: Surface concentration of the reacting species	mol /cm^3
C_{Rd}	: Surface concentration of reacting species	mol/cm^3
C_s	: Surface concentration of reactant on catalyst	mol/cm^3
E	: Potential	Volt
F	: Faraday's constant	C/mol
h	: Planck's constant	m^2kg/s
I	: Current	Amper
i_L	: Limiting current density	A/cm^2
i_o	: Exchange current density	A/cm^2
j	: Flux of reactant per unit area	$mols^{-1}cm^{-2}$
k_b	: Backward reaction (oxidation) rate coefficient	
K_b	: Boltzmann's constant	
k_f	: Forward reaction (reduction) rate coefficient	
m_i	: Mass flow rate of reactant I	g/ min
M_i	: Molecular weight of species i	g/mol
n	: Number of electrons transferred in the overall reaction	
P	: Pressure	kPa
P_{H2O}	: Partial pressure of water vapor	kPa
P_{H2O}^{sat}	: Saturation pressure of water vapor	kPa
Pv	: Water vapor pressure	kPa
Pvs	: Saturation vapor pressure	kPa
R	: Universal gas constant	j/molK
R_i	: Total cell internal resistance	Ωcm^2
slpm	: Standard liter per minute	
sml	: Standard mili liter	

T	: Temperature	^{o}C
V	: Volt	
V_i	: Volumetric flow rate of reactant i	slpm

Greek Letters

ΔG	: Gibbs free energy	J/mol
ΔH	: Enthalpy change of reaction	J/mol
ΔS	: Entropy change of reaction	J/molK
η_a	: Anode over potential	V
η_c	: Cathode over potential	V
λ	: Water content in the electrolyte	
ρ_g	: Density of gas phase	g/cm^3
ρ_w	: Density of the liquid water	g/cm^3
φ	: Relative humidity	
φan	: Relative humidity of anode	
φca	: Relative humidity of cathode	
ξ	: Electro osmotic drag coefficient	
β	: Back diffusion coefficient	
α	: Transfer coefficient	
β	: Symmetry factor	
ν	: Stoichiometry number	

Superscripts

an	: Anode
ca	: Cathode
sat	: Saturation

Subscripts

B	: Bulk
b	: Backward

Ch : Chemical component of the Gibbs free energy

f : Forward

g : Gas phase

I : Gas or liquid species

l : Liquid phase

ox : Oxidation

Rd : Reduction

s : Saturation

w : Liquid water

vs : Saturated vapor

LIST OF ABBREVIATIONS

ABBREVIATIONS

AFC	Alkaline fuel cells
BD	Back diffusion
DMFC	Direct methanol fuel cell
EOD	Electro osmotic drag
GDL	Gas diffusion layer
HOR	Hydrogen oxidation reaction
HTR	Heater
KOH	Potassium hydroxide
MCFC	Molten carbonate fuel cells
MEA	Membrane electrode assembly
NDC	Net drag coefficient
OCV	Open circuit voltage
OFC	Solid oxide fuel cells
ORR	Oxygen reduction reaction
PAFC	Phosphoric acid fuel cells
PEM	Polymer electrolyte membrane
PEMFC	Polymer electrolyte membrane fuel cells
PTFE	Polytetrafluoroethylene
RH	Relative humidity

CHAPTER 1

INTRODUCTION

Energy has been predicted as one of the main problem that humanity must face in the future. Nowadays, primary energy sources in the world consist of fossil fuels including petroleum, coal and natural gas. However, there are some problems with continued use of fossil fuels. They are limited in amount and someday will be depleted. They are causing serious environmental problems, such as global warming, climate changes, acid rains, air pollution, ozone layer depletion, and so on. For these reasons, alternative energy sources are needed. In these sense combined with fuel cells hydrogen energy systems is a good alternative.

Hydrogen is a perfect energy carrier with many unique properties. Together with hydrogen, fuel cells have been getting a lot of attention because they directly and efficiently convert chemical energy of reactants into electrical energy.

Fuel cell is an electrochemical device that convert a chemical reaction energy directly into electrical energy by combining hydrogen with oxygen. In these chemical reactions, only byproducts are heat and water. Fuel cells have many advantages over conventional systems that produce electricity. They have higher efficiency than conventional system.

Within many types of fuel cells, proton exchange membrane (PEM) fuel cells are spectacular because of its compactness, light weight, high power and low cost (Rodríguez et al., 2009). They have been noticed as the most promising power generating device candidates in portable electronic, automotive and distributed power generation applications in future (Ceraolo et al., 2003).

In recent years, research and development activities in fuel cells have been accelerated. Although, there are significant improvements in the technology of proton exchange membrane, the performance, stability, and reliability is not sufficient to replace internal combustion engines and the cost of fuel cell systems is still too high to become acceptable commercial products. The most important problems to be overcome are improvement of their performance and reduction of their cost (Youssef et al., 2010).

In PEM fuel cells, hydrogen and air humidification may be required in order to prevent the fuel cell membrane from dehydration. At high current flow, there is ohmic heating causing drying problems in the polymer membrane and slows ionic transport through the membrane. Because of water generation at the air side, in some fuel cell stacks, humidification is not required. In general fuel cell systems, humidification is required for either the air or hydrogen or both the air and hydrogen at the fuel cell inlets. Water content is very important for the protonic conductivity in proton exchange membranes. If membrane dehydration or drying occurs, the electrical performance decreases due to significant ohmic losses (Zawodzinski et al., 1993).

In METU Chemical Engineering Fuel Cell Technology Laboratory Research Group, development of different carbon support for proton exchange membrane fuel cell electro catalysts (Güvenatam et al., 2012) preparation and performance of membrane electrode assemblies with Nafion and alternative polymer electrolyte membranes (Devrim et al., 2012) electro catalyst development (Bayrakçeken et al., 2008a), effect of components of membrane electrode assembly on PEM fuel cell performance (Bayrakçeken et al., 2008b) and modeling of nonisothermal two-phase flow for PEM fuel cells (Fıçıcılar et al., 2010) were investigated. However, in these studies reactant gases were saturated so the effect of relative humidity of reactant gases on PEM fuel cell performance has not been studied.

The objective of this thesis is to investigate the effect of operating temperature and relative humidity (RH) of reactant gases on proton exchange membrane

(PEM) fuel cell performance by setting the operation temperature of the fuel cell and humidification temperature of the reactant gases. In this study, performance of a single proton exchange membrane (PEM) fuel cell have been studied experimentally using pure hydrogen and air on the anode and cathode side, respectively. Experiments with different fuel cell operating temperatures, different air and hydrogen humidification temperatures have been carried out. The experimental data are presented in the form of polarization curves, which show the effects of the various operating parameters on the performance of the PEM fuel cell. The experimental data have been fit to a zero dimensional model, and the effect of the fuel cell operation and humidification temperatures on the kinetic parameters and the cell resistance have been determined.

CHAPTER 2

LITERATURE SURVEY

2.1 Fuel Cells

Fuel cell is an electrochemical device that convert chemical energy of reactants directly into electrical energy. In some ways a fuel cell is similar to a battery. It has an electrolyte with negative and positive electrodes. Unlike in a battery, a fuel cell generates DC electricity by electrochemical reactions as long as the fuel and oxidant are supplied (Barbir, 2005).

In 1839, Sir William Grove first discovered the operating principle of the typical fuel cell and stated that gaseous fuels could generate electricity (Barbir, 2005). Comparison of fuel cell types are listed in Table 2.1.

Table 2.1 Comparison of fuel cell types (Barbir, 2005)

Type	PEMFC	AFC	PAFC	MCFC	SOFC	DMFC
Electrolyte	Ion exchange membrane	Mobilized or Immobilized Potassium Hydroxide	Mobilized Liquid Phosphoric Acid	Mobilized Liquid Molten Carbonate	Ceramic	Ion exchange membrane
Mobile ion	H^+	OH^-	H^+	CO_3^{2-}	O^{2-}	H^+
Fuel	H_2, reformate	H_2	H_2, reformate	H_2, CO, CH_4,	H_2, CO, CH_4,	Methanol, ethanol
Catalyst	Platinum	Platinum	Platinum	Nickel	Perovskites	Platinum
Operating temperature	60-80 ºC	65-225 ºC	~ 200 ºC	~ 650 ºC	800-1000ºC	80 ºC
Efficiency	25-35%	32-40%	35-45%	40-60%	45-55%	~ 20%
Power density	3.8-2.6 W/cm^2	0.7-8.1 W/cm^2	0.8-1.9 W/cm^2	0.1-1.5 W/cm^2	1.5-2.6 W/cm^2	~ 0.6 W/cm^2
Startup times	sec-min	Min	Hours	Hours	Hours	sec-min
Applications	Electric utility portable power transportation	Military space	Electric utility transportation	Electric utility	Electric utility	Portable power transportation
Stage of development	Commercially available	In use since 1960s	Commercially available	Demonstration	Prototype	Prototype
Advantages	Low corrosion low temperature Quick startups	Air reaction is faster in alkaline electrolyte	Impure H_2 acceptable Less Pt needed	No noble metals needed Efficiency is improved	Less Pt needed Low corrosion Fuel flexibility High eff.	Direct feed of fuel Zero emission
Disadvantages	Cost of catalyst sensitivity to fuel impurities	Expensive removal of CO_2 from fuel	Cost of catalyst Low power Large size	Thermal effects on cell component Corrosion low power	Thermal effects on cell component	Higher system complexity

Fuel cells are grouped according to type of electrolyte used in, namely (Zhang, 2008):

Proton Exchange Membrane Fuel Cells (PEMFC): A thin polymeric membrane is used as electrolyte. Typically, platinum catalyst supported on carbon is used with loadings of about 0.3 mg/cm^2. Generally operating temperature is between 60 °C and 80 ˚C. PEM fuel cells are used mainly in automotive applications together with portable and small scale distributed stationary power generation applications.

Alkaline fuel cells (AFC): Concentrated KOH is used as electrolyte for high operation temperature (250 ˚C) and less concentrated (30-50 wt %) for lower operation temperature (<120 ˚C). A wide range of catalysts like Ag, Ni, noble metals and metal oxides can be used with an electrolyte matrix that is usually asbestos. It is not tolerant to CO_2 existing in either fuel or oxidant. Alkaline fuel cells have been used in the space program (Apollo and Spave Shuttle) since the 1960.

Molten carbonate fuel cells (MCFC): Combination of alkali (K, Na, Li) carbonates, which is preserved in a ceramic matrix of $LiAlO_2$ is used as electrolyte. Operating temperature is generally quite high between 600 °C and 700 ˚C where the carbonates form a highly conductive molten salt, with carbonate ions providing ionic conduction. It is in the demonstration stage for stationary power applications.

Solid oxide fuel cells (SOFC): Solid, nonporous metal oxide, usually Y_2O_3-stabilized ZrO_2 (YSZ) is used as the electrolyte. This type of fuel cells operate at 800 to 1000 ˚C where ionic transport actualized. Like MCFC, these fuel cells are in the demonstration stage for stationary power generation, although smaller units are being developed for portable power and auxiliary power in automobiles.

Phosphoric acid fuel cells (PAFC): Concentrated phosphoric acid used as the electrolyte. Usually, electro catalyst for both H_2 and air is platinum. Operating temperature is generally between 150 and 220 ˚C. They are already semi commercially available in container packages (200 kW) for stationary electricity generation.

2.2 PEM Fuel Cells

Due to PEM fuel cells' high-energy density at low operating temperatures, zero emissions and quick start-up, proton exchange membrane fuel cells (PEMFC) are considered as a possible solution to environmental and energy problems, and are expected to become the most promising energy supplier for automotive, stationary and portable applications (Ji and Dai, 2009).

Figure 2.1 shows a process schematic of a PEMFC. Hydrogen is supplied from anode side to the fuel cell as fuel. When it contact with the anode catalyst layer it oxidized to electrons flowing through the external circuit and protons flowing through fuel cell membrane to the cathode side where they combine with the oxidant O_2 to produce water and heat (Ji and Dai, 2009).

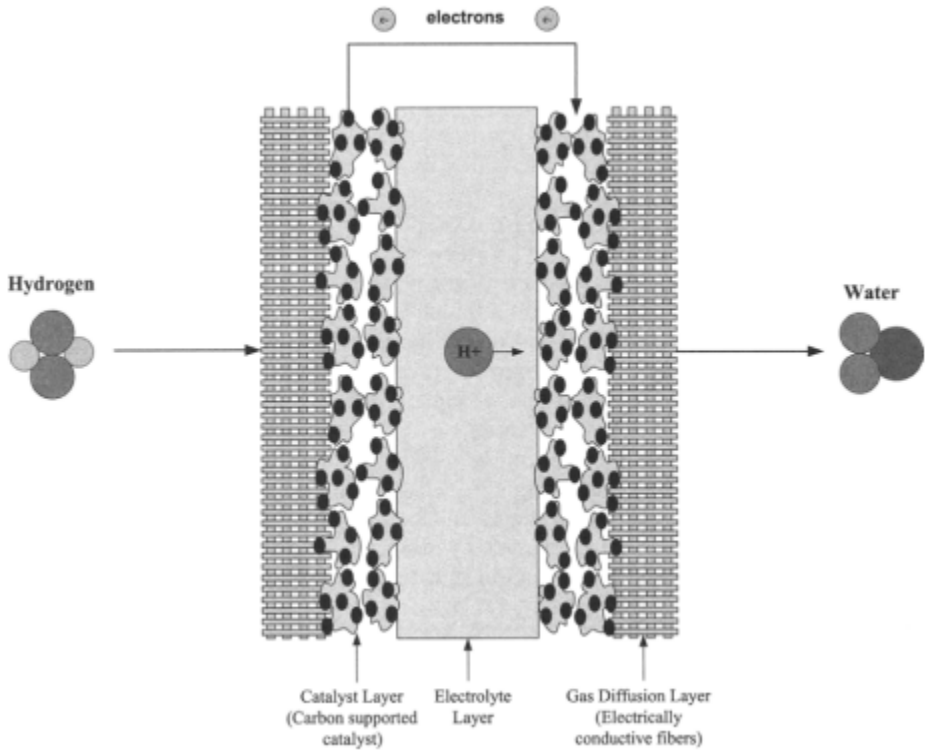

Figure 2.1 A single PEM fuel cell configuration (Ji and Dai, 2009)

2.3 PEM Fuel Cell Components

The design of the components and properties of materials must accommodate the above-listed processes with minimum obstruction and losses. Because in some of the components more than one process takes place, very often with conflicting requirements, the properties and the design must be optimized. Although a fuel cell seems to be a very simple device, numerous processes take place simultaneously. It is therefore important to understand those processes, their mutual interdependence, and their dependence on components design and materials properties (Barbir, 2005).

2.3.1 Membrane

In PEM fuel cells, membrane mainly transport protons from the anode to the cathode; sulfuric group in polymeric membrane activate the transport of protons.

Membrane also keeps the hydrogen and air separated, so this prevents mixing of the gases. That means, the ideal membrane must have sufficient proton conductivity, thermal and chemical stability, low gas permeability, strength, water drag, good availability and cost. The membranes are generally polymers modified to contain ions, such as sulfuric groups. These hydraulic groups allows proton transport across the membrane. Additionally, determining the lifetime of the fuel cell, the lifetime of the membrane is very important. Although thinner membrane increases proton conductivity and so improves the fuel cell performance, membrane mechanical resistance is weaker and cause degradation problems (Zhang, 2008).

2.3.2 Electrodes

A fuel cell electrode is a thin catalyst layer pressed between porous, electrically conductive substrate and the polymer membrane where the electrochemical reactions take place. Electrons travel through electrically conductive substrate, including the catalyst. Protons travel through polymer membrane and the reactant gases travel only through voids (Barbir, 2005).

2.3.3 Gas Diffusion Layer

One of the main components in proton exchange membrane fuel cells is gas diffusion layer. Its primary function is to diffuse the gases. Effective diffusion of each reactant gases to the catalyst layer is facilitated by the porous structure of the backing material. Its material is generally carbon cloth or carbon paper. The other function of the gas diffusion layer is being an electrical connection between bipolar plates and catalyst layer. Additionally, it helps in managing water that produced as a result of electrochemical reactions (Saab et al, 2002).

2.3.4 Bipolar Plates

Bipolar plates in fuel cell have many functions such as supplying reactant gases to the fuel cell by gas flow channels, keeping electrical connection between the individual cells. Gas flow channels design are critical parameters for fuel cell performance because reactants distribution to the fuel cell is partially depend on this configurations (Pantea et al, 2001). And also they must remove the water produced as a result of electrochemical reactions at the cathode side effectively (Wang, 2003). Bipolar plates must have high chemical stability due to acidic environments and corrosion resistance.

2.4 Fuel Cell Electrochemistry and Polarization Curve

2.4.1 Open Circuit Voltage

Exterior with the movement of free electrons between the electrodes of anode and cathode, electric current is obtained. Direct current output of the cell over electrode surface area is called current density (Barbir, 2005).

Theoretical hydrogen/air fuel cell potential is 1.23 V at standard conditions. But, it is generally lower than that theoretical fuel cell potential and this potential is known as open circuit voltage (OCV).

$$H_2 \rightarrow 2H^+ + 2e^- \qquad (E_r = 0\ V) \tag{2.1}$$

$$1/2\,O_2 + 2e^- \rightarrow H_2O \qquad (E_r = 1.23\ V) \tag{2.2}$$

Combined effects of internal short, fuel crossover and parasitic oxidation reactions of air side contribute to the drops the fuel cell voltage (Zhang, 2008). These additional losses in a typical fuel cell occur because of internal electrical and ionic resistances, the kinetics of the electrochemical reactions, internal currents and crossover of reactants and difficulties in transport of the reactants to reaction sites (Barbir, 2005).

The design of the fuel cell stack includes lots of parameters and requires a detailed optimization study. Actually, materials structure and properties, configurations, operating conditions such as pressure regulation, gas flow rates and water and heat management affect fuel cell power output (Zhang, 2008).

2.4.2 Polarization Curve and Voltage Losses

2.4.2.1 Polarization Curve

A polarization curve is used as a standard electrochemical technique for characterizing the fuel cell performance. It is a plot of cell current density against cell potential under a set of constant operating conditions such as system temperature, pressure, humidification, and gas stoichiometry. Polarization curve gives information about the performance losses in the fuel cell under these operating conditions (Zhang, 2008). A typical polarization curve is shown in Figure 2.2. Generally, polarization curves are converted to power density versus current density curves by multiplying the fuel cell potential by the current density at each point of the curve, also seen in Figure 2.2.

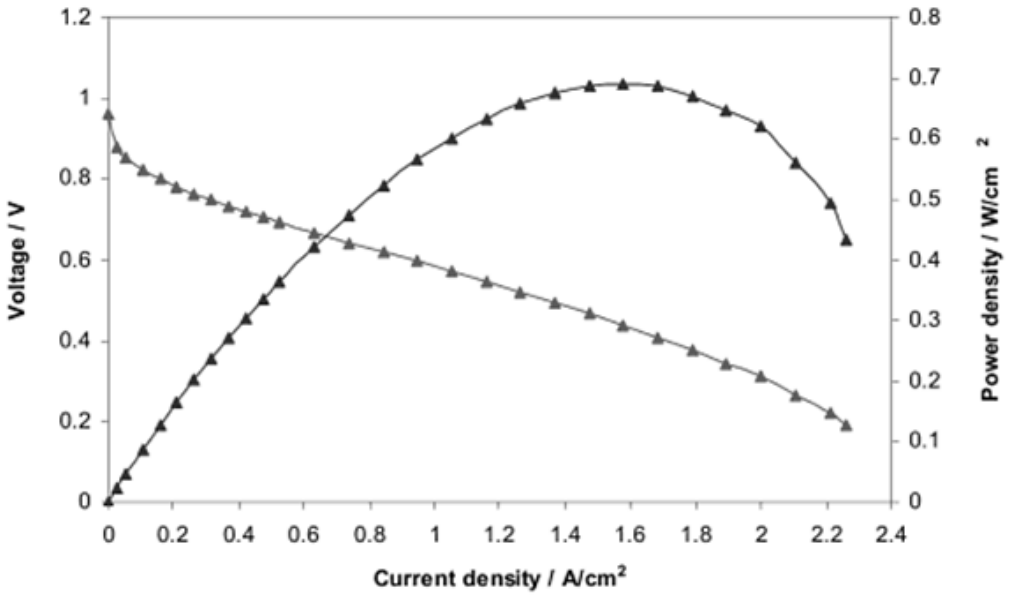

Figure 2.2 Typical polarization curve of PEM fuel cell

2.4.2.2 Voltage Losses

The fuel cell voltage losses are classified into three categories: the concentration loss (concentration polarization), the ohmic loss (ohmic polarization), and the activation loss (activation polarization). Plots of voltage drops caused by each of the losses are shown in Figure 2.3.

The cell potential drops sharply and the majority of these losses are due to the sluggish kinetic of the oxygen reduction reaction (ORR) at low current densities (the region of activation polarization) (Hirano et al, 1997). At intermediate current densities (the region of ohmic polarization), the voltage loss caused by ohmic resistance becomes significant and results mainly from resistance to the flow of ions in the electrolyte and resistance to the flow electrons through the electrode (Zhang, 2008). In this region, the cell potential decreases nearly linearly with current density, while the activation over potential reaches a relatively constant value (Hirano et al, 1997). At high current densities (the region of concentration polarization), mass transport effects dominate due to the transport limit of the reactant gas through the pore structure of the GDLs and electro catalyst layers, and cell performance drops drastically (Zhang, 2008).

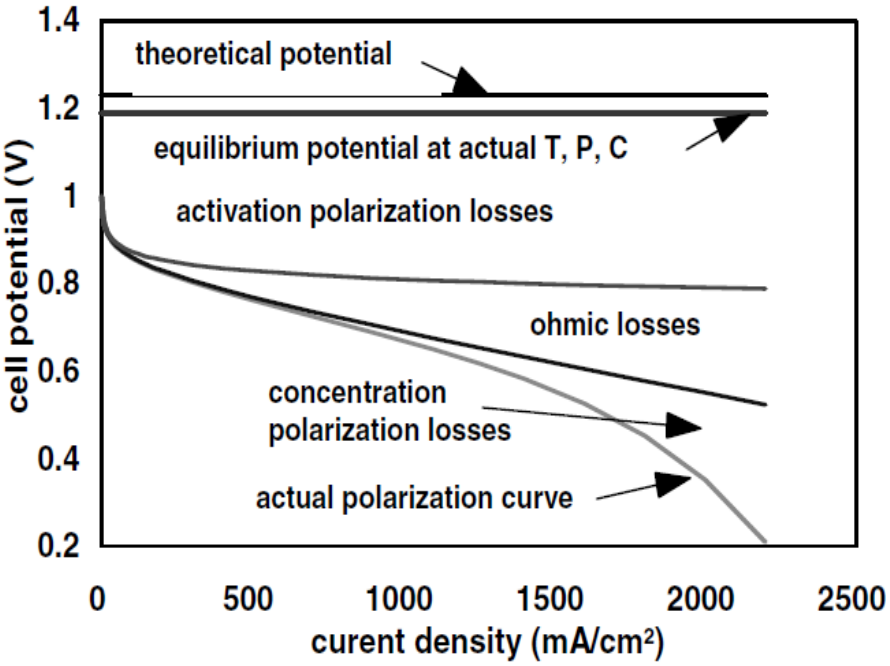

Figure 2.3 PEM fuel cell polarization curve

The output voltage of a single cell, E_{cell}, can be defined as follows:

$$E_{cell} = E_{OCV} - \Delta E_{act} - \Delta E_{ohmic} - \Delta E_{con} \quad (2.3)$$

Where E_{cell} is the voltage for a certain operating condition, E_{OCV} represents the fuel cell theoretical voltage, ΔE_{act} is the voltage drop associated with the activation of the H_2 and of the air, ΔE_{ohmic} is the ohmic voltage drop associated with the conduction of protons and electrons, and ΔE_{con} is the voltage drop resulting from the decrease in the concentration of air and hydrogen.

2.5 Fuel Cell Operating Conditions

A fuel cell power output depends on mainly material properties, cell structure and design, operating conditions. These are gas flow rate, pressure, water and heat management. High power output of a PEM fuel cell requires optimal membrane hydration, temperature and reactants partial pressure (Zhang, 2008).

2.5.1 Operating Pressure

A PEM fuel cell is generally operated at ambient pressure or at a higher pressure. Better performance usually obtained at increased pressures. However, increasing the operating pressure requires extra compression power. Usually, the reactant gases are supplied from pressurized tanks to the fuel cell inlet (Hirano et al, 1997).

2.5.2 Operating Temperature

Temperature is one of the most important parameter in a fuel cell operation. It is generally required high operating fuel cell temperature in order to get a high fuel cell power output. However, a fuel cell design requires an optimal operating temperature to be able to obtain better performance (Zhang, 2008).

The fuel cell reaction is an exothermic reaction that generates heat as a by-product. Heat must be removed from the fuel cell system to maintain the desired temperature. (Hirano et al, 1997).

Additionally, the temperature inside a fuel cell may not be uniform throughout the cell. It may varies from inside to outside, from inlet to outlet or from cathode to anode. Generally, it is surface temperature or leaving air temperature from the fuel cell that is the measured fuel cell temperature (Zhang, 2008).

2.5.3 Reactants Flow Rate

The reactant flow rate at the inlet of a fuel cell must be equal to or greater than the consumption rate of the reactants in the electrochemical reaction of the fuel cell. The ratio between the actual flow rate of a reactant at the cell inlet and the consumption rate of that reactant is called the stoichiometry. Lack of reactants has destructive effect on fuel cell performance because negative cell potential can arise in the absence of reactants. Thus, membrane degradation and failure of the fuel cell is occurred (Zhang, 2008). To overcome these difficulties, high

stoichiometry gas flow rates and suitable gas flow field designs must be required for proper flow of gasses (Zhang, 2008).

2.5.4 Reactant Humidity

An important issue in PEM fuel cell systems is water balance and management that they have a critical effect on lifetime and performance of fuel cell systems. Reactant humidity is required in order to have a sufficient membrane hydration. Generally, inlet relative humidity (RH) of reactant gases equal to or less than 100 % during the fuel cell operation. The proton conductivity of the membrane in a PEMFC is directly proportional to its water content, which depends on the water carried by the humidified reactant gases. Full hydration of the membrane is required in order to maintain good proton conductivity from anode side to cathode side. Membrane hydration can be obtained by giving fully humidified reactant gases to both the anode and the cathode (Zhang, 2008).

Water transport in a PEM fuel cell membrane is affected by mainly four mechanisms. These are the water carried by the humidified reactant gases in to the fuel cell; the water generated as result of electrochemical reaction at the cathode side; the water carried by the protons from the anode to the cathode which is called electro osmotic drag; and the water back diffusion from the cathode side to the anode side. It is apparent that water management in a fuel cell is a critical and complex issue.

Both the lifetime and performance of the fuel cell are degraded by too much or too little water. If the membrane is lack of sufficient hydration, membrane proton conductivity will be decreased. On the other hand, if water is not removed sufficiently from the fuel cell cathode side, liquid water flooding occurs and that leads to unpredictable, unreliable, and unrepeatable PEM fuel cell performance under identical operating conditions. Therefore, achieving a perfect water balance during dynamic fuel cell operation is essential for fuel cell lifetime and performance.

2.6 Water Management

In PEM fuel cells, it is possible that the PEM fuel cell may need a hydrogen humidification system in order to prevent dehydrating under the load. As mentioned before, because of the existence of ohmic heating under high current flow which makes the polymer membrane dry and also slow ionic transport, in the PEM fuel cell , water management is a troublesome event. By reason of the existence of water generation at the air, some of the fuel cell stacks might not need any humidification. However, it is necessary to humidify air or hydrogen together or one of them at the fuel inlets when fuel cell systems are larger.

The humidity is contingent upon the partial pressure of vapor in the mixture , in case of constant total pressure. Fuel cell performance is affected by operating temperature, relative humidity of reactant gases, flow rates and pressures of reactant gases. In order for improving fuel cell performance with regard to reaction kinetics , water management, catalyst CO tolerance, and heat rejection, high temperatures are an essential need for PEM fuel cell to be operated. While the fuel cell is being operated at a high temperature, it is needed to operate at high relative humidity in order to get a useful performance in PEM fuel cell (Rodríguez et al., 2009). So as to diminish extra power losses that applied for heating the reactants to get preferred humidity conditions, commercial applications give preference to low gas humidity conditions. Yet, the decline of water content in the PEMFC, which will result in the performance loss, leads to low gas humidity. The consequences of various feed gas temperatures and humidities were studied to analyze the performance uniformity of PEMFC (Weng et al., 2008).

The membrane hydration that feels necessity for suitable water management decides PEM fuel cell performance and durability. These stand for one of the most important and design issues of PEM fuel cells (Perez et al., 2011). There are several challenges of water management principally flow-field designs or new humidification strategies, and membrane electrode assembly designs (Sauriol et al., 2005). In the event of the ionic conductivity of the proton conducting

membranes, water content takes a crucial part. The electrical performance decreases because of important ohmic losses in the case of membrane dehydration or drying, (Zawodzinski et al., 1993). The situation that excess of water causes condensation must be avoided because liquid water blocks the pores of the gas diffusion layers (GDL). As a result, the transport of reactants are inhibited. Furthermore, it confines active sites in the catalyst layers and blockade the gas transport channels in the flow-field plates. As a consequence of water flooding a non-uniform distribution of reactants over the active catalyst area occurs and this causes inefficient electrical performances (Maranzana et al., 2008).

2.6.1 Water Transport and Balance

In a PEM fuel cell, the oxygen reduction reaction (ORR) generates water at the air side and later the reactant gas flow removes it. As water molecules are reacting, protons drag water molecules through the membrane while they are moving from the anode to the cathode. Currently used in PEMFCs, perfluorosulfonic acid (PFSA) membranes are known to be the most popular membrane type. It acts not only as the separator but also the electrolyte. Many studies such as hydrocarbons (Lee et al., 2007), aromatic polymers (Miyatake et al., 2005), acid–base complexes (Nakamoto et al., 2007), additionally modified or composite PFSA membranes (Verbrugge et al., 1992), have focused on alternative materials (Feng et al., 2008). However, the strict requisites of the proton exchange membrane have been met by far few other commercial membranes.

In current PEMFC technologies, membrane performance and durability include a large effect of water content of the membrane. The effectiveness of the electrochemical reaction is determined by proton conductivity in which hydration of the PFSA membrane acts a crucial role. The requirement of contact with liquid water or water vapor at >80 % RH to keep adequate proton conductivity by PFSA and some sulfonated aromatic systems is shown in Figure 2.4 (Roelofs, 2001). It is still hard to succeed the adjustment between the membrane conductivity (and dry out) and hydration of feed gases and propensity to flooding.

The current understanding of the fundamental structure and properties of Nafion® PFSA materials has been comprehensively reviewed by Mauritz and Moore (2004). For being the structure of the Nafion® ionomer, the water and proton diffusion mechanisms are still debated. To explain some important features of Nafion®, including the rapid diffusion of water and protons through Nafion®, even at low temperatures, a parallel cylindrical water nano channels model has been built by Schmidt-Rohr and Chen (2008). Small-angle scattering data on hydrated Nafion® which is using a recently introduced algorithm was previously published by their quantitatively simulated model . It is still required that membrane fundamentals and satisfactory models should be understood by sufficient experimental data and achieved a better PEMFC design and optimization. Figure 2.4 showed membrane proton conductivity as a function of gas humidification at different temperatures for Nafion membrane.

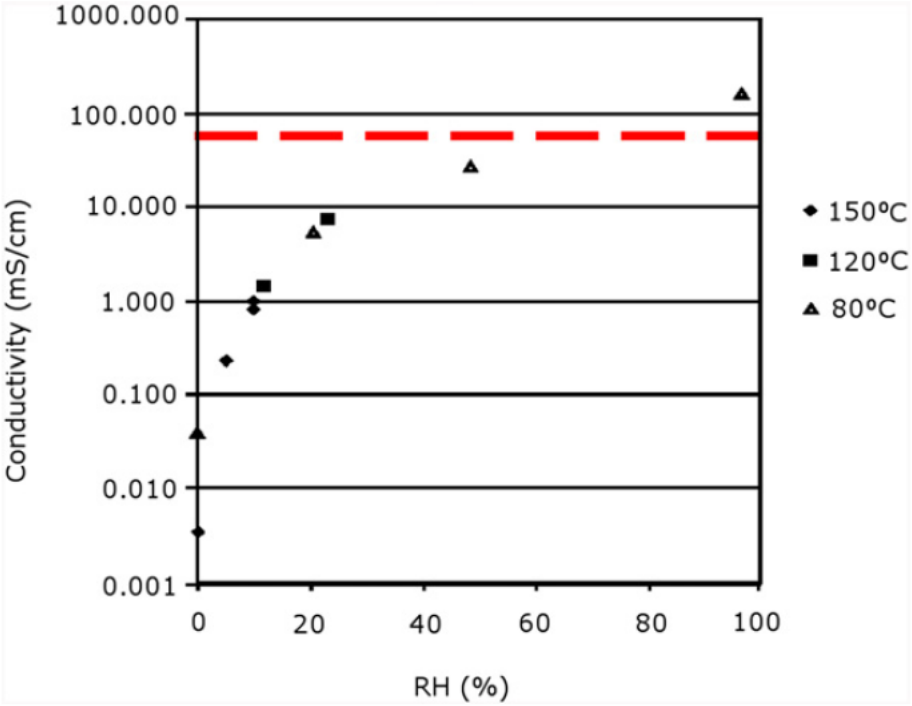

Figure 2.4 Membrane proton conductivity as a function of gas humidification at different temperatures for Nafion membrane (Schmidt-Rohr and Chen, 2008)

High proton conductivity of the membrane that needed adequate water content influenced the efficiency of electrochemical reactions in PEM fuel cell. The reduced proton conductivity probably will lead to lower cell fulfillment in case of

the water content in the membrane being insufficient. A dry membrane is also easily affected by pinhole formation, and this formation can increase the speed of degradation process in the membrane and also result in membrane failure. Still, the pores of the catalyst or gas diffusion layers and limiting reactant mass transport can be obstructed by overabundance of liquid water in the cathode or anode and it leads to a performance fall or cell reversal. Before going into the cell, it is essential to humidify the feed gases in most PEM fuel cell applications. For the time being, removing excess water from the cell to prevent flooding is also very important. Thus water acts interestingly in PEMFCs that is favorable for proton delivery and adverse to mass transfer. To maintain a balance; for achieving better cell performance, water should be dealt with and this the desired way: Supply efficient water for proton exchange to appear through the membrane and be prevented from condensed water blocking the mass-transfer channels (Dai et al., 2009).

Electro-osmotic drag (EOD), back diffusion (BD) usually help water to go through the membrane. On the appliance of a pressure gradient, hydraulic permeation are driven by convection and pressure. Compared with EOD and BD pressure, driven hydraulic permeation is generally insignificant when a pressure gradient is not placed and the operating temperature is under 70 ºC. Yet, during high temperature (>80 ºC) or high back pressures, PEM water balance is considerably influenced by this factor. Because of this reason (Yan et al., 2006). The water transport operation in a common hydrogen PEM fuel cell is shown as a scheme in Figure 2.5. One can realize that EOD, BD and pressure driven hydraulic permeation are included in water transport mechanisms in PEM fuel cells.

Apart from extra water, providing the water in this internal cycle by any means necessary, the best way is to keep water balance. In the event of the water being withdrawn by the exhaust gases, it is reprocessed to humidify the feed gases which are another larger water cycle forms. If the necessities of PEMFC operation are fulfilled by the recycled water, without external humidification water balancing in a single cell or system would be accomplished. As the recycled water

can effortlessly be assessed and formed, for fuel cell implementations, this simplified design is given preference. The PEMFC is known to be a dynamic, multi-scale, multi-phase, and inclusive system. In this system a cell's performance and durability are linked in order to be figured by all parameters. In PEMFCs, water management, being interrelated with thermal and gas management is believed to be an essential issue. In order to obtain a better water management in PEMFCs, it is advisable to keep a water balance in MEA (Dai et al., 2009).

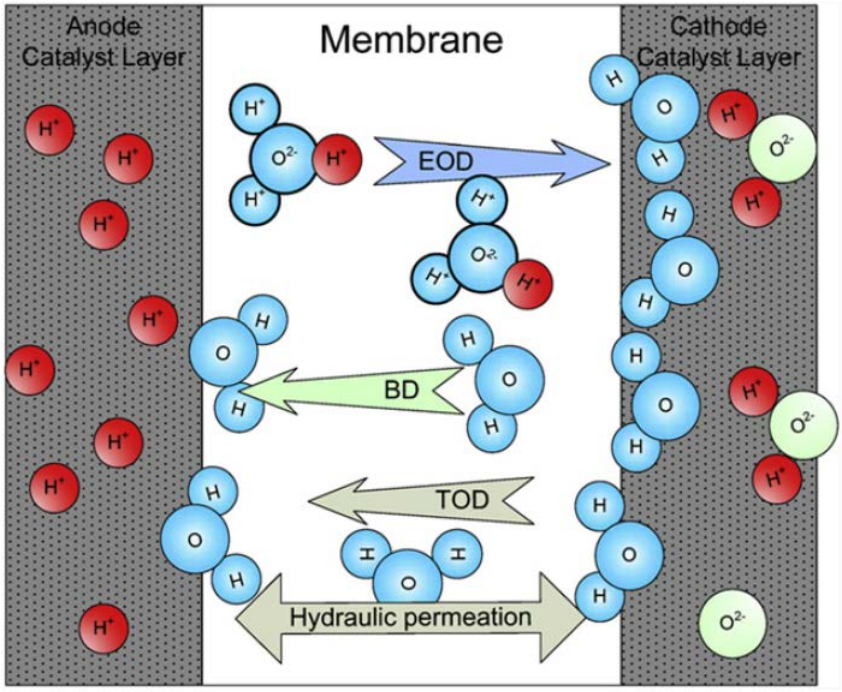

Figure 2.5 Water transport mechanisms in PEMFCs (Dai et al., 2009)

2.6.1.1 Electro Osmotic Drag

A measure of the number of water molecules, carried with each proton brought from the anode to the cathode, is called the electro-osmotic drag (EOD) coefficient. The electro-osmotic coefficient is particularly influenced by temperature and water content (Yan et al., 2006). That at 25 ^{o}C, equalized with saturated water vapor, the transport number of water was 1.4 for a membrane, and with the dehydration of the membrane declined slowly was shown by Fuller et al. (1992).

Electro-osmosis consequences from proton chemistry, through isolated protons in which electron clouds does not exist, can hardly be in existence in solution as independent species (Kreuer, 1996). Alternatively, protons cooperate with the electrons of adjacent water molecules to shape dynamic species such as H_3O^+ (Pivavor et al., 2006).

Some of the EOD factors get by various researchers are listed in Table 2.2. Being ordered from 1.5 to 2.6 under different operating cases, electro-osmotic drag coefficients are attested in literature (Yan et al., 2006). When the temperature increases, EOD coefficients in Nafion ® 117 also increase. Higher back pressures (3.16 H_2O/H_3O^+) or EOD (1.5–2.6 H_2O/H_3O^+) become higher than those at room temperature and ambient pressure (0.9–1.4 H_2O/H_3O^+) as the temperature is higher. That the electro-osmotic drag coefficient are greatly subject to the cell current density including the temperature is also discovered by Husar et al. (2008).

By reason of their EOD coefficient being concluded by the membrane's water content (Zawodzinski et al., 1993), temperature (Verbrugge et al., 1992), current density (Ge et al., 2006), and also membrane thickness (Janssen and Overvelde, 2001), the EOD coefficients of other membranes, including GORE® (1.01 H_2O/H_3O^+), are dissimilar with regard to those of Nafion ® membranes. For the use of better comprehending water balance and designing necessities for the PEMFCs, the systematic data based on experience on EOD coefficients for various membranes (even for the commonly used Nafion ® -series membranes) and various operating conditions (e.g., current density temperature, pressure) is still seen inadequate even though for water transport from H_2 to air, EOD is the main driving power.

Table 2.2 Comparison of the selected EOD coefficients in PEMFCs (Dai et al., 2009)

Researchers	**Measurement**	**PEM**	**T(ºC)**	**EOD coefficient**
Fuller et al. (1992)	Concentrated cell	Nafion 117	25	1.4 (vapor equilibrated) Decreased slowly as the membrane was dehydrated, falling sharply toward zero as the concentration of water approached zero
Zawodzinski et al. (1993)	Electro-osmotic drag cell	Nafion 117 Recast Nafion membrane Nafion 117 Dow XUS Membrane C	30	Nafion 117, λ=22:2.5-2.9 Nafion 117, λ=11: 0.9 Recast Nafion membrane: 2.9-3.4 Nafion 117 λ=22:2.0-2.9 Nafion 117, λ=11:0.9 Dow Membrane: 1.4-2.0 Membrane C: 2.6-4.0 1.0 (vapor equilibrated) 2.5 (liquid equilibrated) Independent of water content over λ=1.4-14 (vapor equilibrated). Not significantly dependent on details of membrane microstructure.
Zawodzinski et al. (1993)				
Zawodzinski et al. (1995)				
Ren et al. (1997)	DMFC analysis Water flux Measurement	Nafion 117	60, 80	3.16@80 ºC, 2.82 bar BP 2.86@60 ºC, 2.82 bar BP λ<4, temperature had no influence on the EOD, λ>4, the EOD coefficient increased with increasing temperature. 1.1 For the water activity=1.0. Linearly increased from 1.8 to 2.7 at 15-85 ºC (liquid equilibrated). Keep constant at 0.05-1.0 A/cm^2 current densities at 75 ºC.
Ge et al. (2006)			30, 50, 80	
Ise et al. (1999)	NMR	Nafion 117	30-80	EOD coefficient increased with increasing temperature and water content (λ=11-20). Λ=13, 1.7@22 ºC and 2.5@79 ºC.
Ye et al. (2007)	Hydrogen pumping cell	GORE-SELECT membranes	80	1.07 (40 and 95 % RH).
Yan et al. (2006)	Water flux measurement	Nafion 117	80	1.5-2.6
Takaichi et al. (2007)	Inserted Pt potential probes	Nafion 211	80	The ratio of EOD coefficient to BD coefficient was constant irrespective of the current density (0.2-200 mA/cm^{-2} at 20, 40, or 60 % RH feed gases).
Husar et al. (2008)	Water flux measurement	Nafion 115	40, 60	0.25-0.4 (0.3-0.8 A/cm^2) at 40 ºC, 0.65-1.05 (0.3-1.0 A/cm^2) at 60 ºC.

2.6.1.2 Back Diffusion

Back diffusion (BD) is water's diffusion from the air to the H_2. Many groups who are using methods including streaming potential NMR (Zawodzinski et al., 1993), flow permeation and sorption (Rivin et al., 2001), water flux measurement (Husar et al., 2008), has examined the water BD coefficient, or the number of water molecules that are diffusing with each proton from the air to the H_2.

the density and dimension changes of Nafion® 117 as a function of water content was evaluated by Morris and Sun (1993) and that the BD coefficient of water in Nafion®117 are mainly related to the water content was discovered. Furthermore, the BD coefficient of Nafion®117 membrane at 30 ºC using NMR was evaluated by Zawodzinski et al. (1993 The dependence of water BD coefficients on concentration was examined by Rivin et al. (2001) by regarding various Nafion® membranes, including Nafion ®112, 115, and 117, and by making use of the flow permeation and sorption method at 32 ºC. ıt was concluded from the results that the water BD coefficient rises easily and droningly with concentration. The estimated water flux across Nafion® 115 membranes with the experimental water flux that was estimated under different flow rates and pressure gradients, was contrasted by Motupally et al. (2000) through measuring water flux. The result of this comparison showed that the experimental data suited the guessed modeling using the Fickian diffusion coefficient got as an information from self-diffusion evaluations stated in the literature.

Temperature and outlet pressure, the diffusivity of water as a function of water movement were evaluated by Husar et al. (2008). The water content gradient that exists across the membrane (Zawodzinski et al., 1993), membrane thickness (Ye and Wang, 2007), temperature (Husar et al., 2008), and pressure gradient (Motupally et al., 2000) have defined the BD coefficien while the experimental data for varied membranes under varied operating circumstances are inefficient, these data are still useful for placing the PEM water balance region,

additionally, selecting a membrane and making the operating circumstances better.

2.6.1.3 Pressure Driven Hydraulic Permeation

Water's move in a PEMFC between the H_2 and the air, known as pressure driven hydraulic permeation, happens because of the pressure gradient. If both the research of EOD and BD are taken into consideration, it can be concluded that research of pressure driven hydraulic permeation has focalized on modeling rather than on experiments. A model showing the influence of a constrained membrane on fuel cell water balance was developed by Weber and Newman, (2004). A non equilibrium force-balance water transport model in a Nafion®-based PEM was formed by Nazarov and Promislow (2007). That mechanical pressure of the membrane can cause a more uniform division of water along the thickness of the membrane is pointed out from this model. It is also predicted from the model that mechanical compression can reduce not only the back diffusion of water within the membrane by up to 20 % but also the membrane water content by 5–30 % by using an original aggregated operational fuel cell Husar et al. (2008) quantified the water pressure driven the hydraulic permeation rate. As a result, rising pressure difference and temperature cause the water pressure driven hydraulic permeation flux to rise. Unlike electro-osmotic drag and back diffusion, pressure driven hydraulic permeation can be neglected under several cases. Yet, to develop the stack performance and lower the stack size, high pressure is favored for some PEM fuel cell applications, such as automotive. Under these circumstances, in order to stabilize the water in the fuel cell, it is essential to consider the water pressure driven hydraulic permeation. Compared to water EOD and BD, water pressure driven hydraulic permeation is generally ignored for ambient pressure fuel cells.

2.6.2 Net Water Drag

By using the net water transport coefficient, in general, the net water transport is described. Commonly, gas pressure, gas stoichiometry, feed gas humidity,

current density, gas stoichiometry, There is probability that the factors like flow field pattern of the fuel cell membrane materials, and water content of the membrane influence the net water transport coefficient. A gradient existing in water activity across the Nafion membrane is the result of the production of water at the air. The diffusion of water from the air to the H_2 will be the effect of this gradient (Yan et al., 2006). the electrical conductivity of Nafion and the diffusion coefficient of water in Nafion were mainly related to the water content, discovered by Morris et al. (1993). As the water is more firmly relevant to the sulfonic acid sites, when the water content declines, correspondingly, the diffusion coefficient is thought to decline, as a function of water content (Yan et al., 2006).

Principally, by using the net water transport coefficient, the net water transport is mainly described. net electro-osmotic drag coefficient or the net drag coefficient (NDC) is generally used in order to make the process easier. The NDC is the net number of water molecules carried away by a single proton from the H_2 to the air. Under several cases, different techniques including H_2 –H_2 cells (Himanen et al., 2006), water flux measurements, electrochemical impedance spectroscopy (EIS) (Andreaus and Scherer, 2004),and humidity sensors (Ye and Wang, 2007) has surveyed the NDC.

Some chosen results for the NDC measured by various research groups are shown in Table 2.3.Although the most well-liked was Nafion®-series membranes. other membranes were still examined. For instance, GORE® -series membranes or MEAs were considered by Wang's research group. ıt can be seen easily from Table 2.3 that compared to those of Nafion® -series membranes, the NDC values of GORE® membranes for which the gas RH conditions are more important than the current density, show differences (Dai et al., 2009). The reason for that is as GORE® -series membranes are Nafion® -based rein- forced composite membranes with various microstructures and so they have various water transport efficiency.

Table 2.3 Comparison of selected net drag coefficients in PEMFCS (Dai et al., 2009)

Researches	**Membrane/ MEA**	**Condition**	**Net drag coefficient (NDC)**
Janssen et al. (2001)	Nafion 112 Nafion 105	Wide range of operating condition and materials	The stoichiometry and the humidity of the inlet gases had a large effect on NDC as well as membrane thickness.
Choi et al. (2000)	Nafion 115 Hanwha membrane	Different current densities	NDC decreased sharply with current density, but nearly constant value over 200mA/cm^2.
Yan et al. (2006)	Nafion 117	Various conditions	NDC ranged from -0.02 to 0.93 and depended on current density, feed gas humidification, and operating conditions.
Cai et al. (2006)	Nafion 112 Nafion 115	Dry H_2 supply	NDC was negative even when the H_2 was humidified and liquid water existed in both sides. High air humidity was a disadvantage for water removal in both sides.
Murahashi et al. (2006)	Nafion112	Various fed gas humidity	FC mod operation: NDC decrease as the air humidity increased. ND<0 when humidity was higher than t_{dc}=75ºC. H_2 mode operation: NDC increased as the air humidity increased.
Liu et al. (2007)	30 µm GORE-SELECT membrane	Various H_2 and air inlet RHs@ 80 ºC and 2 atm	Local current density was dominated by membrane hydration and gas RH has a large effect on NDC. Very small or negative water transport coefficients indicated strong water back diffusion.
Lu et al. (2007)	30 µm GORE-SELECT membrane	Segmented cell	0.47 to 0.025 under 100% RH H_2 and partially humidified air (EOD dominates). 0.19 to -0.24 under partially humidified H_2 and air (negative value indicating back diffusion dominant).
Ye et al. (2007)	GORETM PRIMEA 18 MEA 18 µm GORE-SELECT membrane	In-situ effective water diffusivity diagnostic tool	NDC considerably decreased with increasing current density at 35% - 95% RH. NDC slightly decreased with the increasing RH level of the gas streams at constant current density.
Yang et al. (2005)	Commercial MEA 18 µm membrane	Segmented cell @ 80 ºC and 2 atm	0.05-0.30 even under very dry air conditions, suggesting the presence of strong back diffusion of water from the air to the H_2, despite rather dry air gases.
Himanen et al. (2006)	GORETM PRIME series 58 MEA	Symmetrical H_2-H_2 cell	NDC increased with increasing concentration difference of water over the membrane.

Moreover, the thicknesses of GORE®-series membranes, being 18 mm and 30 mm, are much thinner than Nafion®117 (178 mm), Nafion®105/115 (127 mm), and Nafion ®112 (50 mm). as mentioned before, thinner membranes includes strong back diffusion, with dry-feed gases as well.

2.6.3 Humidification Effect on Net Water Transport

Under different cases , water balance in a polymer electrolyte membrane fuel cell (PEMFC) was examined by measurements of the net drag coefficient (Yan et al., 2006). Actual density and humidification of feed gases is essential for the net drag coefficient of water in the membrane as the former is subjected to the latter and on the fuel cell performance, air inlet gases possessed an important influence. That the membrane resistance rose as the feed gas relative humidity (RH) declined was revealed by the resistance of the working fuel cell. The humidity of each H_2

In case of incorrectly hydrated, the membrane shows higher ionic resistance and also can be inconvertibly harmed in extreme conditions. for keeping high proton conductivity, It is required to hydrate polymer membrane materials which are used in PEM fuel cells and also take out excess water in order to avoid flooding. While the water transport circumstance influences membrane hydration in the membrane, the condition of the inlet gases and the operating parameters of the fuel cell influences the membrane. The fact that the temperature and the hydrogen flow rate are the major parameters affecting the water transport coefficient was discovered (Colinart et al., 2009). Thus, in the course of the operation of PEM fuel cells, keeping an ideal water balance is highly essential. It is important to keep the water balance in order to make sure of ideal performance is obtained (Perez et al, 2011) . The performance and stabilization of a PEMFC are interdependent on numerous operating parameters (Weng et al., 2008).

By Nguyen et al. (1993), a water and heat management model for fuel cell was developed and used to examine the impact of different humidification designs. It is concluded that both H2 stream and the air stream, if air is used, need to be

humidified so as to minimize the ohmic loss. Along with current density, the amount of water that is produced by ORR in air catalyst layer also rose linearly. As a result of the parallel increase of the water concentration gradient existing in the membrane near to the air side and current density, similarly, the back-diffused water from air to H_2 rose. This is the result of decline of the net electro-osmotic drag coefficient. Hydration and proton conductivity of membrane is settled by the equilibration between electro-osmotic drag and back diffusion. It is inferred that so as to avoid membrane dehydration water transport by reason of back-diffusion is not adequate.

Monitored by Perez et al, (2011), in the non-exist condition of humidification, it is presented by the polarization curves of the fuel cell stack that the fuel cell performance got better associated with increase temperature from 20 ºC to 40 ºC. because of the possibility of membranes death, when the temperature is higher, the performance of the fuel cell stack declines. The operation temperature subjects the impact of the humidification temperature on the fuel cell stack performance. In the case of high operation temperature, humidification temperatures must be higher. On the other hand, flooding in some individual cells is caused by the excess of water owing to high humidification temperatures on behalf of low operation temperatures. It was also monitored that in the event of membrane's well humidification, the resistance declines with the operation temperature owing to the membrane conductivity at higher temperatures and the progress of the gas diffusivity (Perez at al., 2011).

Some transports such as the transport of the proton from the H_2 side to the air side through the membrane , the transport of reactant and oxidant gases to active sites of catalyst layer, and the transport of produced water from the air side to the H_2 side by back diffusion mechanism are the mass transport limitation. This limitation has great effects on the performance of PEMFC and it could be decreased through temperatures, pressures, and humidity of reactant gases. In addition, the performance of the fuel cells could be improved with these factors. According to these observations, with the humidified reactant gases temperature

increased and the ideal conditions acted when the temperature was higher. Moreover, there has been more influence on the performance of the PEM fuel cell on compressed air side rather than compressed H_2 side (Amirinejad et al., 2006).

In order to study the impact of the air humidification circumstances on the location of the interworking, a, multi-component, multi-dimensional, computational fluid dynamic model was developed. The cell performance and power density lowers while the relativistic humidity of the air elevates because the condensed water in the pores in the porous media blockades the access of fuel gas, (Lee et al., 2007).

2.7 Fuel Cell Modeling

In order to get ideal performance and design, right system selection, design, and modeling for forecast of performance are required while the fuel cell is a exclusive and perfect system. Possessing an interdisciplinary intellect of electrochemistry, materials, manufacturing, mass and heat transfer is essential in order to take a step in performance, cost, and assurance.

A fuel cell model is thought to be highly important for obtaining the best fuel cell performance. By a suitable model, forecasts of the cell performance under different operating circumstances will be allowed. In the past, consecutive and analytical fuel cell models that compound different ways of heat, mass, and momentum transport characteristics have been suggested. the different parts of the PEM fuel cell such as the polymer electrolyte membrane (proton and water transport), the catalyst layer (reaction site), and the gas diffusion layer / gas flow channel (reactant transport) have seen as a focal point by most modeling efforts. It is likely that water transport and heat impacts might be existed in typical PEM fuel cell models that comprise of transport equations for these respective parts.

Besides leading to cheaper, better, and more effective fuel cells, fuel cell modeling can cause fuel cell design reformations that it is beneficial for fuel

cell developers. In order to be considered as an ideal model, the model should provide fuel cell performance under a great variety of fuel cell operating conditions. the cell, the fuel or oxidant pressures, the weight fraction of each reactant, fuel and oxidant temperatures, and the cell potential are several crucial factors to add in a fuel cell model. better design, optimization , and materials are claimed by important developments for fuel cell performance and operation. These subjects can only be dealt providing veridical mathematical process models are existing.

Butler- Volmer-type expressions are stated by many certain papers, yet Tafel-type expressions can be often seen. More veridical, complex multi-staged reaction kinetics for the electrochemical reactions are used other a few models. The existence of the two phases (liquid and gas) is known. These phases coexist under a different of operating circumstances. Within the air structure, with the purpose of reaching the catalyst layer, there is a possibility that water may condense and blockade the way for fresh oxygen.

Descriptions related to the mass transport aiming the H_2, air, and electrolyte are an essential property for a single modal. Some mass transport models are put to use. Despite using Fick diffusivities, basic Fick diffusion models and efficient Fick diffusion models generally apply efficient transport coefficients that are specified by experiment and do not throw light on convective flow contributions. Consequently, Nernst-Planck mass transport expressions associating Fick's disperse with convective flow is used by many models. Darcy's law, having various formulations of the hydraulic permeability coefficient, is typically used to number the convective flow while Schlogl's formulations for convective flow are used by some models which not only numbers electro osmotic flow but also and can be applicable for mass transport inside the PEM, Using the drag coefficient model is known to be a basic model to associate electro osmotic flow in the membrane. A proportion of water and fuel flow to proton flow are presumed by this model. The Maxwell-Stefan formulation is the other well-known mass transport definition for multi

component mixtures. Although the Maxwell-Stefan formulation has been applied on many models for gas-phase transport, it could be preferable if used for liquid-vapor-phase mass transport. Surface diffusion models and models based on unchangeable thermodynamics are not used very much. Mass transport models using efficient transport coefficients and drag coefficients generally only make a good access to experimental data under a restricted range of operating conditions.

A fully hydrated PEM is ascribed by most models. In some instances, while based upon the change of Gibbs free energy inside the PEM based upon water content, a thermodynamic model is referable. In some other instances, an empirical correlation defines the water uptake. Most of the forms associate an isothermal cell activity and as a result there is a lack of involved energy balances. In the open literature, the description of many PEM fuel cell models regarding simple zero-dimensional and complex three-dimensional models has been made during last decade.

Most models are based in theory, comprehensive and complicated, managing to number circumstance in fuel cells. The models ordinarily deal with one side or section of the fuel cell only. In order to get a general voltage–current relationship some models called semi-empirical are held. Yet, these relations inclined to be particular to one definite fuel cell stack with physical justification which is unreal. For each new fuel cell form, it is essential to re-examine the coefficients existing in the voltage–current that restricts this kind of model that can be predicted. A simplified approach to the electrochemical viewpoints including electrode kinetics and mass transport restrictions in the fuel cell are applied by fuel cell system models that are usually semi-empirical having fluid dynamic relations for the supporter system and extra thermodynamic (Haraldson and Wipke, 2004).

A three-dimensional parametric model, based on the influences of temperature, humidity and pressure was developed by Wang et al. (2003). It is discovered that in case of the inlet gases being completely humidified, with increasing

temperature the performance of the fuel cell developed. However, with under humidified gases dehydration of the membrane may happen leading to lowered conductivity values, as well as lowered cell activity. It is also discovered that except at higher current densities, H_2 humidification is needed at low current densities. The reason of this is when the current densities are high, adequate water is produced at the air in order to maintain the membrane hydrated. As dehydration may take place on the H_2 side and flooding on the air side; in addition to previously mentioned results, it is seen that air humidification has no importance, particularly when current densities are high. As a result, humidifying the air gas stream has no advantage. In Table 2.4 recent mathematical models are compared.

Table 2.4 Comparison of recent mathematical models

No. Of Dimension	Dyn/ SS	H_2 and Air Kinetics	H_2 and Air Phase	Mass Transport (H_2 and Air)	Mass Transport (Electrolyte)	Membrane Swelling	Energy Balance
One dimension, two dimension, or three dimension	Dynamic or steady state	Tafel-type expressions, butlervolmer complex kinetics equations	Gas, liquid, combination of gas and liquid	Effective fick's diffusion, nernstplanck, nernst-planck +schlogl, maxwellstefan	Nernst-planck +schlogl, Nernst-Planck +drag coefficient, Maxwell-Stefan, effective Fick's diffusion	Empirical or thermodynamic models	Isothermal or full energy balance

The needed water inclusion and removal important to keep full membrane humidification at a certain current density are identified by the Bernardi and Verbrugge model (1992). A pseudo two-dimensional model predicting not only water and thermal control but also fuel utilization for a fuel cell operating with developed methanol as the fuel was developed by Fuller and Newman (1993). That for fuel cell stacks water control is strongly attached to thermal control and becomes even more harder can be seen through the model of Wohr et al., (1998). In the inner cells of the stack the temperatures are more than the outer cells coming up with result in membrane dehydration. Water control mainly has relation with thermal control/heat removal. the geometry of the gas flow field is included in other strategies for influential water control.

In mechanistic modeling, getting the most importance in the literature, differential and algebraic equations are came out stood for the physics and electro-chemistry managing the incident internal to the cell. By applying some kind of computational method, these equations are solved. Multi-domain models or single- domain (or unified) models are the categories of mechanistic models.

2.7.1 Zero-D Model

A movement of electrical load and a alteration in Gibbs energy are both included in electrochemical reactions. The activation energy block specifies the rate of an electrochemical reaction. The overwhelm of the charge in travelling from electrolyte to a solid electrode is required or reverse. an electrochemical activation keeps going on the external part of the electrode at the speed and this is the rate where the electrons are freed or "consumed," called the electrical current. The current (of electrons or ions) per unit area of the external part is called current density. It is pursued from Faraday's Law that current density, the current (of electrons or ions) per unit area of the surface, is comparative to the charge carried and the depletion of reactant per unit area:

$$i = nF_j \tag{2.14}$$

in which nF stands for the charge transferred (Coulombs mol^{-1}) , and j stands for the flux of reactant per unit area ($mols^{-1}cm^{-2}$). Thus, by a current-measuring device located outer part to the cell, the reaction rate can be quantified with ease. Yet, the variation between onward and backward current on the electrode is the net current or current density. In general, both oxidation and lessening of the categories are included in an electrochemical reaction:

$$Red \rightarrow Ox + ne^{-} \tag{2.15}$$

$$Ox + ne^{-} \rightarrow Red \tag{2.16}$$

Protons and electrons are the products of the H_2 reactions, known as oxidation of hydrogen where hydrogen and its electrons are separated. During oxygen reduction, water is activated as a product and this occurrence is defined as the air reaction. Reduction , courses, and oxidation happen at identical rates when an electrode is at balanced circumstances that means outer current is not being activated:

$$Ox + ne^{-} \leftrightarrow Red \tag{2.17}$$

The flux related to the onward reaction of Equation (2.17), defined by Equation (2.176), is:

$$j_f = k_f C_{O_x} \tag{2.18}$$

In which k_f means forward reaction (reduction) rate coefficient, and Cox means surface concentration of the reacting species.

in the same way, the flux related to the reverse reaction of Equation (2.18), defined by Equation (2.15), is:

$$j_b = k_b C_{R_d} \tag{2.19}$$

In which k_b stands for reverse reaction (oxidation) rate coefficient, and C_{Rd} for surface concentration of reacting species.

Each two reactions liberates or uses electrons up. The core current generated is the difference between the electrons released and consumed:

Electrons are liberated or used up by each two reactions. The difference between the electrons liberated and used up is called the absolute current activated:

$$i = nF\left(k_f C_{O_x} - k_b C_{R_d}\right) \tag{2.20}$$

Despite the fact that the reaction advances in both directions concurrently, at balanced condition, the absolute current coincides with zero. The rate including these reactions advance at balanced condition is called the exchange *current density*.

That a function of the Gibbs free energy means the reaction velocity coefficient for an electrochemical reaction can be shown in Transition State Theory:

$$k = \frac{k_B T}{h} \exp\left(\frac{-\Delta G}{RT}\right) \tag{2.21}$$

where k_B is Boltzmann's constant and h is Planck's constant.

That the Gibbs free energy for electrochemical reactions is composed of not only chemical terms but also electrical terms can be regarded. At this stage, reduction reaction :

$$\Delta G = \Delta G_{ch} + \alpha_{Rd} FE \tag{2.22}$$

an oxidation reaction:

$$\Delta G = \Delta G_{ch} - \alpha_{Ox} FE \tag{2.23}$$

The subscript "ch" signifies the chemical component of the Gibbs free energy, E infers the potential, F means the Faraday's constant, α stands for a transfer coefficient, E infers the potential. In the literature the transfer coefficient related to the transfer coefficient, α , and the symmetry factor, β, includes some disordinance. For a single-step reaction including a single electron (n = 1), the symmetry factor, β , may most certainly be used. Although its amount is between 0 and 1 in theory, the amount approximately for the reactions on a metallic surface is principally approximately 0.5. As β is identified in a method that needs the union of that the total of the symmetry factors in the anodic and cathodic direction. Regarding that β is for reduction, it is obliged to be (1 - β) for the backward, oxidation reaction. Yet, oxygen reduction and hydrogen oxidation called electrochemical reactions electron, include more step and electron rather than one. Therefore, the slowest step in the range, also called as rate-determining step, identified that the rate of all steps have to be like at steady state. experimental parameter, referred the transfer coefficient α, is applied rather than the symmetry factor, β, on defining a multistep process. In this stage, the equality of $\alpha_{Rd} + \alpha_{Ox}$ to unity is not much needed. As a matter of fact $(\alpha_{Rd} + \alpha_{Ox}) = n/\nu$ stands for the number of times the rate-determining step have to happen to lead to the occurrence of the overall reaction, n refers the number of electrons carried in the overall reaction and ν means the stoichiometry number. In Equation (2.20) the parameter of the onward (reduction) and reversal (oxidation) reaction rate is shown then successively:

$$k_f = k_{0,f} \exp\left[\frac{-\alpha_{Rd} FE}{RT}\right]$$

$$k_b = k_{0,b} \exp\left[\frac{-\alpha_{Ox} FE}{RT}\right] \quad (2.24)$$

The net current density is acquired after including into Equation (2.20)

$$i = nF\left\{k_{0,f} C_{Ox} \exp\left[\frac{-\alpha_{Rd} FE}{RT}\right] - k_{0,b} C_{rd} \exp\left[\frac{\alpha_{Ox} FE}{RT}\right]\right\} \quad (2.25)$$

Despite the fact that in both directions the reaction advances at once, at balanced condition, E stands for the potential, and the net current is zero,. the exchange current density means the rate at which these reactions advance at balanced condition:

$$i_0 = nFk_{0,f}C_{Ox}\exp\left[\frac{\alpha_{Rd}FE_r}{RT}\right] = nFk_{0,b}C_{Rd}\exp\left[\frac{\alpha_{Ox}FE_r}{RT}\right] \quad (2.26)$$

A connection between potential and the current density is acquired by conjoining the Equations (2.26) and (2.27),

$$i = i_0\left\{\exp\left[\frac{-\alpha_{Rd}F(E-E_r)}{RT}\right] - \exp\left[\frac{\alpha_{Rd}F(E-E_r)}{RT}\right]\right\} \quad (2.27)$$

E_r is the invertible or balanced condition potency, called as Butler-Volmer Equation. 0 V is the invertible or balanced condition potency at the fuel cell H_2 and 1.229 V (at 25°C and atmospheric pressure) stands for the invertible potential at the fuel cell air, with temperature and pressure it varieties. Over potential is the dissimilarity between the invertible potential and the electrode potential. This potential dissimilarity is needed in order to engender current.

The Butler-Volmer Equation (2.27) is suitable H_2 and air reaction in a fuel cell:

$$i_a = i_{0,a}\left\{\exp\left[\frac{-\alpha_{Rd,a}F\left(E_a - E_{r,a}\right)}{RT}\right] - \exp\left[\frac{\alpha_{Ox,a}F\left(E_a - E_{r,a}\right)}{RT}\right]\right\}$$

$$I_c = i_{0,c}\left\{\exp\left[\frac{-\alpha_{Rd,c}F\left(E_c - E_{r,c}\right)}{RT}\right] - \exp\left[\frac{\alpha_{Ox,c}F\left(E_c - E_{r,c}\right)}{RT}\right]\right\} \quad (2.28)$$

The over potential on the H_2 is positive ($E_a > E_{r,a}$,) which causes the first term of the Equation (2.28) to be insignificant in comparison with the second term, that is, the oxidation current is predominant and the equation may be reduced to:

The over potential on the H_2 is positive ($E_a > E_{r,a}$,)

Compared to the second term, the over potential on the H_2 is positive ($E_a > E_{r,a}$,) causing the first term of the Equation (2.28) to be insignificant. Therefore, the oxidation current is most effective and the equilibrium may be decreased to:

$$i_a = -i_{0,a}\exp\left[\frac{\propto_{Ox,a} F(E_a - E_{r,a})}{RT}\right] \quad (2.29)$$

A negative sign existing in the resulting current stands for the parting of the electrons from the electrode (net oxidation reaction). In the same way, the over potential on the air is negative ($E_c < E_{r,c}$) causing the first term of the Equation (2.28) to be larger compared with the second term. Therefore, the oxidation current is most effective and the equilibrium may be decreased

$$i_c = i_{0,c}\exp\left[\frac{-\propto_{Rd,c} F(E_c - E_{r,c})}{RT}\right] \quad (2.30)$$

It is appeared that for hydrogen/oxygen fuel cells applying Pt catalyst has value around 1 in the former equations related to the transfer coefficients. An n parameter in the former equations signifying the number of electrons included appears in some literature. Regarding that n = 2, on the fuel cell H_2 side and n = 4, on the air side, the product of nα has value around 1. α in range between 0.2 and 2 is stated by Newman (1991) and a value of α = 0.5 for the hydrogen fuel cell H_2 (including two electrons) and also α = 0.1 to 0.5 for the air are inscrolled.

If the rate constant in chemical reactions is compared to Exchange current density, io, in electrochemical reactions, it can be seen that exchange current density is depended on concentration that can be seen directly from Equation 2.26. A function of electrode catalyst charging and catalyst particular surface area are also the part of the influential exchange current density (per unit of electrode active area).

For advance with the electrochemical reaction, exchange current density is a measurement of an electrode's preparedness. High exchange current density leads to higher activity on the surface of the electrode. The exchange current density at the H_2 at the air is not as high as that in a hydrogen/oxygen fuel cell., when the exchange current density is larger, contrarily, the energy barrier gets smaller. Moreover, when the exchange current density is larger, the amount of current is created at any over potential increases. Because the H_2 exchange current density in hydrogen/oxygen fuel cells is several orders of magnitudes larger than the air current density ($\sim 10^{-4}$ vs. $\sim 10^{-9}$ Acm^{-2} Pt, at 25 °C and 1 atm), the over potential on the air is much larger than the H_2 over potential. Thence, the connection between the cell potential and current is frequently converged only by Equation (2.30).

CHAPTER 3

EXPERIMENTAL

3.1 Materials

High-purity hydrogen, nitrogen and dry air (Linde Company) were used as the fuel, oxidant and inert gases, respectively. The flow stoichiometry for hydrogen and the air was 1.2/2.0, respectively (Barbir, 2005). The polarization curve data for commercial PEM MEA was obtained from Paxitech and the required flow rate of the reactant gases for the experiments were calculated according to these data. The calculations and polarization curve are given in Appendix C and Figure C.1, respectively. A membrane electrode assembly (MEA) having active surface area of 5 x 5 cm^2 (Paxitech) and a single test cell having 5 x 5 cm^2 active area (Paxitech) were used during the experiments.

3.2 Experimental Setup

3.2.1 Fuel Cell Test Station

Fuel cell test station with a capacity of 600 W (Henatech ^{TM}, HENAtwin^{TM}) was used for PEM fuel cell performance tests. Test station can be used for both methanol and PEM fuel cell testing. A schematic representation and a photo of the test station are given in Figure 3.1 and 3.2, respectively.

The system mainly consists of 7 sub-systems. These are hydrogen and methanol fuel distribution system, the oxidant gas distribution system, linear electronic load, fuel cell heater control system, the I/O capabilities, and Hardwired Emergency Stop system.

For each entry in the gas system, there are pressure transducers and each gas is allowed to enter the system by secure computer-controlled solenoid valves. Gas flow rates are controlled by pressure regulators.

There is also an isolated purge system in the fuel cell test station. This purge system can be used for purging the fuel mixture gas line in the emergency situation. Back pressure regulators are used to increase the pressure of the system up to 10 bars. These adjustable back pressures can be read on the front panel of HENAtwin^{TM} test unit.

Online electronic load sub-system acts as a variable power resistor. Electronic load connections, the fuel cell current and voltage monitors are located on the front panel of the unit. The amount of impedance, electronic load, the power to spend or how much current and voltage will pass was controlled by user-control software, selecting any of such conditions. In the meantime, current and voltage values are continuously monitored by computer. These parameters are used to calculate and monitor the amount of power consumed by the load sub-system at any time. An internal fan is running continuously to cool the electronic load.

There are three thermocouple input HENAtwin^{TM} testing unit. One of the thermocouples used to measure the fuel cell temperature and the other ones are used to measure the hydrogen and air gas transmission lines temperatures before entering the cell, respectively.

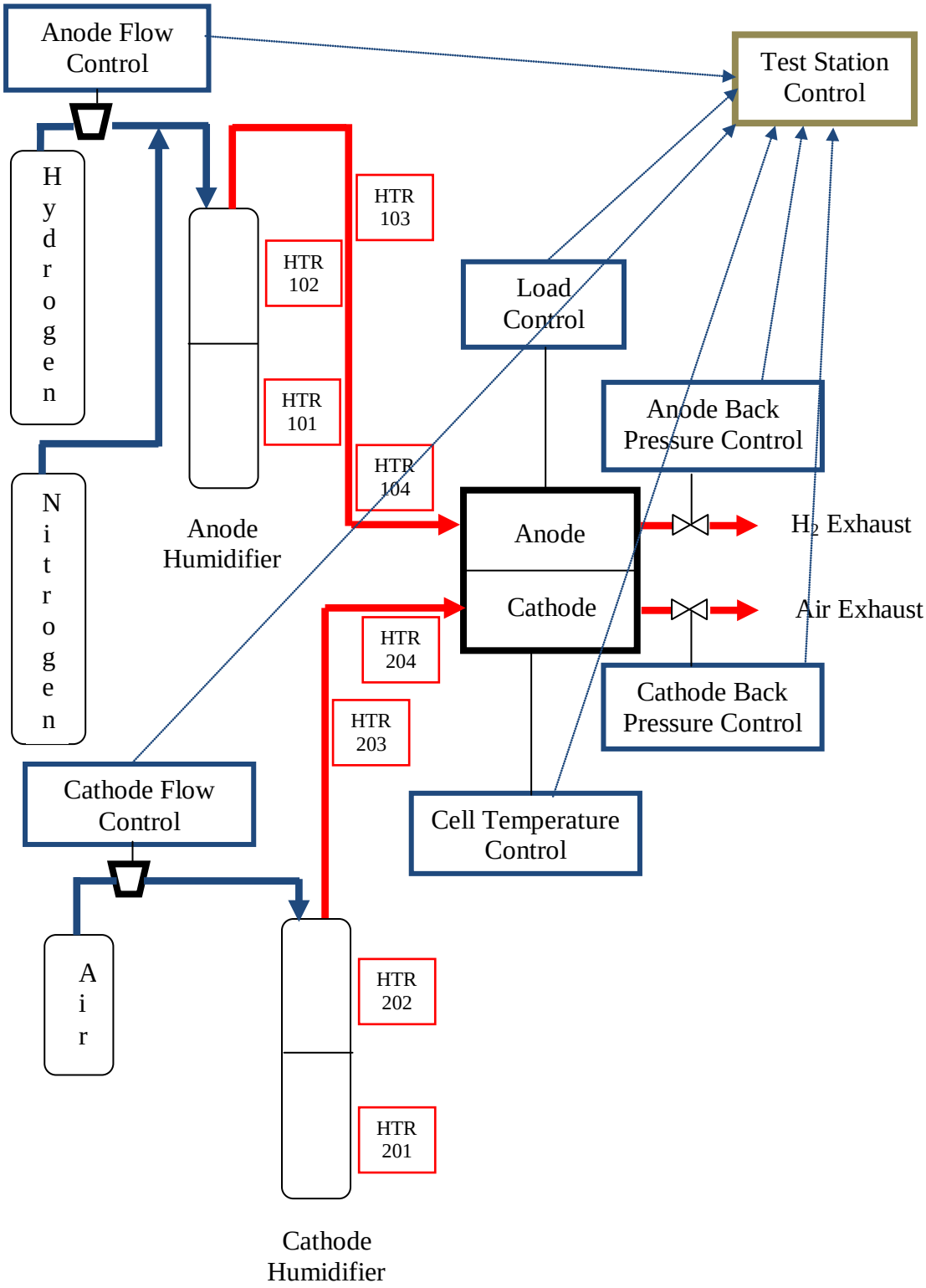

Figure 3.1 Schematic representation of fuel cell test station

Fuel (H_2) and oxidant gas (air) are supplied to the system from pressurized tanks. Gas flow into the fuel cell controlled by mass flow controllers in order to obtain desired flow rates.

Hydrogen and air are passed through heated humidifiers to bring the desired relative humidity of inlet gases before entering to the fuel cell. The relative humidity of the inlet gases were controlled through changing the temperature of the humidifier. The description of some part in the schematic representation is shown in Table 3.1. In the meantime, gases are kept at the desired temperature with the help of resistance heaters to prevent any water vapor condensation in the gas distribution channels. Hydrogen and air waste gases are thrown out from the gas discharge channels. The screen shot of data logging software is shown in Figure 3.3 and 3.4.

Table 3.1 Description of the heaters shown in schematic representation of fuel cell test station

Heaters	Function	Temperature range (^oC)
HTR 101	H_2 humidifier liquid water phase heater	54.8 - 80
HTR 102	H_2 humidifier vapor phase heater	54.8 - 80
HTR 103	H_2 gas transfer line heater	54.8 - 80
HTR 104	Heater of humidified H_2 inlet to the fuel cell	54.8 - 80
HTR 201	Air humidifier liquid water phase heater	36.1 - 80
HTR 202	Air humidifier vapor phase heater	36.1 - 80
HTR 203	Air gas transfer line heater	36.1 - 80
HTR 204	Heater of humidified air inlet to the fuel cell	36.1 - 80

Figure 3.2 Photo of PEM fuel cell test station

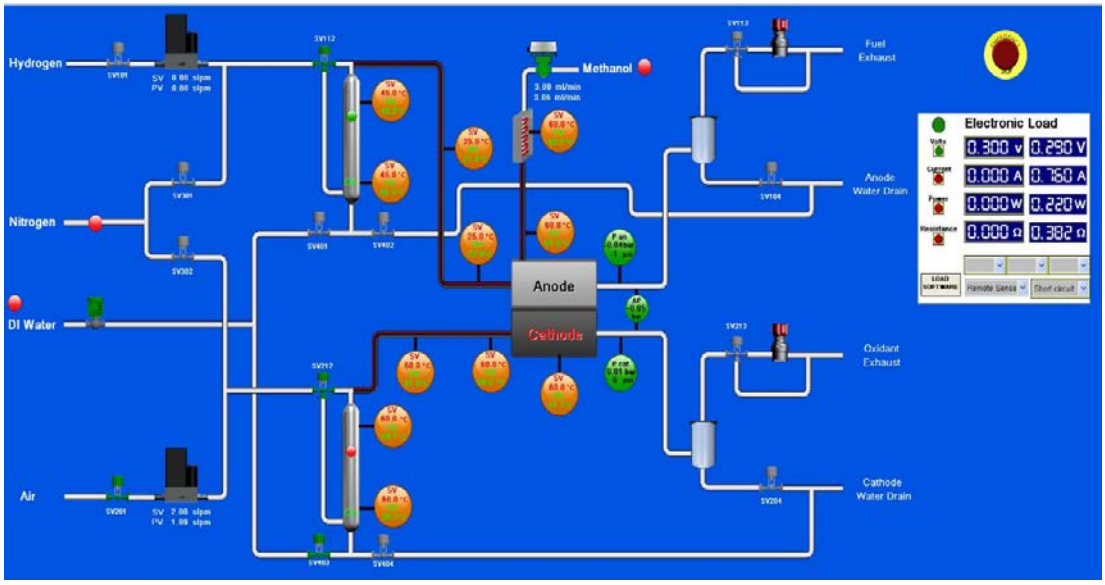

Figure 3.3 The screen shot of data logging software

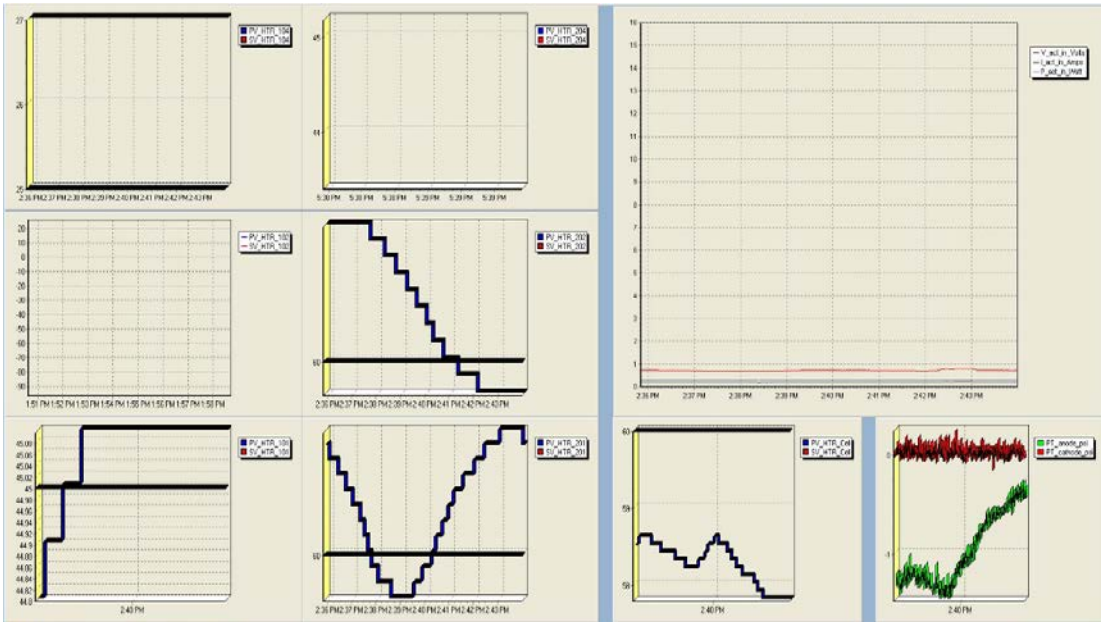

Figure 3.4 The screen shot of data logging software

3.2.2 Fuel Cell Testing Unit

A single test cell composed of two graphite plates having 3-fold serpentine gas flow channel was used in the experiments. Two current collector plates located behind the graphite bipolar plates, two insulator sheets that is preventing the fuel cell from electric short circuits, and two end plates were used to tighten the cell together. 1 mm, 2 mm and 3.2 mm diameter holes was drilled in the graphite bipolar plates in order to measure the voltage and temperature. These test cells are all equipped with “swagelock” type fittings matching 6 mm diameter gas pipes. The photo of the test PEM fuel cell is shown in Figure 3.5.

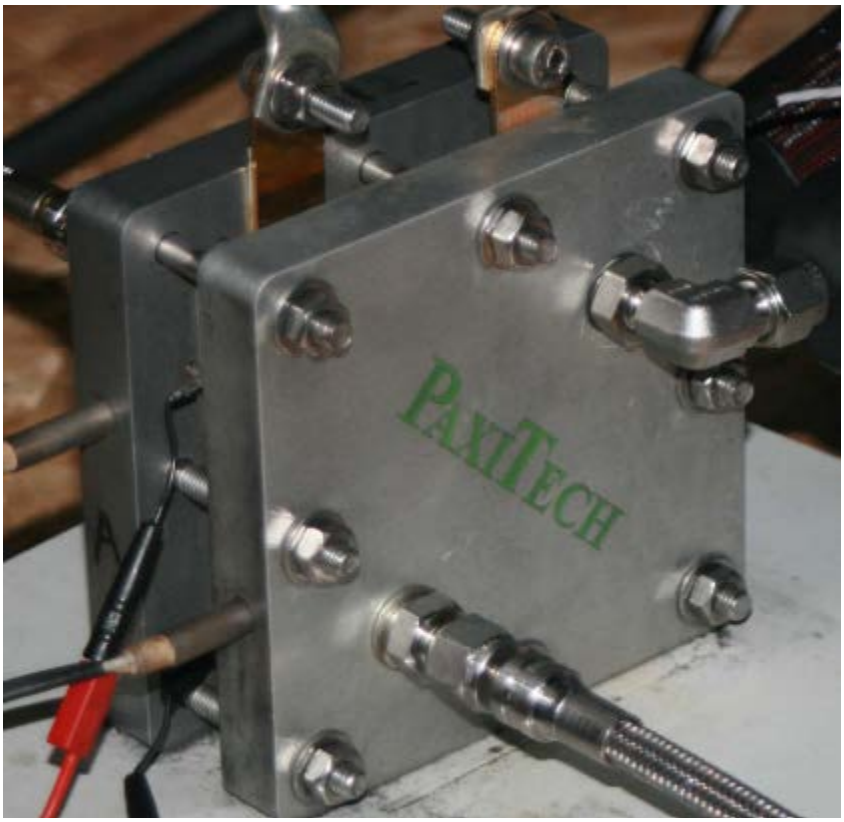

Figure 3.5 Photo of test PEM fuel cell (PaxiTech)

3.2.3 Membrane Electrode Assembly (MEA)

In order to realize fuel cell tests, an active surface area of 5 x 5 cm^2 PEM fuel cell MEA was obtained from Paxitech. Catalyst loading is 0.5 mg Pt/cm^2 for both anode and cathode side of MEA. Membrane thickness is 70 µm of Nafion 212.

Electrode gas diffusion layer is composed of both the macro porous as well as micro porous layers with the components of carbon non-woven felt, 10 % PTFE and carbon 30 % PTFE, respectively. Gas diffusion layer thickness is 215 µm. Commercial PEM MEA specifications and a photo of PEM MEA is shown in Table 3.2 and Figure 3.6, respectively.

Table 3.2 Commercial PEM MEA (Paxitech) specifications

Active area	25 cm^2
GDL	215 µm (carbon non-woven felt – 10% PTFE)
H_2	Pt/C – 0.5 mg/cm^2
Air	Pt/C – 0.5 mg/cm^2
Membrane thickness	70 µm
Micro porous layer	(carbon + PTFE)

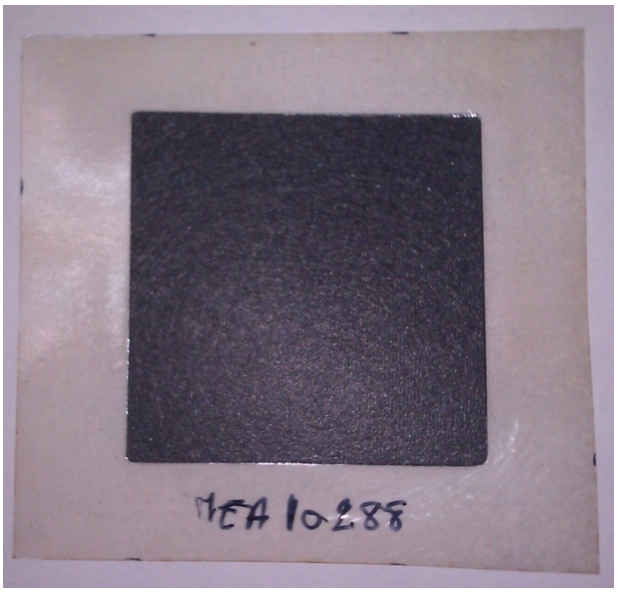

Figure 3.6 Commercial PEM MEA (Paxitech)

3.3 Experimental Procedure

The commercial MEA was placed into the test cell and the bolts were tightened at a torque of 8-10 Nm on eight bolts. . In order to be in safe and prevent the use of gases in vain, before starting the experiments gas leakages from the fuel cell was tested with a liquid gas detector.

3.3.1 Performance Procedure

The following procedure has been followed for performance tests.

1) The cell temperature was adjusted and the temperatures of humidifiers and gas transfer lines were set desired values for each experiment.
2) Before passing the reactant gases, the anode and the cathode side were purged with nitrogen in order to ensure that no H_2 and air were present in the anode and the cathode side or there was no leak in the cell.
3) After the cell passed the required level of safety and set temperatures were achieved, hydrogen and air are supplied to the cell at a rate of 0.3 and 1 slpm, respectively.
4) The cell was operated at 0.6 V until it came to steady state, which took about 4 hours.
5) After steady state was achieved, starting from the OCV value, the current-voltage data was logged by changing the load and polarization curve (voltage versus current density) was obtained.
6) For each experiment, three polarization curves were obtained after purging the system with nitrogen for one hour.

3.3.2 Polarization Curve Procedure

A polarization curve reflects the performance of a fuel cell. After the normal operating procedure is performed, polarization curve procedure is performed as below. Experimental data was taken at multiple voltage points. Starting from OCV, 12 or 13 points between 300 mV/cell and 900 mV/cell, with 5 minutes dwell at each point, corresponding current was read and the data for five (5) minutes was averaged and then plotted as average current versus average voltage.

3.4 Scope of the Experiments

Fuel cell performance test was performed with the commercial MEA obtained from Paxitech. In this way, it was tried to determine the most appropriate

operating conditions for single cell PEM fuel cell. Effect of relative humidity of reactant gases and cell temperatures on fuel cell performance was carried out. In order to obtain desired relative humidity, the required dew point at the fuel cell temperature was calculated and this value was set to the fuel cell station. These calculations are shown in Appendix C. In this context, while the relative humidity of hydrogen was constant, effect of relative humidity of air on the system performance was tried to examine. At the best RH of air condition, 50 % RH of hydrogen was also tested in order to see the effect of relative humidity of hydrogen. Tests were carried out at of 60, 70 and 80 ^{o}C cell temperatures. Test conditions for commercial PEM MEA are given in Table 3.3 and experimental data obtained at these conditions are given in Appendix A.

Table 3.3 Test conditions of performed experiments with commercial PEM MEA, H_2 flow rate 0.3 slpm, air flow rate 1slpm

Test Condition	Cell T (^{o}C)	RH of air (%)	RH of H_2 (%)	H_2 dew point (^{o}C)	Air dew point (^{o}C)
1	60	30	100	60	36.1
2	60	50	100	60	45.7
3	70	20	100	70	36.9
4	70	30	100	70	44.5
5	70	50	100	70	54.8
6	70	70	100	70	62
7	70	100	100	70	70
8	70	70	50	54.8	62
9	80	20	100	80	44.8
10	80	30	100	80	52.9
11	80	50	100	80	63.8
12	80	70	100	80	71.4
13	80	100	100	80	80
14	80	100	50	63.8	80

Two different relative humidity of air were tested at 100 % RH of H2 with a stoichiometry of 1.2/2 for hydrogen and air, at 60 ^{o}C cell temperature, respectively. Five different relative humidity of air were tested at 100 % relative humidity of H_2 and at the best relative humidity of air (70 %) condition, 50 % relative humidity of H_2 was also tested with a stoichiometry of 1.2/2 for H_2 and air at 70 ^{o}C cell temperature, respectively. Five different relative humidity of air were tested at 100 % relative humidity of H_2 and at the best relative humidity of air (100 %) condition, 50 % relative humidity of H_2 was also tested with a stoichiometry of 1.2/2 for H_2 and air at 80 ^{o}C cell temperature, respectively.

CHAPTER 4

RESULTS AND DISCUSSION

In this work, the simultaneous effect of cell temperature and relative humidity of reactant gases on the performance of the fuel cell has been studied. In this way, sets of experiments were carried out where the operation temperature of the fuel cell was varied from 60 to 80 ºC, and the humidification temperature for inlet gases were varied from 36.1 to 80 ºC in order to achieve different relative humidity of reactant gases. The polarization curves were obtained for each set of experiments and zero dimensional mathematical models was fitted to experimental data. Experimental data and modeling results are given in Appendix A and B, respectively.

4.1 Performance of PEM Fuel Cell at Different Temperatures

4.1.1 Performance at 60 °C

The effect of air inlet relative humidity on PEM fuel cell performance have been tested at 60 ^{o}C fuel cell temperature and atmospheric pressure with a flow rate of 0.3 slpm for H_2 and 1 slpm for air. The operating conditions are shown in Table 4.1. Tests were repeated for three times for each experiments and a single polarization curve was obtained taking the arithmetic average of these three experiments. The standard deviations are 0.022 and 0.020 for 30 % and 50% RH air, respectively. It is mean that the average value is consistent with these three curves. So the mean value was used in the results.

Table 4.1 OCV values at 60 °C PEMFC, air flow rate 1 slpm, H_2 flow rate 0.3 slpm

RH of air (%)	RH of H_2 (%)	H_2 dew point (ºC)	Air dew point (ºC)	OCV (V)
30	100	60	36.1	0.97
50	100	60	45.7	0.96

In order to obtain the best polarization curve the commercial PEM MEA was tested at different cell, humidifier, and gas transfer line temperatures. During the tests, all the parameters such as pressure, air and H_2 flow rate were kept constant. The polarization curves and power outputs of commercial PEM MEA are shown in Figure 4.1 and 4.2, respectively.

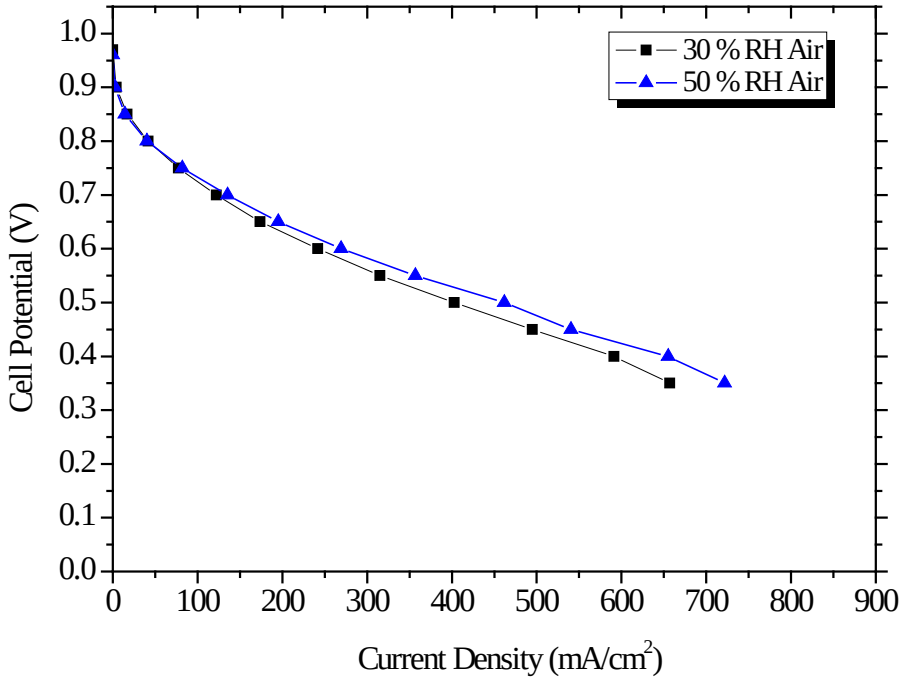

Figure 4.1 Cell potential vs. current density at 60 ^{o}C cell temperature, 100 % RH of H_2

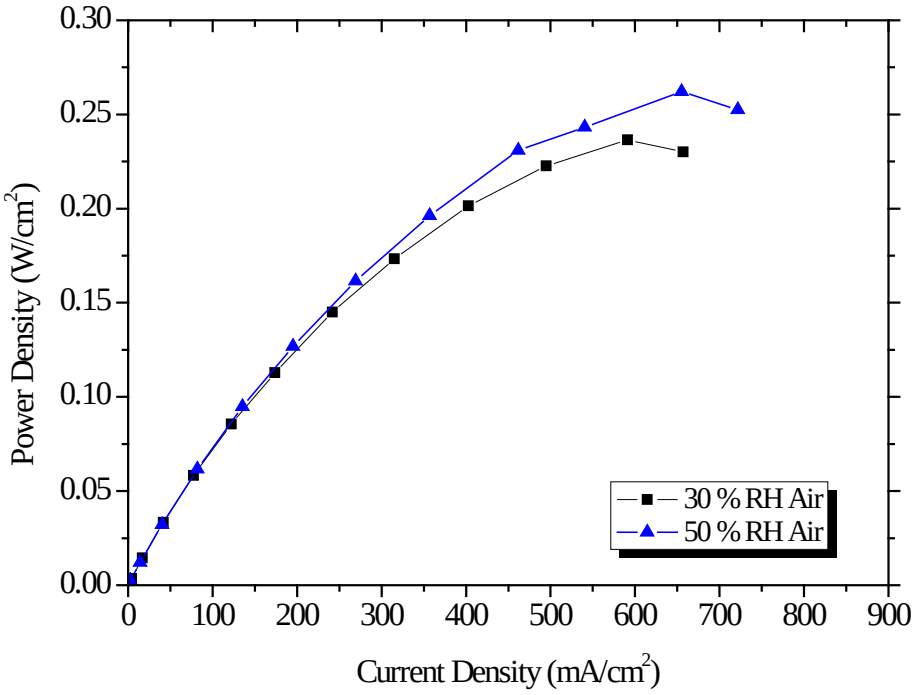

Figure 4.2 Power density vs. current density at 60 °C cell temperature, 100 % RH of H_2

As shown in Figure 4.1 and 4.2, the best performance and highest power output is obtained at 50 % RH of air with a constant RH of H_2 (100%). As it can be seen from the Figure 4.1, open circuit potentials (OCV) are 0.97 V and 0.96 V for 30 % RH and 50 % RH, respectively. It is usually lower than theoretical cell potential (1.2 V). However, in practice this potential is usually less than 1V.

The current density at 0.6 V for 30 % RH is 270 mA/cm^2 and 50 % RH is 275 mA/cm^2. The current density at 0.4 V for 30 % RH is 580 mA/cm^2 and 50 % RH is 650 mA/cm^2. As RH of air decreases, almost 2 % decrease at 0.4 V and 10 % decrease at 0.6 V was observed for the current densities. As it can be seen from Figure 4.3, the maximum power density is 0.23 W/cm^2 for 30 % RH and 0.26 W/cm^2 for 50 % RH.

At low current densities, the activation voltage losses are nearly the same at 30 % and 50 % RH of air. At low relative humidity, the ohmic voltage losses are higher than that of high relative humidity. Therefore in the ohmic region, the resistance is

higher between the anode and cathode if the relative humidity is lower. Sufficient membrane hydration is required to transmit protons from anode to cathode side of the fuel cell. At 30 % RH, membrane may not be hydrated sufficiently to transmit protons.

4.1.2 Performance at 70 °C

The effect of air inlet relative humidity on the performance of PEM fuel cell have been tested at 70 ^{o}C fuel cell temperature and atmospheric pressure with a flow rate of 0.3 slpm for H_2 and 1 slpm for air. The operating conditions are shown in Table 4.2. Tests were repeated for three times for each experiments and a single polarization curve was obtained taking the arithmetic average of these three experiments. The standard deviations are 0.019, 0.011, 0.024, 0.021, and 0.012 for 20, 30, 50, 70 and 100% RH of air, respectively. It is mean that the average value is consistent with these three curves. So the mean value was used in the results.

Table 4.2 OCV values at 70 °C PEM fuel cell, air flow rate 1 slpm, H_2 flow rate 0.3 slpm

RH of air (%)	RH of H_2 (%)	H_2 dew point (^{o}C)	Air dew point (^{o}C)	OCV (V)
20	100	70	36.9	0.98
30	100	70	44.5	0.98
50	100	70	54.8	0.97
70	100	70	62	0.95
100	100	70	70	0.94
70	50	54.8	62	0.94

During the tests, all the parameters such as pressure, air and H_2 flow rate were kept constant. The polarization curves and power outputs of commercial PEM MEAs are shown in Figure 4.3 and 4.4, respectively.

In Figure 4.3 and 4.4, polarization curves are compared for the fuel cell operating conditions from 20 % RH to 100 % RH of air, keeping the H_2 inlet at 100 % RH.

As seen from the Table 4.2, OCV values are 0.98 V, 0.98 V, 0.97 V, 0.95, 0.94 V for 20, 30, 50, 70, 100 RH of air with 100 % RH H_2 and 0.93 V for 50 % RH H_2 with 70 % RH air. At open circuit voltage, in a fuel cell internal currents and crossover losses may have a dramatic effect on fuel cell potential. OCV of hydrogen/air fuel cells is generally below 1V, most likely about 0.94 to 0.97 V depending on operating pressure. Hydrogen cross over is a function of membrane permeability, membrane thickness, and hydrogen partial pressure difference across the membrane, as the main driving force. As RH of hydrogen increases, partial pressure of hydrogen in gas mixture will decrease. Therefore while increasing the RH, OCV values decreases.

The best performance of 230 mA/cm^2 was obtained at 0.6 V for 50 % RH of air and 530 mA/cm^2 at 0.4 V for 70 % RH of air with a constant 100 % RH of hydrogen was obtained.

As it can be seen from the Figure 4.3, the current densities at 0.4 V are 350 mA/cm^2, 400 mA/cm^2, 528 mA/cm^2, 530 mA/cm^2, 529 mA/cm^2 and at 0.6 V are 180 mA/cm^2, 200 mA/cm^2, 230 mA/cm^2, 175 mA/cm^2, 150 mA/cm^2 for 20, 30, 50, 70, 100 % RH of air with a constant 100 % RH of H_2, respectively.

As it can be seen from Figure 4.4, the maximum power densities are 0.14 W/cm^2 , 16 W/cm^2 , 21 W/cm^2 , 22 W/cm^2 , 23 W/cm^2 for 20, 30, 50, 70,100 % RH of air with a constant 100 % RH of hydrogen, respectively.

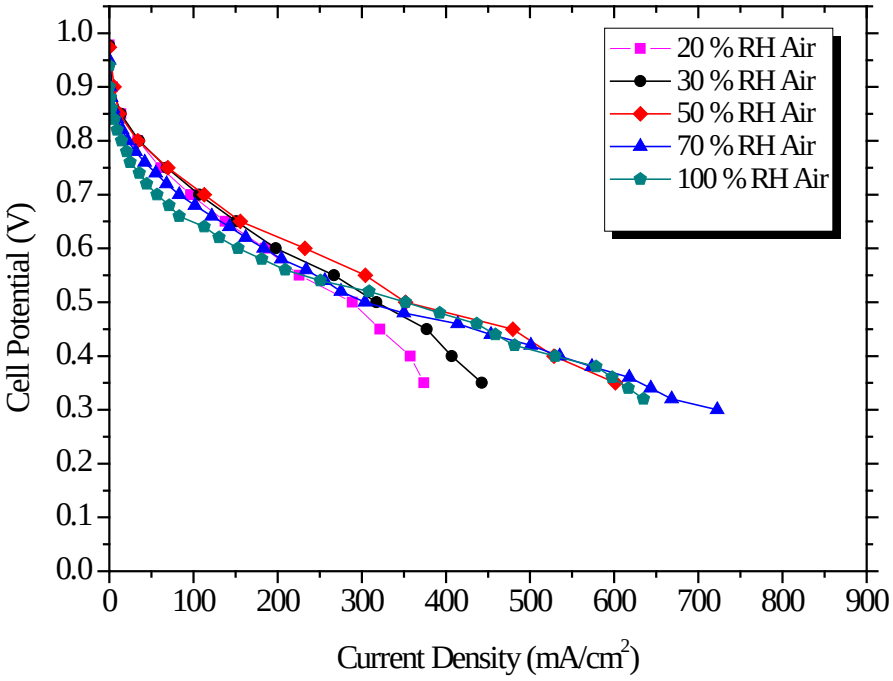

Figure 4.3 Current density vs. cell potential at 70 ^{o}C cell temperature and 100 % RH of H_2

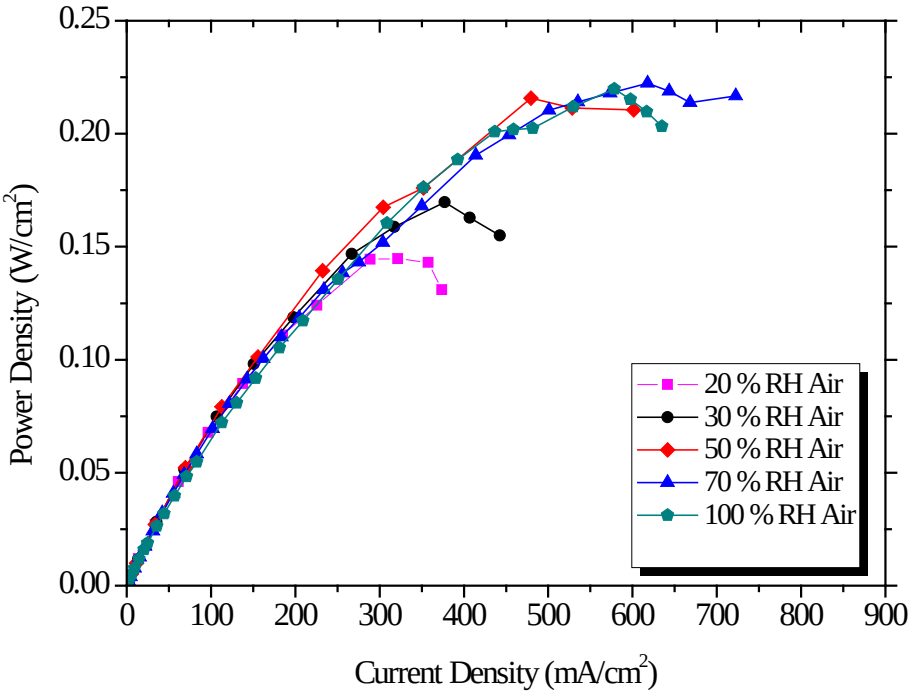

Figure 4.4 Power density vs. current density at 70 ^{o}C cell temperature and 100 % RH of H_2

As shown in Figure 4.3 and 4.4, at low current density region, the cell performance is the best for 50 % RH of air and the worst for 100 % RH of air with a constant 100 % RH of hydrogen. It is seen from the Figure 4.3 that increasing the relative humidity of air from 20 to 50 %, increases the cell performance at low current densities but further increment in RH of air decreases the cell performance at these current densities. At high current densities, increasing the RH of air increases the cell performance. However, there is not much performance difference between 50, 70 and 100 % RH of air with a constant RH of hydrogen (100 %) at that region.

As mentioned before, water is mainly transported inside the membrane by electro-osmotic drag and back diffusion. They affect the water balance in a PEMFC and determine the membrane hydration. In order to achieve good cell performance, there must be an optimal water balance between anode and cathode (Yan et al., 2006). Water transport through the membrane by EOD and BD is affected by current density, fuel cell temperature, membrane water content and humidity of inlet gases.

Fuel cell temperature and water content affect the electro-osmotic coefficient. Yan et al. (2006) was observed that while the current density increasing, the flow of protons and water from the anode to cathode increased linearly with current density. Meanwhile, water was produced at the cathode by oxygen reduction reaction (ORR). The quantity of produced water also increased linearly as current density increased. Therefore the water concentration gradient in the membrane close to the cathode side increased and produced water in the cathode may back diffuse through the membrane from the cathode to the anode. The balance between electro-osmotic drag and back diffusion determines hydration and proton conductivity of membrane.

In their two-dimensional PEMFC model, Nguyen and White (1993) stated that, at high current density, EOD exceeds BD and this cause membrane drying. As the membrane becomes dehydrated, the membrane pores shrink, which further limits

the back diffusion of water. Therefore, it was concluded that water transport due to BD is not sufficient to prevent membrane dehydration. So, it is seen from the Figure 4.3 that increasing RH of air improves the cell performance at high current density region.

As shown in Figure 4.3, at high operating voltages the cell performance decreases with increasing RH of air with a constant 100 % RH of H_2. This may be the because of different channel type configuration like serpentine. Because the cell performance in PEMFC and water management is affected by relative humidity of reactants and flow field designs in the bipolar plates.

In Figure 4.5 and 4.6, polarization curves are compared for the fuel cell operating conditions with 50 % RH and 100 % RH of H_2, keeping the air inlet at 70 % RH. The current density at 0.6 V decreases from 175 mA/cm^2 to 130 mA/cm^2, almost 25 % decrease is observed. As it can be seen from Figure 4.6, the maximum power density is 0.22 W/cm^2 for 100 % RH and 0.15 W/cm^2 for 50 % RH.

As shown in Figure 4.5 and 4.6, the cell performance is higher for 100 % RH of H_2 than 50 % RH of H_2 with a constant 70 % RH of air. As it can be seen from Figure 4.5 that increasing RH of H_2 improves the cell performance with a constant RH of air. As current density is gradually increased, the contribution of RH of H_2 became more important. Yan et al. (2006) observed that when dry hydrogen was supplied to anode as saturated air was supplied to cathode, effective drag coefficient decreased dramatically. With low humidity of hydrogen at anode side, it is fed less water to the anode side of the fuel cell and this cause less water transport from anode to fuel cell membrane leading partial dehydration of membrane.

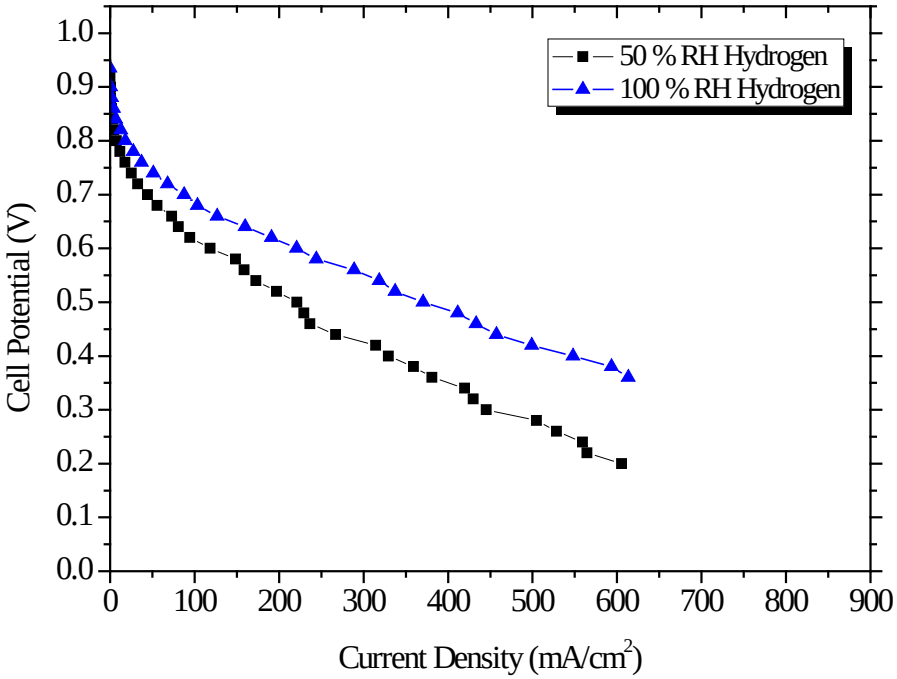

Figure 4.5 Current density vs. cell potential at 70 ^{o}C cell temperature, 70 % RH of air

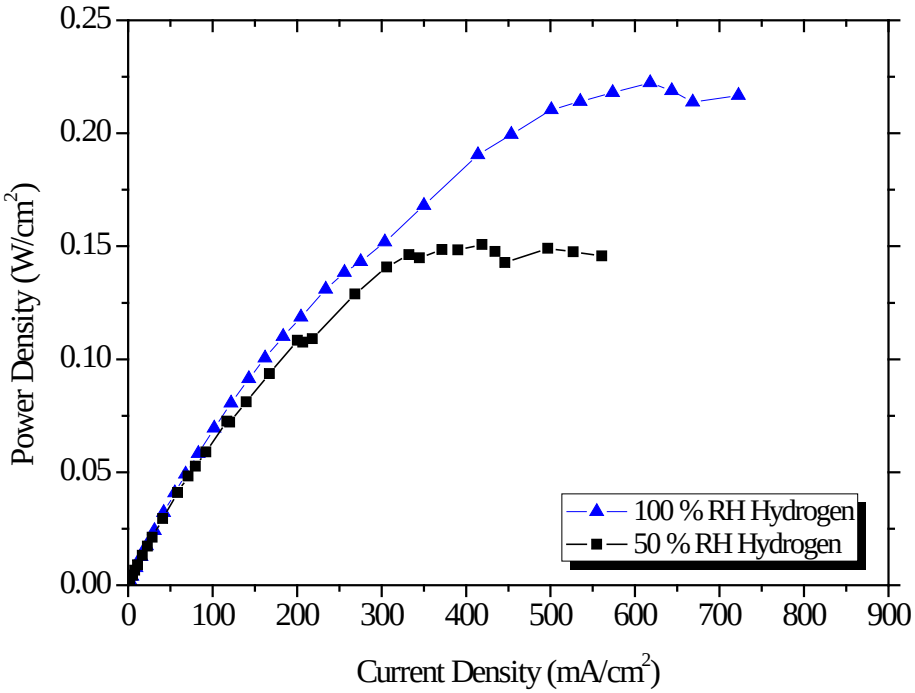

Figure 4.6 Current density vs. power density at 70 ^{o}C cell temperature, 70 % RH of air

4.1.3 Performance at 80 °C

The effect of air inlet relative humidity on the performance of PEM fuel cell have been tested at 80 ^{o}C fuel cell temperature and atmospheric pressure with a flow rate of 0.3 slpm for H_2 and 1 slpm for air. The operating conditions are shown in Table 4.3. Tests were repeated for three times for each experiments and a single polarization curve was obtained taking the arithmetic average of these three experiments. The standard deviations are 0.008, 0.022, 0.010, 0.022, and 0.019 for 20, 30, 50, 70 and 100% RH of air, respectively. It is mean that the average value is consistent with these three curves. So the mean value was used in the results.

Table 4.3 OCV values at 80 °C PEM fuel cell, air flow rate 1 slpm, H_2 flow rate 0.3 slpm

RH of air (%)	RH of H_2 (%)	H_2 dew point (ºC)	Air dew point (ºC)	OCV (V)
20	100	80	44.8	1.0
30	100	80	52.9	0.98
50	100	80	63.8	0.97
70	100	80	71.4	0.97
100	100	80	80	0.94
100	50	63.8	80	0.92

During the tests, all the parameters such as pressure, air and H_2 flow rate were kept constant. The polarization curves and power outputs of commercial PEM MEAs are shown in Figure 4.7 and 4.8, respectively.

In Figure 4.7 and 4.8, polarization curves are compared for the fuel cell operating conditions from 20 % RH to 100 % RH of air, keeping the hydrogen inlet at 100 % RH. The current density at 0.6 V decreases from 200 mA/cm^2 to 80 mA/cm^2, almost 60 % decrease is observed. Also, the current density at 0.4 V decreases from 530 mA/cm^2 to 225 mA/cm^2, almost 60 % decrease is observed. As it can be seen from Figure 4.8, the maximum power density is 0.23 W/cm^2 for 100 % RH and 0.09 W/cm^2 for 20 % RH.

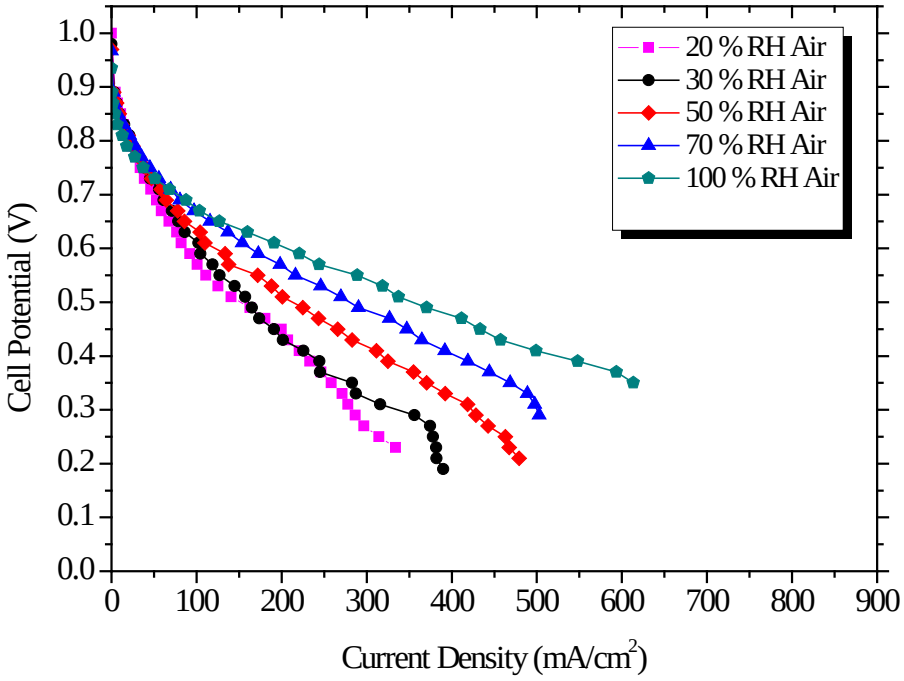

Figure 4.7 Current density vs. cell potential at 80 °C cell temperature, 100 % RH of H_2

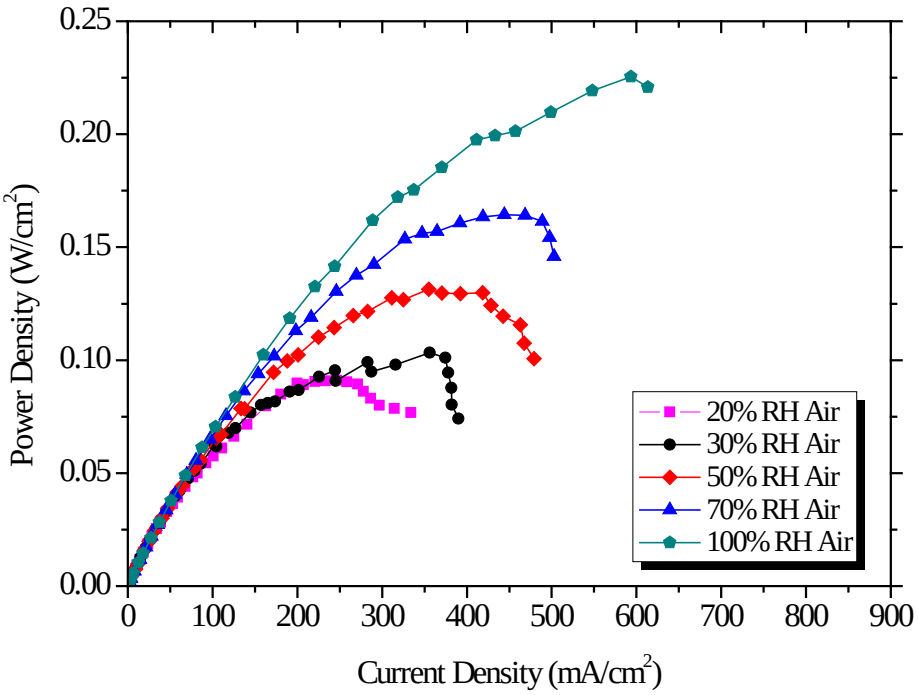

Figure 4.8 Power density vs. current density at 80 °C cell temperature, 100 % RH H_2

In Figure 4.9 and 4.10, polarization curves are compared for the fuel cell operating conditions with 50 % RH and 100 % RH of H_2, keeping the air inlet at 100 % RH. The current density at 0.6 V decreases from 200 mA/cm^2 to 125 mA/cm^2, and at 0.4 V decreases from 530 mA/cm^2 to 325 mA/cm^2 , almost both 40 % decrease is observed. Also, from Figure 4.10, the maximum power density is 0.23 W/cm^2 for 100 % RH and 0.14 W/cm^2 for 50 % RH.

As shown in Figure 4.9 and 4.10, the cell performance is higher for 100 % RH of H_2 than 50 % RH of H_2 with a constant 100 % RH of air. As it can be seen from Figure 4.9 that increasing RH of H_2 improves the cell performance with a constant RH of air. As current density was gradually increased, the contribution of RH of H_2 became more important.

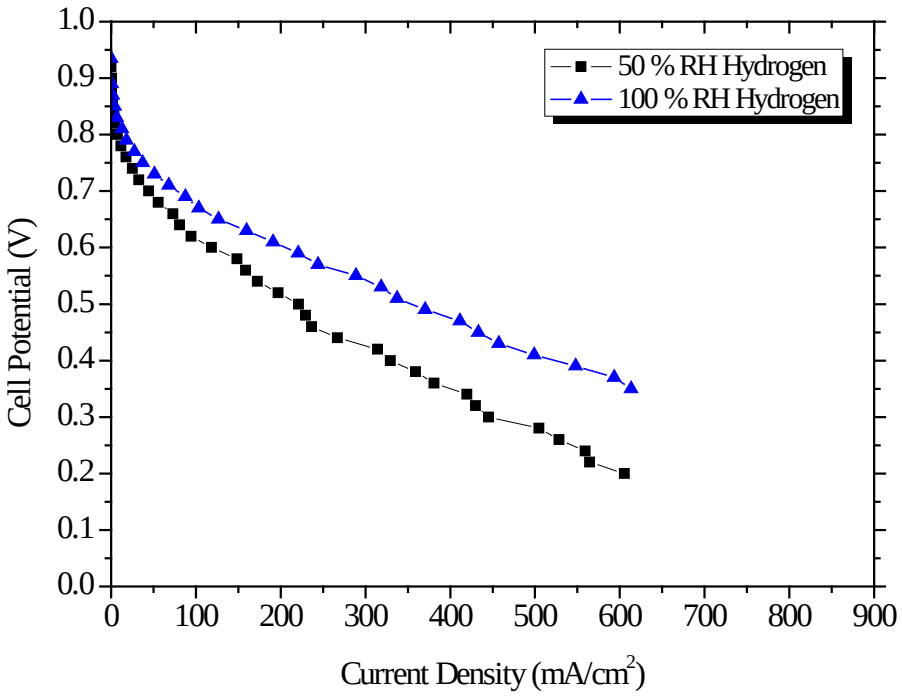

Figure 4.9 Current density vs. cell potential at 80 ^oC cell temperature, 100 % RH air and 50-100 % RH H_2

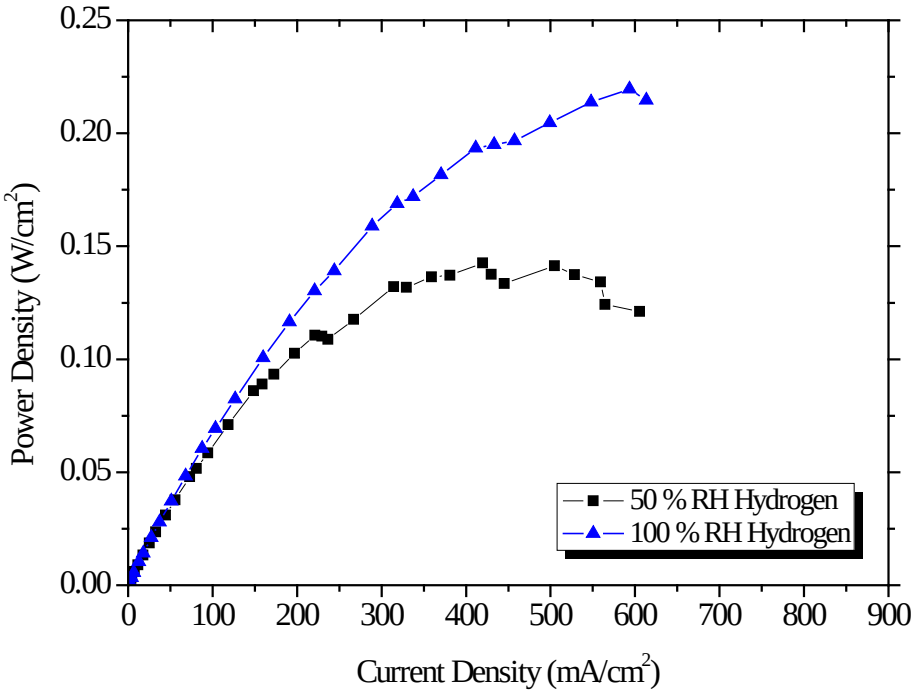

Figure 4.10 Current density vs. power density at 80 °C cell temperature, 100 % RH air and 50-100 % RH H_2

4.1.4 Performance Comparison at 70 °C and 80 °C

The effect of the operation temperature on the performance of the fuel cell is shown in Figures 4.11 and Figures 4.12 with fully saturated air and hydrogen (100 % RH).

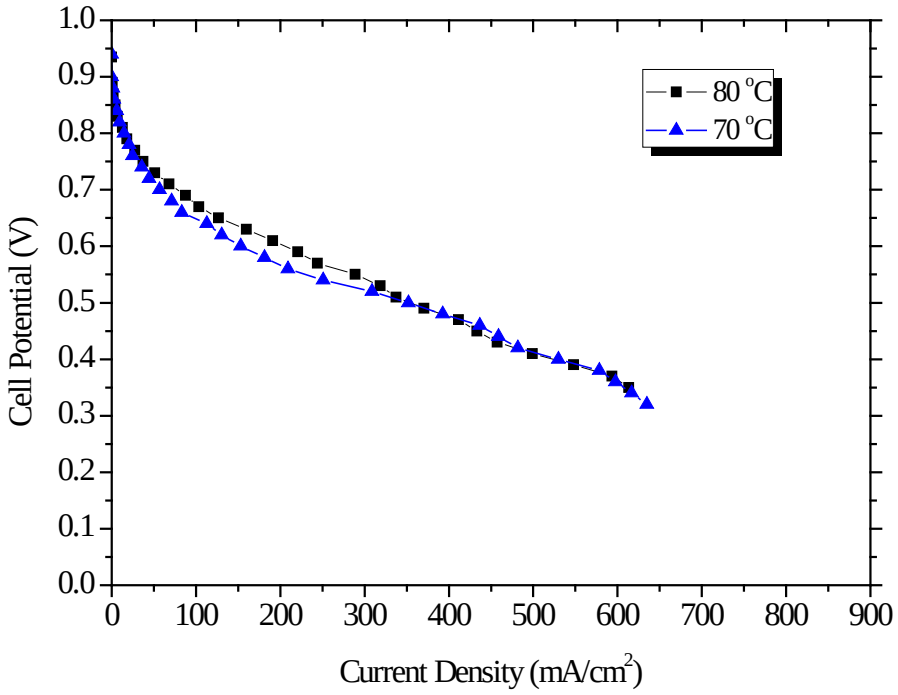

Figure 4.11 Polarization curves for different fuel cell temperatures. The H_2 and air are fully saturated

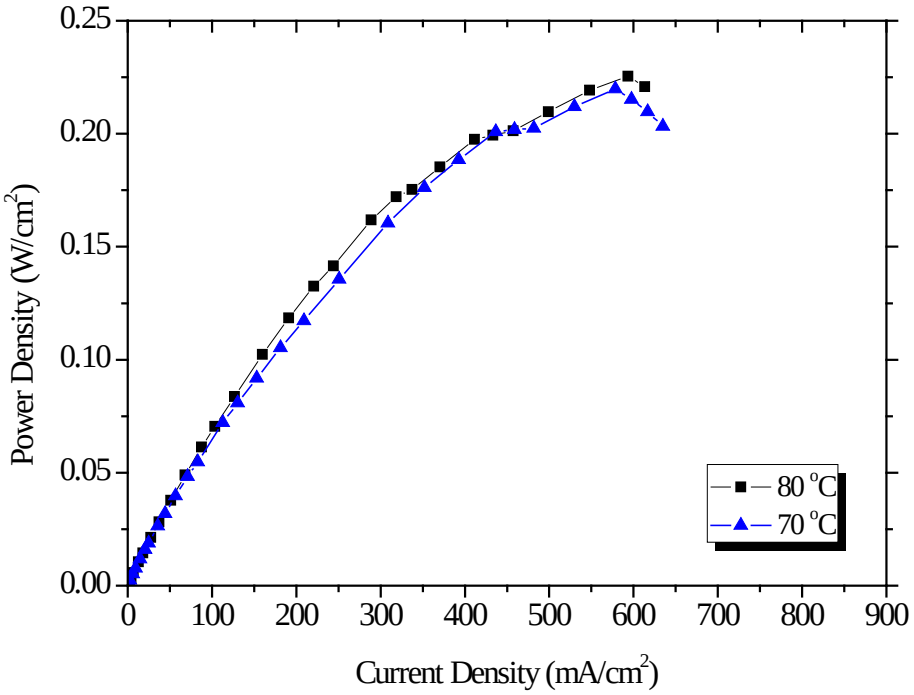

Figure 4.12 Polarization curves for different fuel cell temperatures. The H_2 and air humidification temperatures are equal to the fuel cell temperature

In this set of experiments, by keeping the reactants fully saturated the effect of fuel cell temperature on the cell performance is tried to observe.

Figure 4.11 shows that increasing fuel cell temperature improves PEM fuel cell performance. The slope of the linear portion of the curve decreases as fuel cell temperature increases. The limiting current density increases with the increase of the fuel cell temperature as well, due to the improvement of mass transport. It can be seen from the Figure 4.11 that, there is no significant difference between the polarization curves at 70 and 80 ºC. However, there are some differences at the ohmic region. In the high temperature the diffusivity increases and mass transport resistance decreases. Also, the increase in ohmic-ion conductivity of Nafion membrane occurs in elevated temperature (Amirinejad et al., 2006).

4.1.5 Water balance

Table 4.4 summarizes the current obtained at 0.4 V for all experiments. The water flow rate entering and leaving the fuel cell are estimated by the following procedure and the results are tabulated in Table 4.4 at these conditions. Sample calculations for the mass balance are given in Appendix C.

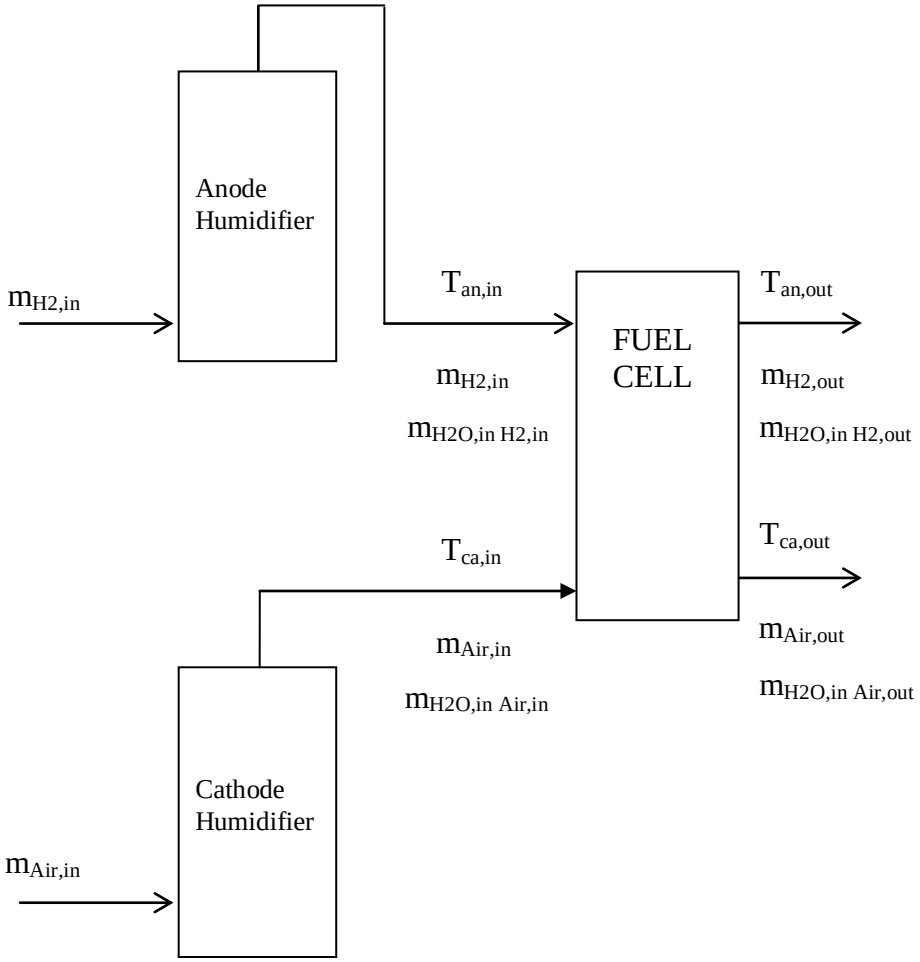

Assumptions:

1) The inlet gases are humidified to the assigned relative humidity in the humidifiers.
2) Humidifiers are operated at dew point temperature.
3) Gases leaving the humidifiers are in thermal equilibrium with the liquid at dew point temperature.
4) Gases are saturated with water vapor at humidifier temperature.
5) Gas inlet temperatures are equal to humidifier outlet temperatures. (Gas lines are heated to eliminate any condensation of vapor).
6) Gases outlet temperatures are equal to fuel cell operating temperature.
7) Both anode and cathode inlet and outlet pressures are taken as 1 atm.
8) Pressure drop between humidifiers and fuel cell connections are negligible.

9) Water transfer from anode to cathode by electro osmotic drag is considered as each proton accompanied by 1 water molecule.
10) Net electro osmotic drag coefficient is assumed as 0.93.

Reactant flow rates are calculated by Faraday's Law:

Water vapor in hydrogen inlet to the fuel cell in $gmin^{-1}$

$$m_{H_2O,in\ H_2,in} = S_{H_2} \frac{M_{H_2O}}{2F} \frac{\varphi_{an} P_{vs}(T_{an,in})}{P_{an} - \varphi_{an} P_{vs}(T_{an,in})} I * n_{cell} * 60$$

n_{cell} = 1 (single cell PEM fuel cell). It will be taken as 1 for the following calculations

Water vapor in air inlet to the fuel cell in $gmin^{-1}$

$$m_{H_2O,in\ Air,in} = \frac{S_{O_2}}{r_{O_2}} \frac{M_{H_2O}}{4F} \frac{\varphi_{ca} P_{vs}(T_{ca,in})}{P_{ca} - \varphi_{ca} P_{vs}(T_{ca,in})} I * n_{cell} * 60$$

Water content in hydrogen exhaust in $gmin^{-1}$

$$m_{H_2O,in\ H_2,out} = m_{H_2O,in\ H_2,in} - m_{H_2O,ED} + m_{H_2O,BD}$$

Electro osmotic drag was calculated as:

$$m_{H_2O,ED} = \xi \frac{M_{H_2O}}{F} I * n_{cell}$$

Where ξ = 1 (each proton is accompanied by 1 water molecule) (Barbir, 2005)

Yan et al. (2006) obtained the net electro osmotic drag coefficient ranged from − 0.02 to 0.93, and was dependent on the operating conditions, the current load and the level of humidification.

It is assumed that the net drag coeffcient is 0.93. Then
Net electro osmotic drag = Electro osmotic drag coefficient (EOD) – back diffusion coefficient (BD)

NDC = ξ- β

$$0.93 = 1 - \beta \quad \Rightarrow \quad \beta = 0.07$$

$$m_{H_2O,BD} = \beta m_{H_2O,ED} = \beta\xi \frac{M_{H_2O}}{F} I * n_{cell}$$

Water vapor at anode exhaust calculated as:

$$m_{H_2O,inH_2,out\,V} = \min\left[(S_{O2} - 1)\frac{M_{H_2O}}{2F}\frac{P_{vs}(T_{out,an})}{P_{an} - \Delta P_{an} - P_{vs}(T_{out,an})} I * n_{cell}\,,\; m_{H_2O,in\,H_2,out}\right]$$

Liquid water at anode exhaust calculated as:

$$m_{H_2O,inH_2,out\,L} = m_{H_2O,inH_2,out} - m_{H_2O,in\,H_2,out\,V}$$

Water content in the cathode exhaust in gmin^{-1}

$$m_{H_2O,in\,Air,out} = m_{H_2O,in\,Air,in} + m_{H_2O,qen} + m_{H_2O,ED} - m_{H_2O,BD}$$

$$m_{H_2O,in\,Air,out\,V} = \min\left[\frac{S_{O_2} - r_{O_2,in}}{r_{O_2,in}}\frac{M_{H_2O}}{4F}\frac{P_{vs}(T_{out,ca})}{P_{ca} - \Delta P_{ca} - P_{vs}(T_{out,ca})} I * n_{cell}\,, m_{H_2O,in\,Air,out}\right]$$

$$m_{H_2O,in\,Air,out\,L} = m_{H_2O,in\,Air,out} - m_{H_2O,in\,Air,out\,V}$$

It is seen from Table 4.4 that decreasing hydrogen relative humidity from 100 to 50, the amount of water obtained at the cathode exhaust decreases about 40 % at 70 ^{o}C cell temperature for both in liquid and vapor phases. At 80 ^{o}C cell temperature decreasing the RH of hydrogen from 100 to 50 %, decreases the cathode exhaust water content 40 % for both liquid and vapor phases.

Yan et al. (2006) obtained the net electro osmotic drag coefficinet ranged from -0.02 to 0.93. It is seen that at 60 ^{o}C cell temperature the anode exhaust water was obtained as vapor. However there is no liquid water formation at the anode exhaust. At cathode side the higher amount of cathode exhaust was obtained as liquid water. For 70 ^{o}C cell temperature, the anode exhaust was also obtained as vapor and no liquid water is observed. Higher amount of cathode exhaust was obtained as vapor except for the relative humidity of 100 % for both air and hydrogen. At 80 ^{o}C, the similar anode exhaust behavior was obtained. Vapor was obtained at the anode exhaust and there is no liquid water. However, up to 70 % RH air with a costant 100 % RH hydrogen, there is no liquid water at the cathode exhaust, all the water was obtained as vapor. At 70 and 100 RH air, the higher amount of water was obtained as vapor but both the liquid and vapor phase was observed.

Table 4.4 Inlet and outlet water flow rates

TC	Cell T (ºC)*	RH of air (%)*	RH of H_2 (%)*	I (A)* (0.4V)	Mass flow rate of water at H_2 inlet (g/min)**	Mass flow rate of water at air inlet (g/min)**	Mass flow rate of water vapor at H_2 outlet (g/min)**	Mass flow rate of liquid water at H_2 outlet (g/min)**	Mass flow rate of water vapor at air outlet (g/min)**	Mass flow rate of liquid water at air outlet (g/min)**
1	60	30	100	14.5	0.024	0.007	0.004	0.000	0.085	0.154
2	60	50	100	16.25	0.027	0.022	0.004	0.000	0.095	0.187
3	70	20	100	9	0.027	0.003	0.004	0.000	0.096	0.052
4	70	30	100	10.25	0.031	0.008	0.005	0.000	0.109	0.063
5	70	50	100	13.5	0.040	0.030	0.007	0.000	0.143	0.103
6	70	70	100	13.5	0.040	0.064	0.007	0.000	0.143	0.137
7	70	100	100	13.5	0.040	0.160	0.007	0.000	0.143	0.233
8	70	70	50	8.5	0.005	0.040	0.004	0.000	0.090	0.086
9	80	20	100	5.75	0.034	0.003	0.006	0.000	0.095	0.000
10	80	30	100	5.75	0.034	0.007	0.006	0.000	0.099	0.000
11	80	50	100	8	0.047	0.028	0.008	0.000	0.156	0.000
12	80	70	100	10	0.059	0.079	0.010	0.000	0.210	0.029
13	80	100	100	13.25	0.078	0.311	0.013	0.000	0.278	0.245
14	80	100	50	8.25	0.007	0.193	0.008	0.000	0.173	0.152

*Experimental

**Calculated

By using the net water transport coefficient, in general, the net water transport is described. Commonly, gas pressure, gas stoichiometry, feed gas humidity, current density, gas stoichiometry, There is probability that the factors like flow field pattern of the fuel cell membrane materials, and water content of the membrane influence the net water transport coefficient. A gradient existing in water activity across the Nafion membrane is the result of the production of water at the air. The diffusion of water from the air to the H_2 will be the effect of this gradient (Yan et al., 2006).

Principally, by using the net water transport coefficient, the net water transport is mainly described. Net electro-osmotic drag coefficient or the net drag coefficient (NDC) is generally used in order to make the process easier. The NDC is the net number of water molecules carried away by a single proton from the anode to the cathode. NDC ranged from -0.02 to 0.93 and depended on current density, feed gas humidification, and operating conditions (Yan et al., 2006). Fuel cell performance is affected mainly by relative humidity of both hydrogen and air gases. Membrane resistance increased as the feed gas relative humidity (RH) decreased.

Along with current density, the amount of water that is produced by ORR in air catalyst layer also rose linearly. As a result of the parallel increase of the water concentration gradient existing in the membrane near to the air side and current density, similarly, the back-diffused water from air to H_2 rose. This is the result of decline of the net electro-osmotic drag coefficient. Hydration and proton conductivity of membrane is settled by the equilibration between electro-osmotic drag and back diffusion (Yan et al., 2006).

4.2 Comparison of Performance Curve with Zero-D (Butler-Volmer) Model

Series of polarization curves with different fuel cell operation temperatures and relative humidity of reactants have been studied. From the polarization curves, the

values of kinetic parameters such as exchange current density, internal resistance and transfer coefficient have been calculated with the fit of the experimental data to a zero dimensional model of Butler Volmer. Model equation and modeling results are shown in Appendix B. Model parameters are shown in Table 4.4. Model was developed in MATLAB and the code for solving the equations are shown in Appendix B.

The Butler Volmer equation gives the fundamental relationship between the current and the applied voltage. The equation is as:

$$E_{cell} = E_{r,T,P} - \frac{RT}{\propto F}\ln\left(\frac{i}{i_0}\right) - \frac{RT}{nF}\ln\left(\frac{i_L}{i_L - i}\right) - iR_i \quad (4.1)$$

Experimental data were fitted to Butler Volmer equation. Limiting current density values was obtained from the polarization curves. It is the current density that a fuel cell cannot produce more current than it. As an example, at 70 °C cell temperature 100 % RH of air with 100 % RH of H_2 and 70 % RH of air with 50 % RH of H_2 was shown in Figure 4.13 and 4.14, respectively. The other modeling results are shown in Appendix B. The kinetic parameters obtained from the modeling results are shown in Table 4.4.

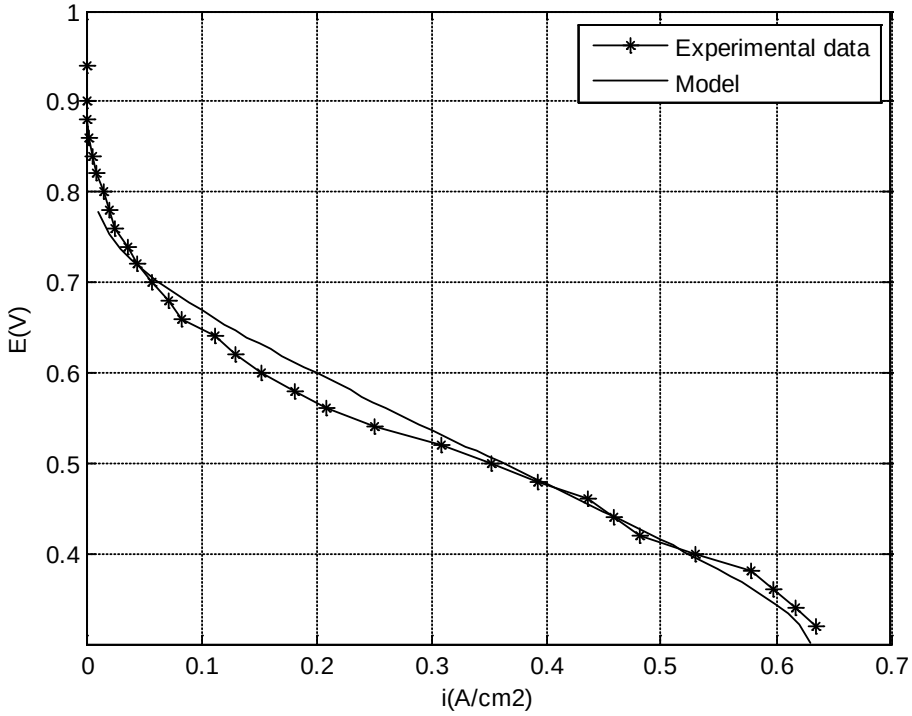

Figure 4.13 Comparison of the modeling results with the experimental data for polarization curve at 70 °C, 100 % RH air, 100 % RH H_2

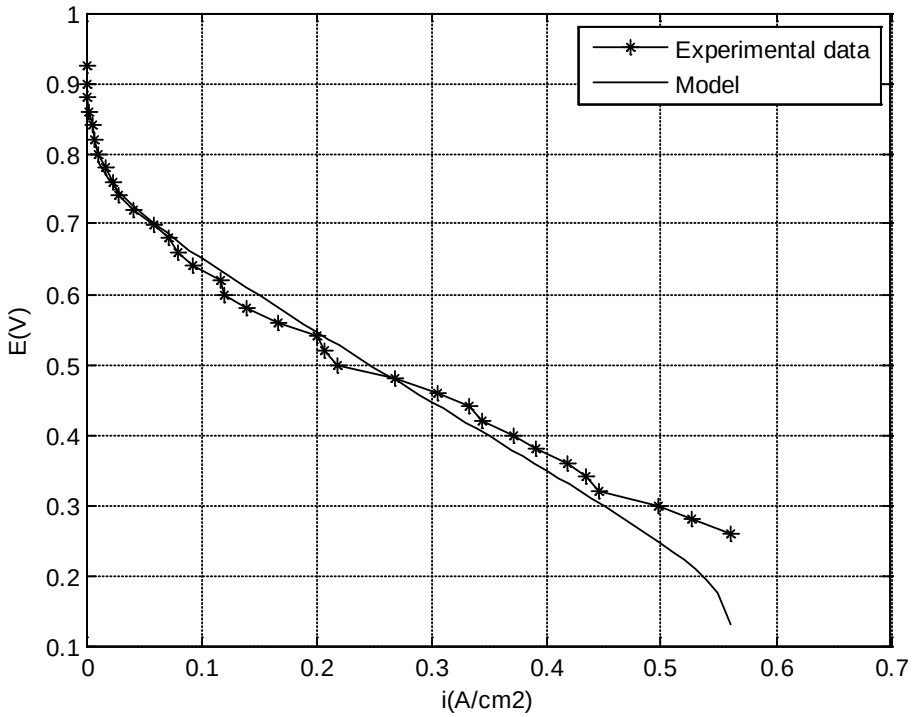

Figure 4.14 Comparison of the modeling results with the experimental data for polarization curve at 70 °C, 70 % RH air, 50 % RH H_2

The model includes electrochemical reaction in the catalyst layers and formulation for electrical resistance in the membrane, electrodes, and bipolar plates, and employs engineering correlation for the reactant gas transport in the flow channels and through the electrodes. It is shown that the present model predictions are in reasonable agreement with known experimental observations, indicating that the present model can be employed for fuel cell stack and system modeling. The eject of various operating and design parameters on the cell performance has been investigated. It is found that mass transport limitations are the largest cause of performance loss in the fuel cell when graphite is used as the material for bipolar plates and electrodes. If conducting polymers are substituted as construction materials, cell performance is expected to super considerably at high current densities due to their reduced electrical conductivity.

It is seen from the Figure 4.13, an example of data fitting at 60 ^{o}C and 30 % RH air and 100 % RH H_2 conditions, experimental data was well fitted to model.

Transfer coefficient, exchange current density and limiting current density values were found from the modeling results.

Transfer coefficient represented as α. In theory, it varies between 0 and 1, depending on the symmetry of the transition state in the electrochemical reaction. Experimentally, it has been determined to be about 0.5 (Hoogers, 2003).

Concentration of reactants and products do not change in a chemical reaction at equilibrium. It means that forward and backward reaction rates are equal to each other. At equilibrium, the current density of forward and backward reaction are equal to each other. This is called the **exchange current density**. It is a kinetic parameter that depends on the reaction and on the electrode surface. Exchange current density is defined as a rate of redox reactions at equilibrium. Exchange current density is mainly affected by electrode catalyst loading, active catalyst surface area, distribution of catalyst particles and thickness of the catalyst layer (Barbir, 2005).

In the manner of operation variables, fuel cell temperature effect the exchange current density (Santarelli et al, 2006).

It's magnitude ease the electrochemical reaction on the electrode surface. A small exchange current means that a high over potential is required to achieve a high current flow, while a large exchange current density indicates that only a small over potential is needed to produce a large current flow.

The exchange current density can be used as a comparison between different catalysts: the smaller the activation energy, the larger the exchange current density and the better the catalyst (Hoogers, 2003).

In a PEM fuel cell, typical exchange current density values are: $i_{0,a} = 0.2$ A cm^{-2} and $i_{0,c} = 1 \times 10^{-4}$ A cm^{-2} (Larminie and Dicks, 2000). You and Liu (2001) found a unique value is considered: $i_0 = 4.84 \times 10^{-8}$ A cm^{-2}.

Bevers et al. (1997), found the considered exchange current density value is: $i_0 = 1 \times 10^{-6}$ A cm^{-2}. Finally, Parthasarathy et al. (1992) found the exchange current value in the range from $i_{0,c} = 6 \times 10^{-5}$ A cm^{-2} at T = 30 °C to $i_{0,c} = 2.6 \times 10^{-4}$ A cm^{-2} at T = 70 °C.

However, limiting current density is not particularly discussed in the literature. Lee et al. (1998), a typical value for a PEM is reported: $i_L = 0.9$ A cm^{-2}. Amphlett et al. (1995) described an analytical expression, where the limiting current is function of the diffusion coefficient of the reactant in the electrode, of the electrode thickness and of the reactant concentration above the diffusion in the electrode. Pisani et al. (2002) found $i_L = 0.810$ A cm^{-2} in case of Nafion 115 fed by H_2/air, operating at atmospheric pressure, at 70 ^{o}C.

Table 4.5 Model parameters

Cell Temperature (^oC)	Relative Humidity of H_2 (%)	Relative Humidity of air (%)	Transfer coefficient (α)	Exchange Current Density (i_o) (A/cm^2)	Limiting Current Density (i_L) (A/cm^2)	Internal Resistance (Ri) (Ω-cm^2)
60	100	30	0.778	$8.834x10^{-7}$	0.720	0.495
60	100	50	1.254	$1.975x10^{-9}$	0.790	0.538
70	100	20	1.310	$2.068x10^{-9}$	0.374	0.957
70	100	30	1.372	$1.434x10^{-9}$	0.443	0.866
70	100	50	1.327	$1.545x10^{-9}$	0.602	0.704
70	100	70	0.770	$4.927x10^{-7}$	0.723	0.461
70	100	100	1.075	$2.566x10^{-9}$	0.636	0.475
70	50	70	1.155	$1.458x10^{-9}$	0.561	0.839
80	100	20	0.409	$1.152x10^{-4}$	0.334	0.986
80	100	30	0.364	$2.114x10^{-4}$	0.391	0.800
80	100	50	0.495	$3.332x10^{-5}$	0.480	0.687
80	100	70	0.605	$8.169x10^{-6}$	0.503	0.560
80	100	100	0.778	$5.423x10^{-7}$	0.614	0.443
80	50	100	0.726	$5.129x10^{-7}$	0.606	0.667

It is seen from Table 4.4 that higher exchange current density was obtained at 30 % RH of air than 50 % RH with a constant 100 % RH of H_2 at 60 ° cell temperature At 70 ^oC cell temperature, the highest exchange current density was obtained at 70 % RH of air and the lowest was obtained at 30 % RH of air with constant 100 % RH of H_2. On the other hand, with constant 70 % RH of air, 100 % RH of H_2 gives the higher exchange current density than that of 50 % RH of H_2. At 80 ^oC cell temperature, the highest exchange current density was obtained at 30 % RH of air and the lowest was obtained at 100 % RH of air with constant 100 % RH of H_2. Besides, with constant 100 % RH of air, 100 % RH of H_2 gives the higher exchange current density than that of 50 % RH of H_2. It is seen that relative humidity of reactant gases have a significant effect on exchange current density.

It is seen from Figure 4.15 that higher internal resistance was obtained at 50 % RH of air than 30 % RH with a constant 100 % RH of H_2 at 60 ° cell temperature At 70 ^oC cell temperature, the lowest internal resistance was obtained at 70 % RH of air and the highest internal resistance was obtained at 20 % RH of air with constant 100 % RH of H_2. On the other hand, with constant 70 % RH of air, 50 % RH of H_2 gives the higher internal resistance than that of 100 % RH of H_2. At 80 ^oC cell temperature, the lowest internal resistance was obtained at 100 % RH of air and the highest internal resistance was obtained at 20 % RH of air with constant 100 % RH of H_2. Besides, with constant 100 % RH of air, 50 % RH of H_2 gives the higher internal resistance than that of 100 % RH of H_2. It is seen that relative humidity of reactant gases have a significant effect on internal resistance. Increasing relative humidity of reactant gases improves the fuel cell performance as decreasing internal resistances.

Internal resistance is associated with ohmic losses. Ohmic losses vary directly with current, increasing over the entire range of current density. These are due to the resistance to the flow of protons in the electrolyte membrane and resistance to flow of electrons through the stack materials, electrode materials, electrode backing, interconnects current collector plates and constant resistance between

various interfaces. This may be the because of non-properly hydration, it exhibits higher ionic resistance. At the same time excess water must be removed to prevent flooding. This also causes internal resistance in the fuel cell.

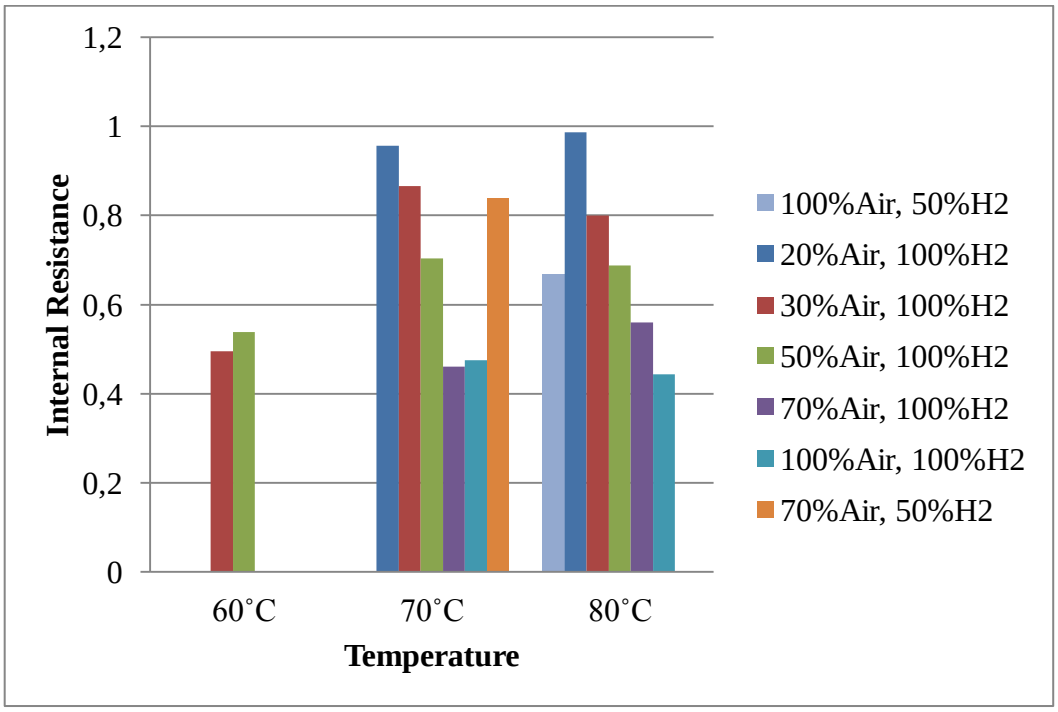

Figure 4.15 Internal resistances at different cell temperatures and relative humidity of reactants

It is seen from Figure 4.16 that higher transfer coefficient was obtained at 50 % RH of air than 30 % RH with a constant 100 % RH of H_2 at 60 ° cell temperature At 70 ^oC cell temperature, the highest transfer coefficient was obtained at 30 % RH of air and the lowest transfer coefficient was obtained at 70 % RH of air with constant 100 % RH of H_2. On the other hand, with constant 70 % RH of air, 50 % RH of H_2 gives the higher transfer coefficient than that of 100 % RH of H_2. At 80 ^oC cell temperature, the highest transfer coefficient was obtained at 100 % RH of air and the lowest transfer coefficient was obtained at 30 % RH of air with constant 100 % RH of H_2. Besides, with constant 100 % RH of air, 100 % RH of H_2 gives the higher transfer coefficient than that of 50 % RH of H_2. It is seen that as a general trend increasing the relative humidity of reactant gases increase the transfer coefficient.

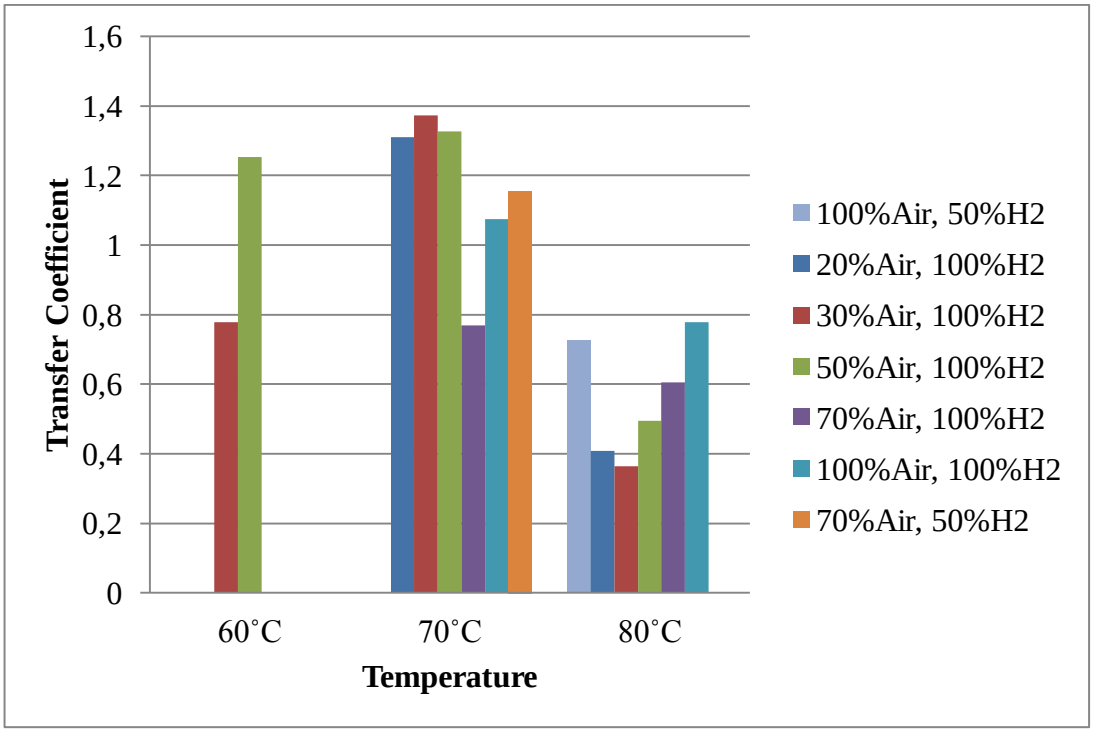

Figure 4.16 Transfer coefficients at different cell temperatures and relative humidity

It is seen from Figure 4.17 that higher limiting current density was observed at 50 % RH of air than 30 % RH with a constant 100 % RH of H_2 at 60 ° cell temperature At 70 ^oC cell temperature, the highest limiting current density was obtained at 70 % RH of air and the lowest limiting current density was obtained at 20 % RH of air with constant 100 % RH of H_2. On the other hand, with constant 70 % RH of air, 100 % RH of H_2 gives the higher limiting current density than that of 50 % RH of H_2. At 80 ^oC cell temperature, the highest limiting current density was obtained at 100 % RH of air and the lowest limiting current density was obtained at 20 % RH of air with constant 100 % RH of H_2. Besides, with constant 100 % RH of air, 100 % RH of H_2 gives the higher limiting current density than that of 50 % RH of H_2. It is seen that as a general trend increasing the relative humidity of reactant gases increase the limiting current density.

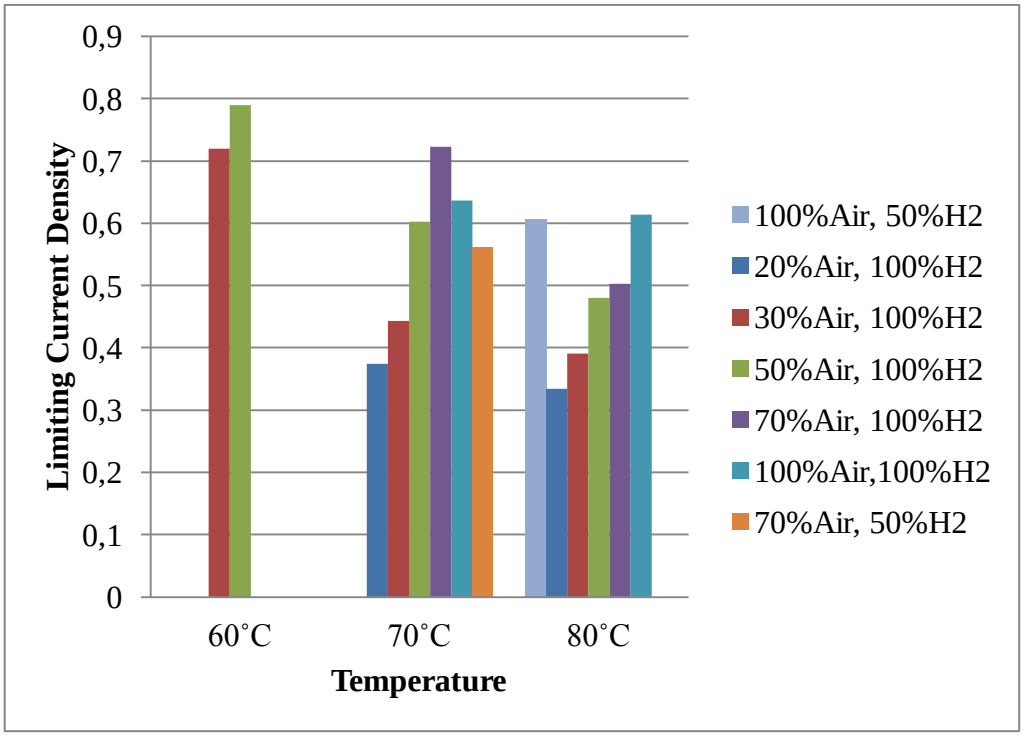

Figure 4.17 Limiting current density at different cell temperatures and relative humidity

When the membrane is well hydrated, increasing the operation temperature improves the performance of the fuel cell stack, due to the increase of the exchange current density, which reduces the activation losses, and to the increase in the gas diffusivity and membrane conductivity at higher temperatures. The hydration of the membrane is better at low temperatures than at high temperatures, but the kinetics was slower at low operation temperatures than at high temperatures. The trade-off between water retention and kinetics may be responsible for the similar performances in the low current range. At higher current, the positive impact of accelerated reaction kinetics at high temperatures on the performance may overwhelm the negative impact of less hydration of membrane, resulting in higher performance. . This could be because at this high operation temperature, the membrane material in the catalyst layer may not be fully hydrated. The water is more easily vaporizes at high temperatures. This could cause a decrease in the membrane conductivity and in the active surface area of the catalyst, and then, a decrease of the fuel cell stack performance (Perez, 2011). The increase of the operation temperature would cause an increase of the

exchange current density, because a higher temperature value allows an improvement of the reaction activation (Santarelli et al, 2006)

CHAPTER 5

CONCLUSION AND RECOMMENDATIONS

The aim of this study was to observe the effect of different operating temperature and relative humidity of reactant gases on the performance of PEM fuel cell. Experiments have been carried out at 60, 70 and 80 °C cell temperature and relative humidity of air was changed from 20 to100 % RH and relative humidity of 50 % and 100 % of hydrogen were tested. The experimental results are presented in the form of polarization curves. These curves data have been fit to a zero dimensional model, and the effect of the fuel cell operation temperature and relative humidity of reactant gases on the kinetic parameters and the cell resistance have been detected.

It was concluded that increasing the relative humidity of both hydrogen and air have a significant effect on fuel cell performance. Increasing the relative humidity of air improves the fuel cell performance for 60 ^{o}C, 70 ^{o}C and 80 ^{o}C cell temperatures. Also, higher relative humidity of hydrogen increases the fuel cell performance.

From the modeling results, increasing the relative humidity of reactants decreases the internal resistance in the fuel cell. However, increasing the relative humidity increases the transfer coefficient and limiting current density.

It is seen that relative humidity of reactant gases have a significant effect on internal resistance. Increasing relative humidity of reactant gases improves the fuel cell performance as decreasing internal resistances.

It is seen that fuel cell performance is highest at 60 ^{o}C fuel cell temperature but it was only tested for two different relative humidity of air condition. So, this temperature can be more test in order to observe the relative humidity of reactants on the fuel cell performance at this temperature.

REFERENCES

Amirinejad, M., Rowshanzamir, S., Eikani, M. H., *Effects of operating parameters on performance of a proton exchange membrane fuel cell*, J Power Sources, 161: 872–875, (2006).

Amphlett, J. C., Baumert, R. M., Mann, R. F., Peppley, B. A., Roberge, P. R., *Performance modelling of the Ballard Mark IV solid polymer electrolyte fuel cell*, J. Electrochem. Soc., 142:1–15, (1995).

Andreaus, B., Scherer, G. G., *Proton-conducting polymer membranes in fuel cells – humidification aspects***,** Solid State Ionics, 168 (3–4): 311–320, (2004).

Barbir, F., *PEM Fuel Cells: Theory and Practice*, Elsevier Academic Press:USA, (2005).

Bayrakçeken, A., Türker, L., Eroğlu, İ., *Improvement of carbon dioxide tolerance of PEMFC electrocatalyst by using microwave irradiation technique*, Int. J. Hydrogen Energy, 33:7527:7537, (2008a).

Bayrakçeken, A., Erkan, S., Türker, L., Eroğlu, İ., Effects of membrane electrode assembly components on proton exchange membrane fuel cell performance, Int. J. Hydrogen Energy, 33:165:170, (2008b).

Bernardi, D. M., Verbrugge, M. W., *Mathematical model of a gas diffusion electrode bonded to a polymer electrolyte*, AIChE J., 37 (8): 1151–1163, (1992).

Bevers, D., Wohr, M., Yasuda, K., Oguro, K., *Simulation of a polymer electrolyte fuel cell electrode*, J. Appl. Electrochem., 27: 1254–1264, (1997).

Cai, Y. H., Hu, J., Ma, H. P., Yi, B. L., Zhang, H. M., *Effect of water transport properties on a PEM fuel cell operating with dry hydrogen*, Electrochim Acta, 51 (28): 6361–6366, (2006).

Ceraolo, M., Miulli, C., Pozio, A., *Modelling static and dynamic behaviour of proton exchange membrane fuel cells on the basis of electro-chemical description*, J. Power Sources, 113 (1): 131-144, (2003)

Choi, K. H., Peck, D. H., Kim, C. S., Shin, D. R., Lee, T. H., *Water transport in polymer membranes for PEMFC***,** J Power Sources, 86 (1–2): 197–201, (2000).

Colinart, T., Chenu, A., Didierjean, S., Lottin, O., Besse, S., *Experimental study on water transport coefficient in Proton Exchange Membrane Fuel Cell*, Journal of Power Sources, 190 (2): 230–240, (2009).

Dai, W., Haijiang, W., Xiao-Zi, Y., Jonathan, J. M., Daijun, Y., Jinli, Q., Jianxin, M., *A review on water balance in the membrane electrode assembly of proton exchange membrane fuel cells*, Int. J. Hydrogen Energy, 34: 9461-9478, (2009).

Devrim, Y., Erkan, S., Baç, N., Eroğlu, İ., *Improvement of PEMFC performance with Nafion/inorganic nanocomposite membrane electrode assembly prepared by ultrasonic coatng technique*, xxx: I-II, (2012).

Feng, S. G., Xie, X. F., Shang, Y. M., Jin, H., Xu, J. M., Zhou, Q. F., *Membranes from sulfonated block copolymer for use in proton exchange membrane fuel cells*, Prog Chem, 20 (1): 117–25, (2008).

Fıçıcılar B., Eroğlu İ., Nguyen T.V., *A Five Layer One-Dimensional PEMFC Model with Detailed Electrode Kinetics*, ECS Transactions, 33(1): 1515-1527, (2010).

Fuller, T. F., Newman, J., *Experimental Determination of the Transport Number of Water in Nafion 117 Membrane,* J. Electrochem. Soc., 139 (5): 1332–1337, (1992).

Fuller, T. F., Newman, J., *Water and thermal management in solid–polymer–electrolyte fuel cells*, J. Electrochem. Soc., 140: 1218–1225, (1993).

Ge, S. H., Yi, B. L., Ming, P. W., *Experimental determination of electro-osmotic drag coefficient in Nafion membrane for fuel cells*, J Electrochem Soc., 153 (8): 1443–50, (2006).

Güvenatam, B., Fıçıcılar, B., Bayraçeken, A., Eroğlu, İ., *Hollow core mesoporous shell carbon supported Pt electroctalysts wit high Pt loading for PEMFCs*, Int. J. Hydrogen Energy, 37: 1865-1874, (2012).

Haraldsson, K.,Wipke, K., Evaluating PEM fuel cell system models, J Power Sources, 126 (1-2): 88-97, (2004).

Himanen, O., Hottinen, T., Mikkola, M., Saarinen, V., *Characterization of membrane electrode assembly with hydrogen–hydrogen cell and ac-impedance spectroscopy – Part I,* Experimental Electrochim Acta, 52 (1): 206–214,(2006).

Hirano, S., Kim, J., Srinivasan, S., *High performance proton exchange membrane fuel cells with sputter-deposited Pt layer electrodes*, Electrochim Acta, 42: 1587-93, (1997).

Hoogers, G., *Fuel Cell Technoogy Handbook*, CRC Press, Boca Raton, FL, (2003).

Husar, A., Higier, A., Liu, H., *In situ measurements of water transfer due to different mechanisms in a proton exchange membrane fuel cell*, J Power Sources, 183 (1): 240–6, (2008).

Ise, M., Kreuer, K. D., Maier, J., *Electroosmotic drag in polymer electrolyte membranes: an electrophoretic NMR study Solid State Ionics*, 125 (1–4): 213–223, (1999).

Janssen, G. J. M, Overvelde, M. L. J., *Water transport in the proton-exchange-membrane fuel cell: measurements of the effective drag coefficient*, J Power Sources, 101 (1): 117–25, (2001).

Ji, M., Dai, Z., *A Review of Water Management in Polymer Electrolyte Membrane Fuel Cells*, Energies, 2 (4): 1057-1106, (2009).

Kreuer, K. D., *Proton conductivity: materials and applications,* Chem Mater, 8 (3): 610–41, (1996).

Larminie, J., Dicks, A., *Fuel Cell Systems Explained*, John Wiley & Sons Ltd., Chichester, GB, 2003.

Lee, J. M., Ito, T., Yamaguchi, T., *Development and modification of a PEMFC electrode by using a hydrocarbon lonomer for high utilization of catalyst*, J Chem Eng Jpn, 40 (9): 773–9, (2007).

Lee, J. H., Lalk, T. R., Appleby A. J., *Modeling electrochemical performance in large scale proton exchange membrane fuel cell stacks*, J. Power Sources, 70: 258–268, (1998).

Liu, F. Q., Lu, Wang, C. Y., *Water transport coefficient distribution through the membrane in a polymer electrolyte fuel cell***,** J Membr Sci, 287 (1): 126–131, (2007).

Lu, G. Q., Liu, F. Q., Wang, C. Y., *An approach to measuring spatially resolved water crossover coefficient in a polymer electrolyte fuel cell***,** J Power Sources, 164 (1): 134–140, (2007).

Maranzana, G., Lottin, O., Colinart, T., Chupin, S., Didierjean, S., J. Power Sources, *A multi-instrumented polymer exchange membrane fuel cell: Observation of the in-plane non-homogeneities*, 180 (2): 748–754, (2008).

Mauritz, K. A., Moore, R. B., *State of understanding of nafion*, Chem Rev., 104 (10): 4535–86, (2004).

Miyatake, K., Watanabe, M., *Recent progress in proton conducting membranes for PEFCs. Electrochemistry,* 73 (1): 12–9, (2005).

Morris, D. R., Sun, X., *Water-sorption and transport properties of Nafion 117 H, J Appl Polym Sci,* 50 (8): 1445–1452, (1993).

Motupally, S., Becker, A. J., Daidner JW., *Diffusion of water in Nafion 115 membranes*. J Electrochem Soc., 147 (9): 3171–3177, (2000).

Murahashi, T., Naiki, M., Nishiyama, E., *Water transport in the proton exchange-membrane fuel cell: comparison of model computation and measurements of effective drag***,** J Power Sources, 162 (2): 1130–1136, (2006).

Nakamoto, H., Watanabe, M., *Bronsted acid–base ionic liquids for fuel cell electrolytes*, Chem Commun., 24: 2539–41, (2007).
Nazarov, I., Promislow, K., *The impact of membrane constraint on PEM fuel cell water management*, J Electrochem Soc., 154 (7): 623–30, (2007).

Newman, J. S., *Electrochemical Systems*, Second ed.,Prentice Hall, Englewood Cliffs, NJ, (1991).

Nguyen, T.V., White, R.E., *A water and heat management model for proton-exchange-membrane fuel-cells*, J Electrochem Soc, 140 (8): 2178–2186, (1993).

Pantea, D., Darmstadt, H., Kaliaguine, S., Summchen, ., Roy, C., Electrical conductivity of thermal carbon blacks:Influence of surface chemistry, Carbon, 39: 1147-58, (2001).

Parthasarathy, A., Supramaniam, S., Appleby, A. J., Martin, C. R., *Temperature dependence of the electrode kinetics reduction at the platinum/Nafion interface—a microelectrode investigation*, J. Electrochem. Soc., 139: 2530–2537, (1992).

Pérez, P. M., Pérez-Herranz, V., *Effect of the Operation and Humidification Temperatures on the Performance of a Pem Fuel Cell Stack on Dead-End Mode*, Int. J. Electrochem. Sci., 6 (1): 492 – 505, (2011).

Pisani, L., Murgia, G., Valentini, M., D'Aguanno, B., *A new semi-empirical approach to performance curves of polymer electrolyte fuel cells*, J. Power Sources, 108: 192–203, (2002).

Pivovar, B. S., *An overview of electro-osmosis in fuel cell polymer electrolytes*, Polymer, 47 (11): 4194–202, (2006).

Ren, X. M., Henderson, W., Gottesfeld, S., *Electro-osmotic drag of water in ionomeric membranes – new measurements employing a direct methanol fuel cell*, J Electrochem Soc, 144 (9): 267–270, (1997).

Rivin, D., Kendrick, C. E., Gibson, P. W., Schneider, N. S., *Solubility and transport behavior of water and alcohols in Nafion(TM)*, Polymer 42 (2): 623–35, (2001).

Rodatz, P., Büchi, F., Onder, C., Guzzella, L., *Operational aspects of a large PEFC stack under practical conditions*, J. Power Sources, 128 (2): 208-217, (2004).

Rodríguez, M. B., Araceli Rosas Paleta, M. G., Antonio Rivera Marquez, J., Belén Tapia Pachuca, A., Roberto García de la Vega, J., *Effect of a Rigid Gas*

Diffusion Media Applied as Distributor of Reagents in a PEMFC in Operation, Part I: Dry Gases, Int. J. Electrochem. Sci., 4: 1754 – 1760, (2009).

Roelofs, M., *Membrane issues for PEM fuel cells*, NSF Workshop, Arlington, Virginia, November 14, 2001.

Saab, P., Garzan, F. H., Zawodzinski, T. A., *Determination of ionic and electronic resistivities in carbon/polylelectrolyte fuel cell composite electrodes,* J Electrochem Soc., 149: 1541-6, (2002).

Santarelli, M. G., Torchio, M. F., Cochis, P., *Parameters estimation of a PEM fuel cell polarization curve and analysis of their behavior with temperature*, Journal of Power Sources, 159: 824–835, (2006).

Sauriol, P., Kim, G., Bi, H. T., Stumper, J., St-Pierre, J., *Comparison between Pemfc Water Management Model and in-Situ Water Transfer Measurements,* AIChE Annual Meeting, 2005.

Schmidt-Rohr, K., Chen, Q., *Parallel cylindrical water nanochannels in Nafion fuel cell membranes.* Nat Mater,7(1): 75-83, (2008).

Springer, T. E., Zawodzinski, T. A., Gottesfeld, S., *Polymer electrolyte fuel-cell model***,** J Electrochem Soc, 138 (8): 2334–2342, (1991).

Squadrito, G., Maggio, G., Passalacqua, E., Lufrano, F., Patti, A., *An empirical equation for polymer electrolyte fuel cell (PEFC) behaviour*, J. Appl. Electrochem., 29: 1449–1455, (1999).

Takaichi, S., Uchida, H., Watanabe, M., *Response of specific resistance distribution in electrolyte membrane to load change at PEFC operation*, J Electrochem Soc., 154 (12): 1373–1377, (2007).

Verbrugge, M. W., Schneider, E. W., Conell, R. S., Hill, R. F., *The effect of temperature on the equilibrium and transport-properties of saturated poly(perfluorosulfonic acid) membranes*, J Electrochem Soc., 139 (12): 3421–8, (1992).

Wang, L., Husar, A., Zhou, T., Liu, H., *A parametric study of PEM fuel cell performances,* Int. J. Hydrogen Energy, 28: 1263–1272, (2003).

Weber, A. Z., Newman, J., *A theoretical study of membrane constraint in polymer–electrolyte fuel cells,* AlChE J., 50 (12): 3215–26, (2004).

Weng, F. B., Yan, W. M, Duan, Y. Y., Wang, X. D., *Effect of humidity of reactants on the cell performance of PEM fuel cells with parallel and interdigitated flow field designs*, Journal of Power Sources, 176 (1): 247-258, (2008).

Wohr, M., Holwin, K., Schurnberger, W., Fischer, M., Neubrnad, W., Eigenberger, G., *Dynamic modeling and simulation of a polymer membrane fuel cell including mass transport limitation*, Int. J. Hydrogen Energy, 23 (3): 213–218, (1998).

Yan, Q. G., Toghiani, H., Wu, J. X., *Investigation of water transport through membrane in a PEM fuel cell by water balance experiments*, J Power Sources, 158 (1): 316–325, (2006).

Yang, X. G., Burke, N., Wang, C. Y., Tajiri, K., Shinohara K., *Simultaneous measurements of species and current distributions in a PEFC under low-humidity operation*, J Electrochem Soc, 152 (4): 759–766, (2005).

Ye, X. H., Wang, C. Y., *Measurement of water transport properties through membrane electrode assemblies – Part II. Air diffusion media*, J Electrochem Soc., 154 (7): 683–6, (2007).

You, L., Liu, H., A *parametric study of the air catalyst layer of PEM fuel cells using a pseudo-homogeneous model*, Int. J. Hydrogen Energy, 26: 991–999, (2001).

Youssef E. M., Khairia E.AL-NAdi, Moataz H.Khalil, *Lumped Model for Proton Exchange Membrane Fuel Cell (PEMFC)*, Int. J. Electrochem. Sci., 5 (1): 267 – 277, (2010).

Yu, X., Zhou, B., Sobiesiak, A., *Water and Thermal Management for Ballard PEM Fuel Cell Stack*, J. Power Sources, 147 (1-2): 184-195, (2005).

Zawodzinski, T. A., Davey, J., Valerio, J., Gottesfeld, S., *The water-content dependence of electroosmotic drag in proton-conducting polymer electrolytes*, Electrochim Acta, 40 (3): 297–302, (1995).

Zawodzinski, T. A., Derouin, C., Radzinski, S., Sherman, R. J., Smith, V. T., Springer, S., Gottesfeld, T. E., *Water Uptake by and Transport Through Nation 117 Membranes*, J. Electrochem. Soc., 140 (4): 1041–1047, (1993).

Zhang, J., *Pem Fuel Cell Electrocatalyst and Catalyst Layers Fundementals and Applications*, Springer, Canada, 1-50, (2008).

APPENDIX A

EXPERIMENTAL DATA

Table A.1 Polarization curve data obtained at 60 °C

100 % RH H_2			
% RH Air			
30		50	
Voltage (V)	Current (A)	Voltage (V)	Current (A)
0.97	0.00	0.96	0.00
0.90	0.10	0.90	0.07
0.85	0.43	0.85	0.36
0.80	1.04	0.80	1.01
0.75	1.94	0.75	2.05
0.70	3.05	0.70	3.39
0.65	4.34	0.65	4.88
0.60	6.04	0.60	6.73
0.55	7.88	0.55	8.92
0.50	10.07	0.50	11.54
0.45	12.37	0.45	13.51
0.40	14.78	0.40	16.38
0.35	16.43	0.35	18.04

Table A.2 Polarization curve data obtained at 70 °C

100 % RH H_2										50 % RH H_2	
% RH Air										% RH Air	
20		30		50		70		100		70	
Voltage (V)	Current (A)	Voltage (V)	Current (A)	Voltage (V)	Current (A)	Voltage (V)	Current (A)	Voltage (V)	Current (A)	Voltage (V)	Current (A)
0.98	0	0.98	0	0.97	0	0.95	0	0.94	0	0.93	0
0.9	0.09	0.9	0.08	0.9	0.15	0.9	0.01	0.9	0	0.88	0.03
0.85	0.35	0.85	0.34	0.85	0.3	0.88	0.05	0.88	0.04	0.86	0.05
0.8	0.85	0.8	0.88	0.8	0.85	0.86	0.11	0.86	0.07	0.84	0.13
0.75	1.54	0.75	1.71	0.75	1.74	0.84	0.23	0.84	0.16	0.82	0.2
0.7	2.42	0.7	2.67	0.7	2.83	0.82	0.38	0.82	0.24	0.8	0.28
0.65	3.44	0.65	3.77	0.65	3.89	0.8	0.54	0.8	0.37	0.78	0.43
0.6	4.62	0.6	4.95	0.6	5.81	0.78	0.78	0.78	0.52	0.76	0.57
0.55	5.64	0.55	6.68	0.55	7.61	0.76	1.06	0.76	0.62	0.74	0.72
0.5	7.22	0.5	7.94	0.5	8.8	0.74	1.38	0.74	0.89	0.72	1.03
0.45	8.04	0.45	9.43	0.45	11.99	0.72	1.7	0.72	1.11	0.7	1.47
0.4	8.94	0.4	10.18	0.4	13.22	0.7	2.08	0.7	1.42	0.68	1.78
0.35	9.35	0.35	11.07	0.35	15.04	0.68	2.55	0.68	1.78	0.66	2
						0.66	3.05	0.66	2.08	0.64	2.31
						0.64	3.57	0.64	2.82	0.62	2.93
						0.62	4.05	0.62	3.26	0.6	3.01

Table A.2 (Cont'd) Polarization curve data obtained at 70 °C

100 % RH H_2										50 % RH H_2	
% RH Air										% RH Air	
20		30		50		70		100		70	
Voltage (V)	Current (A)	Voltage (V)	Current (A)	Voltage (V)	Current (A)	Voltage (V)	Current (A)	Voltage (V)	Current (A)	Voltage (V)	Current (A)
						0.6	4.58	0.6	3.83	0.58	3.5
						0.58	5.11	0.58	4.54	0.56	4.18
						0.56	5.85	0.56	5.23	0.54	5.02
						0.54	6.41	0.54	6.28	0.52	5.17
						0.52	6.88	0.52	7.72	0.5	5.46
						0.5	7.59	0.5	8.81	0.48	6.72
						0.48	8.75	0.48	9.82	0.46	7.66
						0.46	10.35	0.46	10.92	0.44	8.31
						0.44	11.34	0.44	11.47	0.42	8.62
						0.42	12.52	0.42	12.05	0.4	9.29
						0.4	13.38	0.4	13.25	0.38	9.76
						0.38	14.34	0.38	14.46	0.36	10.47
						0.36	15.44	0.36	14.94	0.34	10.86
						0.34	16.09	0.34	15.42	0.32	11.15
						0.32	16.71	0.32	15.88	0.3	12.42

Table A.3 Polarization curve data obtained at 80 ℃

100 % RH H_2										50 % RH H_2	
% RH Air										% RH Air	
20		30		50		70		100		100	
Voltage (V)	Current (A)	Voltage (V)	Current (A)	Voltage (V)	Current (A)	Voltage (V)	Current (A)	Voltage (V)	Current (A)	Voltage (V)	Current (A)
1	0	0.98	0	0.97	0	0.97	0	0.94	0	0.92	0
0.89	0.12	0.89	0.09	0.89	0.06	0.89	0.05	0.89	0.02	0.9	0.01
0.87	0.18	0.87	0.16	0.87	0.15	0.87	0.09	0.87	0.05	0.88	0.01
0.85	0.27	0.85	0.23	0.85	0.22	0.85	0.2	0.85	0.1	0.86	0.05
0.83	0.36	0.83	0.38	0.83	0.3	0.83	0.35	0.83	0.17	0.84	0.08
0.81	0.46	0.81	0.52	0.81	0.49	0.81	0.53	0.81	0.32	0.82	0.11
0.79	0.59	0.79	0.64	0.79	0.63	0.79	0.7	0.79	0.45	0.8	0.19
0.77	0.72	0.77	0.81	0.77	0.8	0.77	0.88	0.77	0.69	0.78	0.29
0.75	0.85	0.75	0.98	0.75	1	0.75	1.13	0.75	0.93	0.76	0.44
0.73	0.97	0.73	1.14	0.73	1.18	0.73	1.39	0.73	1.28	0.74	0.63
0.71	1.16	0.71	1.4	0.71	1.46	0.71	1.74	0.71	1.7	0.72	0.82
0.69	1.32	0.69	1.53	0.69	1.61	0.69	2.01	0.69	2.19	0.7	1.11
0.67	1.47	0.67	1.77	0.67	1.94	0.67	2.42	0.67	2.59	0.68	1.39
0.65	1.7	0.65	1.96	0.65	2.14	0.65	2.9	0.65	3.17	0.66	1.82
0.63	1.92	0.63	2.15	0.63	2.6	0.63	3.43	0.63	4	0.64	2.02
0.61	2.05	0.61	2.56	0.61	2.75	0.61	3.85	0.61	4.78	0.62	2.36
0.59	2.31	0.59	2.62	0.59	3.33	0.59	4.31	0.59	5.52	0.6	2.96
0.57	2.52	0.57	2.97	0.57	3.44	0.57	4.95	0.57	6.1	0.58	3.71
0.55	2.78	0.55	3.18	0.55	4.3	0.55	5.4	0.55	7.23	0.56	3.97

Table A.3 (Cont'd) Polarization curve data obtained at 80 °C

100 % RH H_2										50 % RH H_2	
% RH Air										% RH Air	
20		30		50		70		100		100	
Voltage (V)	Current (A)	Voltage (V)	Current (A)	Voltage (V)	Current (A)	Voltage (V)	Current (A)	Voltage (V)	Current (A)	Voltage (V)	Current (A)
0.53	3.13	0.53	3.62	0.53	4.7	0.53	6.15	0.53	7.97	0.54	4.32
0.51	3.51	0.51	3.93	0.51	5.02	0.51	6.74	0.51	8.43	0.52	4.93
0.49	4.07	0.49	4.13	0.49	5.62	0.49	7.26	0.49	9.27	0.5	5.53
0.47	4.51	0.47	4.35	0.47	6.09	0.47	8.17	0.47	10.29	0.48	5.74
0.45	4.99	0.45	4.78	0.45	6.65	0.45	8.67	0.45	10.84	0.46	5.91
0.43	5.18	0.43	5.04	0.43	7.07	0.43	9.12	0.43	11.44	0.44	6.68
0.41	5.52	0.41	5.65	0.41	7.78	0.41	9.8	0.41	12.48	0.42	7.86
0.39	5.83	0.39	6.12	0.39	8.12	0.39	10.48	0.39	13.7	0.4	8.24
0.37	6.16	0.37	6.13	0.37	8.88	0.37	11.1	0.37	14.84	0.38	8.98
0.35	6.46	0.35	7.07	0.35	9.27	0.35	11.72	0.35	15.34	0.36	9.52
0.33	6.78	0.33	7.18	0.33	9.81	0.33	12.23			0.34	10.49
0.31	6.95	0.31	7.9	0.31	10.47	0.31	12.44			0.32	10.75
0.29	7.17	0.29	8.9	0.29	10.71	0.29	12.57			0.3	11.13
0.27	7.41	0.27	9.36	0.27	11.06					0.28	12.62
0.25	7.86	0.25	9.44	0.25	11.57					0.26	13.21
0.23	8.35	0.23	9.54	0.23	11.69					0.24	13.98
		0.21	9.55	0.21	11.98					0.22	14.11

APPENDIX B

MODELING RESULTS

In order to fit experimental data to Butler Volmer equation, MATLAB code is as below and the model results are given in the figures from Figure B1 to B14.

```
x=[0.0001; 0.004; 0.01707; 0.04173; 0.0776; 0.12213; 0.1736; 0.24173; 0.3152;
0.40293; 0.4948; 0.59107; 0.6572];
y=[0.96967; 0.9; 0.85; 0.8; 0.75; 0.7; 0.65; 0.6; 0.55; 0.5; 0.45; 0.4; 0.35];


E0=1.2; % Volt
R=8.31434; % J/kmol.K
F=96485; % C/mol
% alfa=1.5;
% io=3*10^(-6); % A/cm2
% Res=0.15;  % ohm.cm2
% iL=1.6; % A/cm2
T= 333; % K
n=2; % electron
maxIL=0.6573;
mymodel = @(alpha, I0, IL, Ri, x)...
   E0-((R*T)./(alpha*F)).*log(x./I0)-((R*T)./(n*F)).*log(IL./(IL-x))-x.*Ri;

% cevap=fit(x,y,mymodel,'StartingPoint',[0.5,0.4,0.3,0.1],'Lower',
[0,0.0000000001,0.83,0], 'Robust', 'LAR')
% cevap=fit(x,y,mymodel,'Lower', [0,0.0000000001,0.83,0],'Upper', [Inf,1,1,Inf],
'Robust', 'LAR')
[cevap,gof]=fit(x,y,mymodel,'Startpoint', [0.7,5e-7,0.6574,1],'Lower',
[0,0.0000000001,x(length(x)),0],'Upper', [Inf,1,maxIL,Inf], 'Robust', 'LAR')
alpha=cevap.alpha;
I0=cevap.I0;
IL=cevap.IL;
Ri=cevap.Ri;

figure;
plot(x,y,'k*-');
```

```
hold on;
x=[0:0.01:maxIL];
plot(x,E0-((R*T)./(alpha*F)).*log(x./I0)-((R*T)./(n*F)).*log(IL./(IL-x))-x.*Ri,'k-
');
hold off;
xlabel('i(A/cm2)');
ylabel('E(V)');
title(['E vs. I when IL=' num2str(maxIL)])

grid on;
```

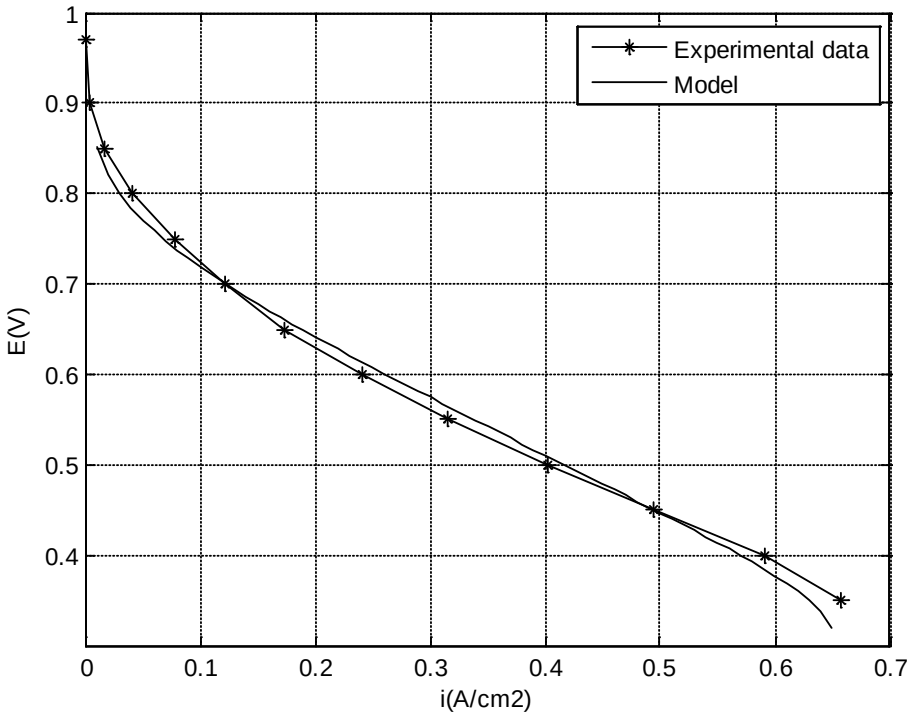

Figure B.1 Comparison of the model with the experimental polarization data obtained at 60 °C, 30 % RH air, 100 % RH H_2

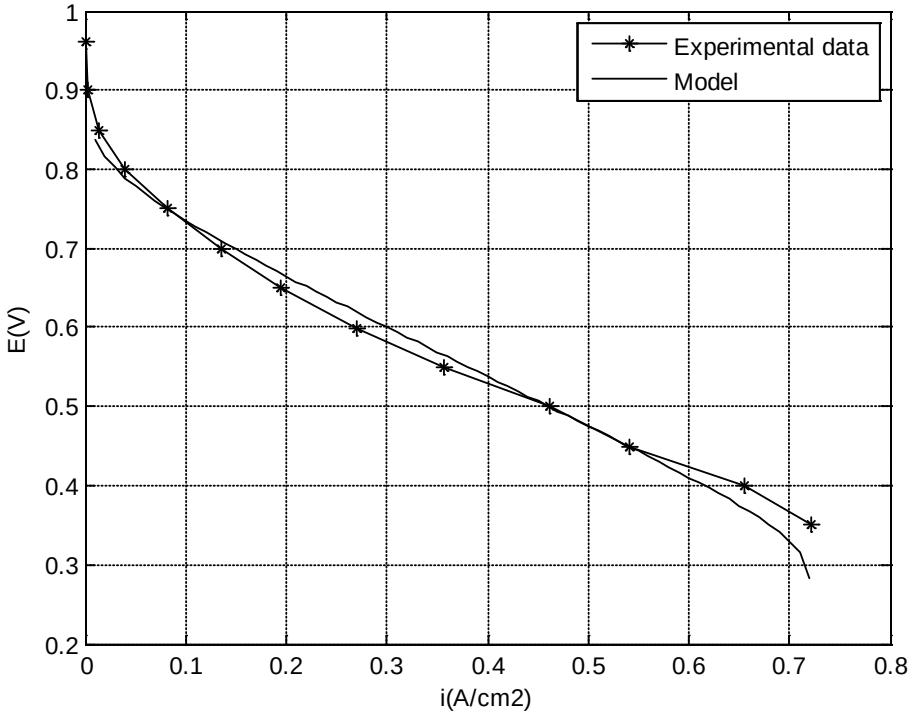

Figure B.2 Comparison of the model with the experimental polarization data obtained at 60 °C, 50 % RH air, 100 % RH H_2

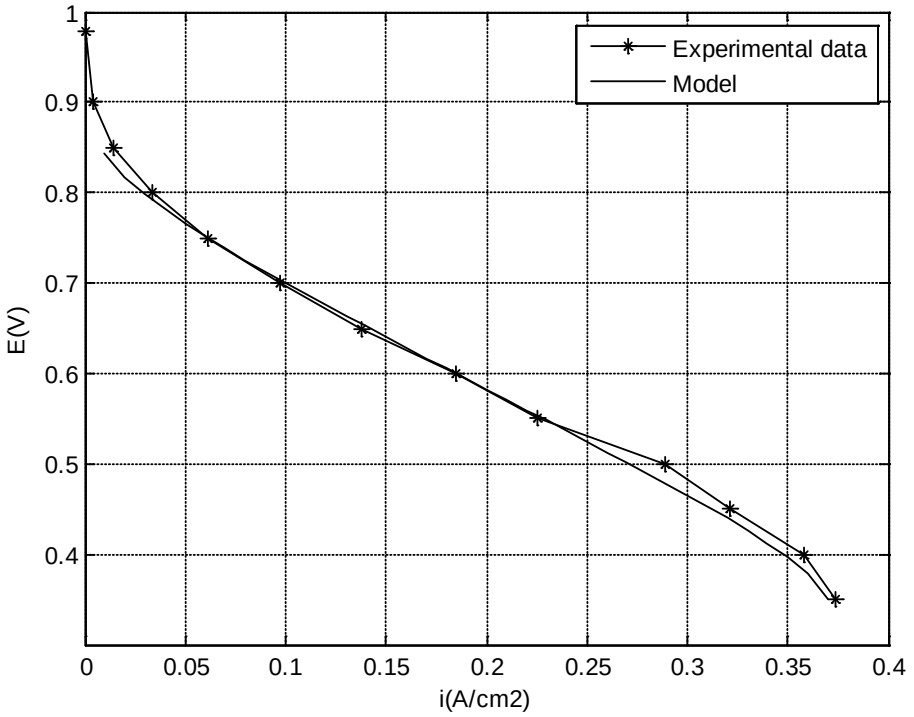

Figure B.3 Comparison of the model with the experimental polarization data obtained at 70 °C, 20 % RH air, 100 % RH H_2

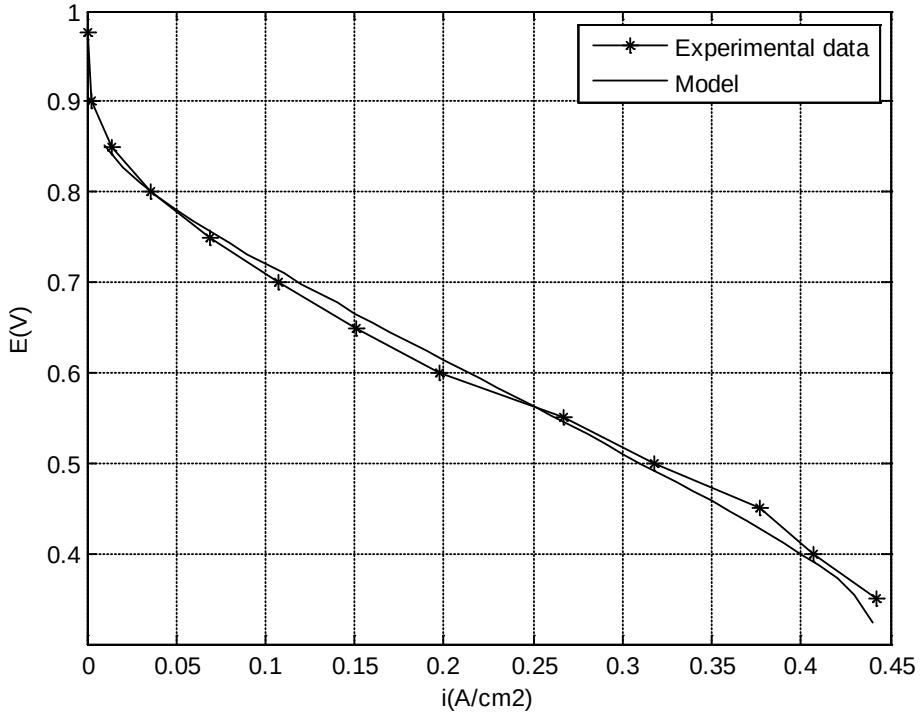

Figure B.4 Comparison of the model with the experimental polarization data obtained at 70 °C, 30 % RH air, 100 % RH H_2

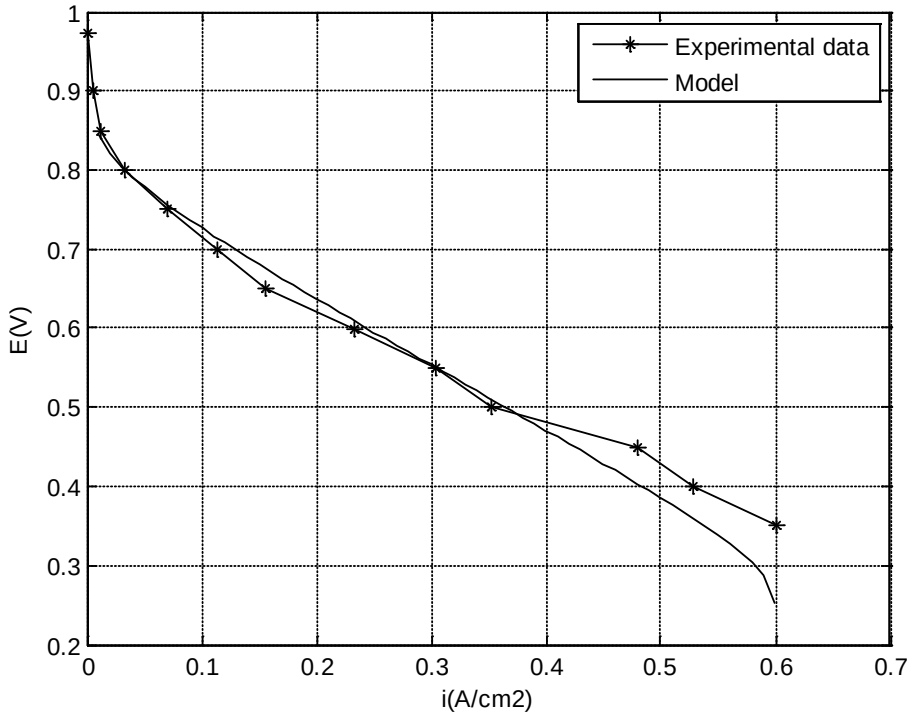

Figure B.5 Comparison of the model with the experimental polarization data obtained at 70 °C, 50 % RH air, 100 % RH H_2

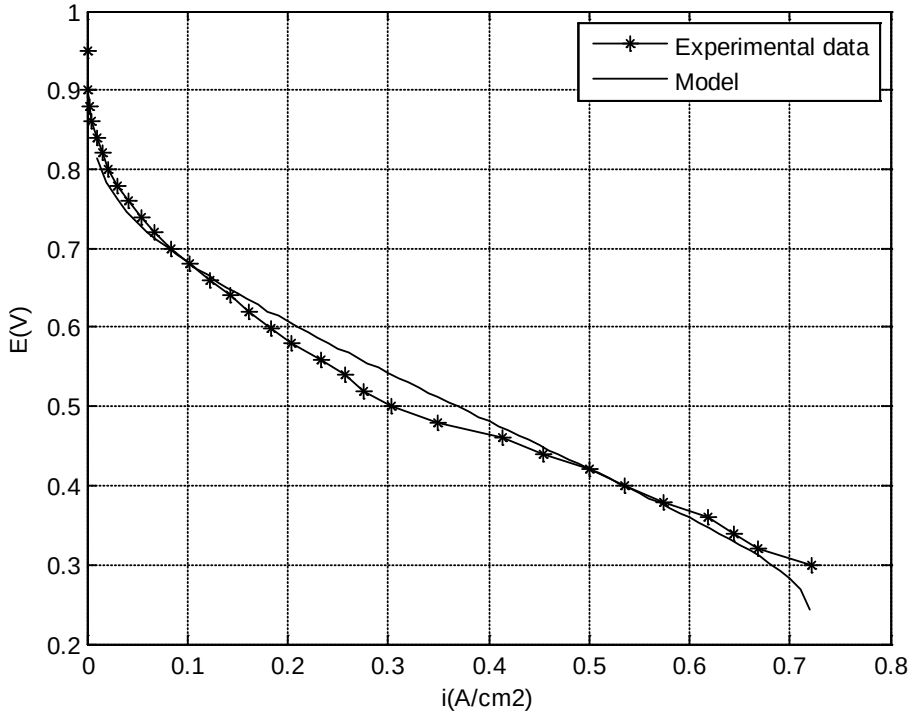

Figure B.6 Comparison of the model with the experimental polarization data obtained at 70 °C, 70 % RH air, 100 % RH H_2

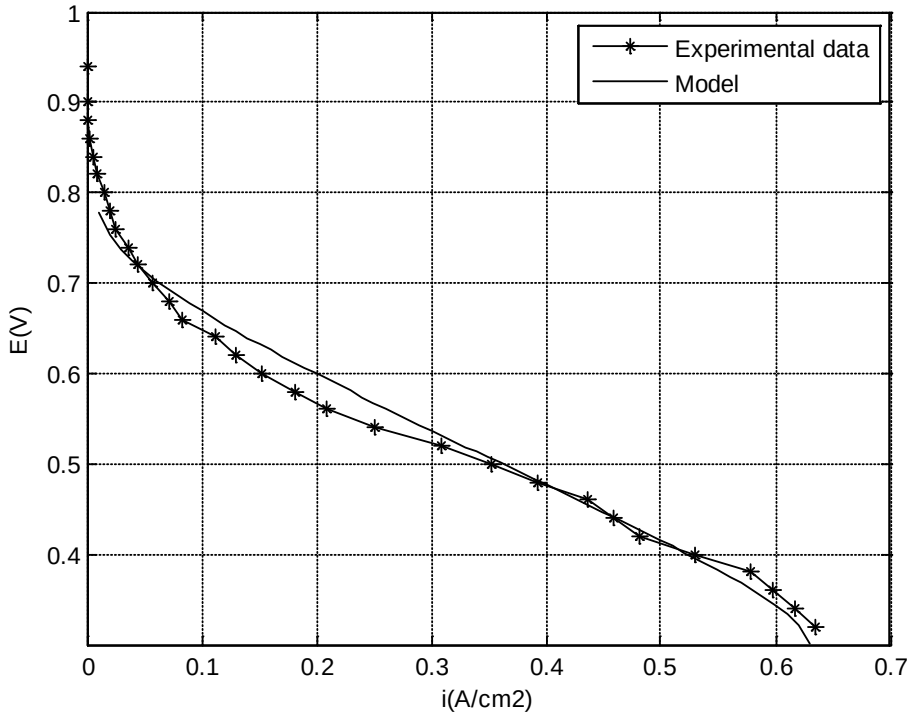

Figure B.7 Comparison of the model with the experimental polarization data obtained at 70 °C, 100 % RH air, 100 % RH H_2

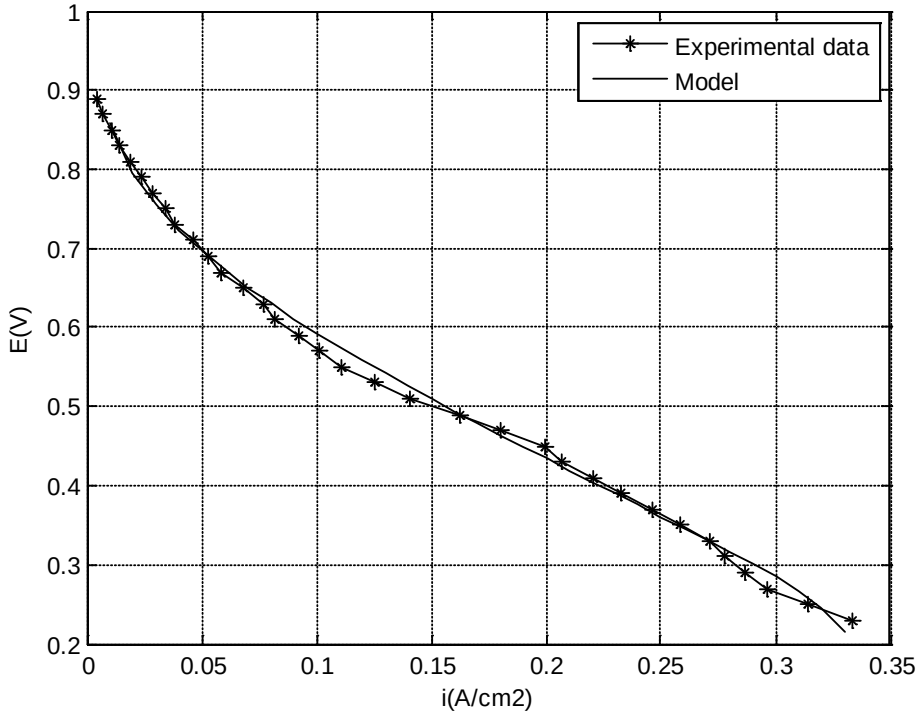

Figure B.8 Comparison of the model with the experimental polarization data obtained at 80 °C, 20 % RH air, 100 % RH H_2

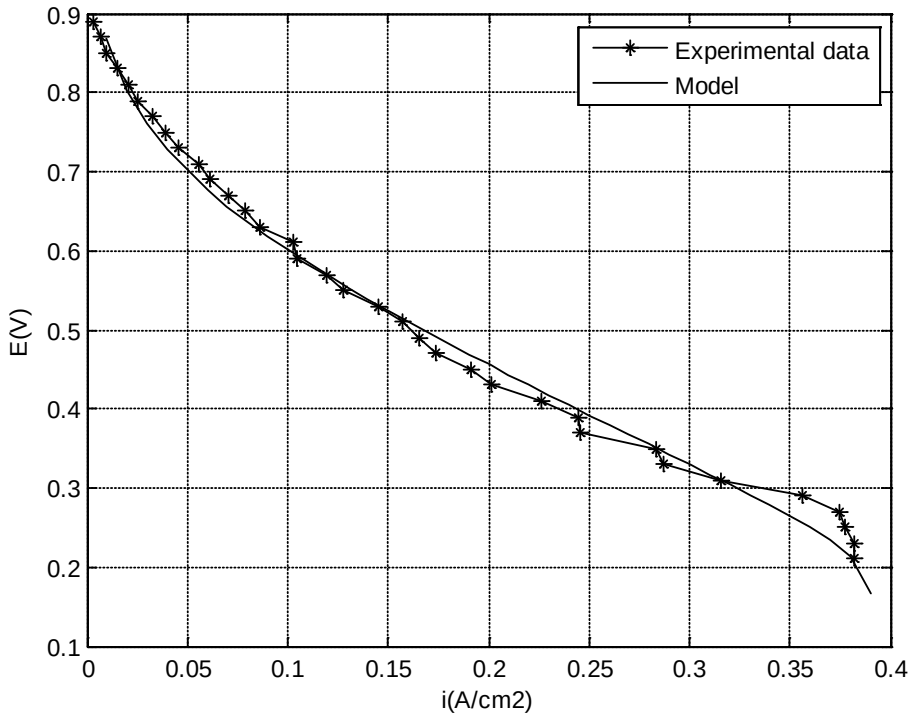

Figure B.9 Comparison of the model with the experimental polarization data obtained at 80 °C, 30 % RH air, 100 % RH H_2

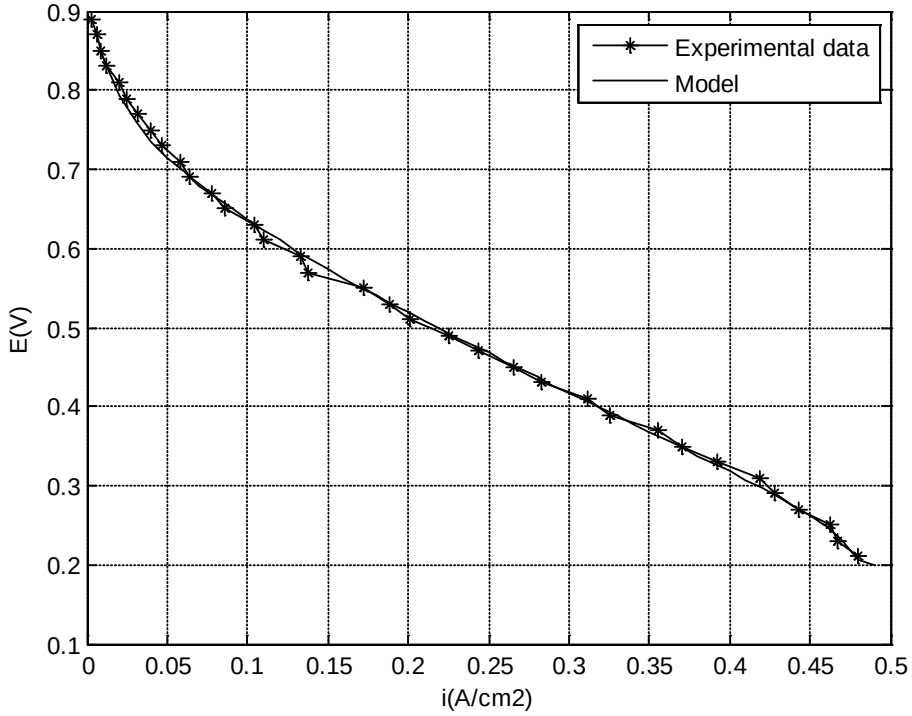

Figure B.10 Comparison of the model with the experimental polarization data obtained at 80 °C, 50 % RH air, 100 % RH H_2

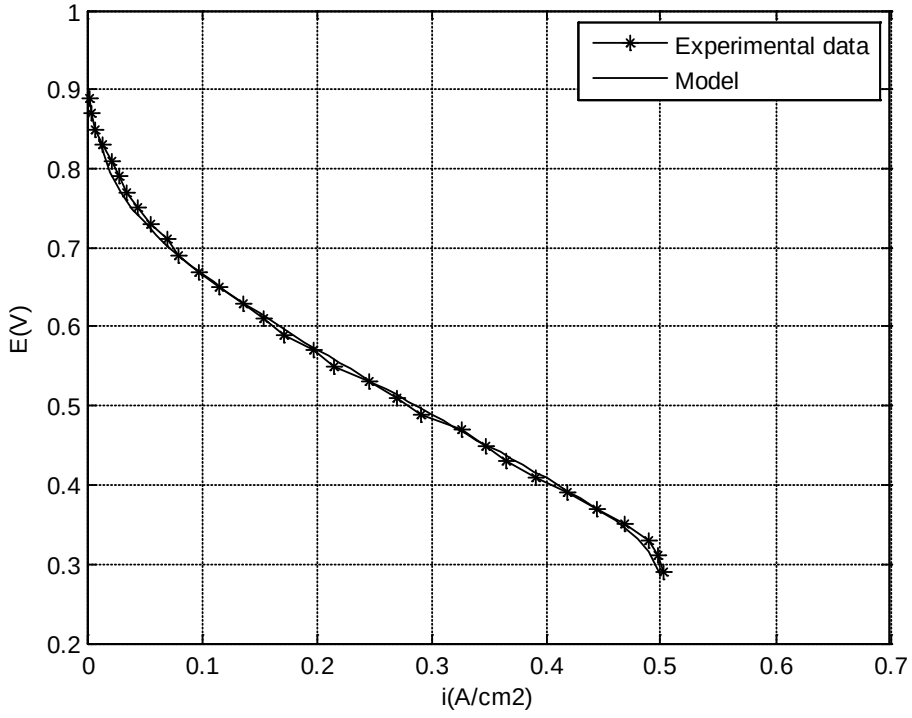

Figure B.11 Comparison of the model with the experimental polarization data obtained at 80 °C, 70 % RH air, 100 % RH H_2

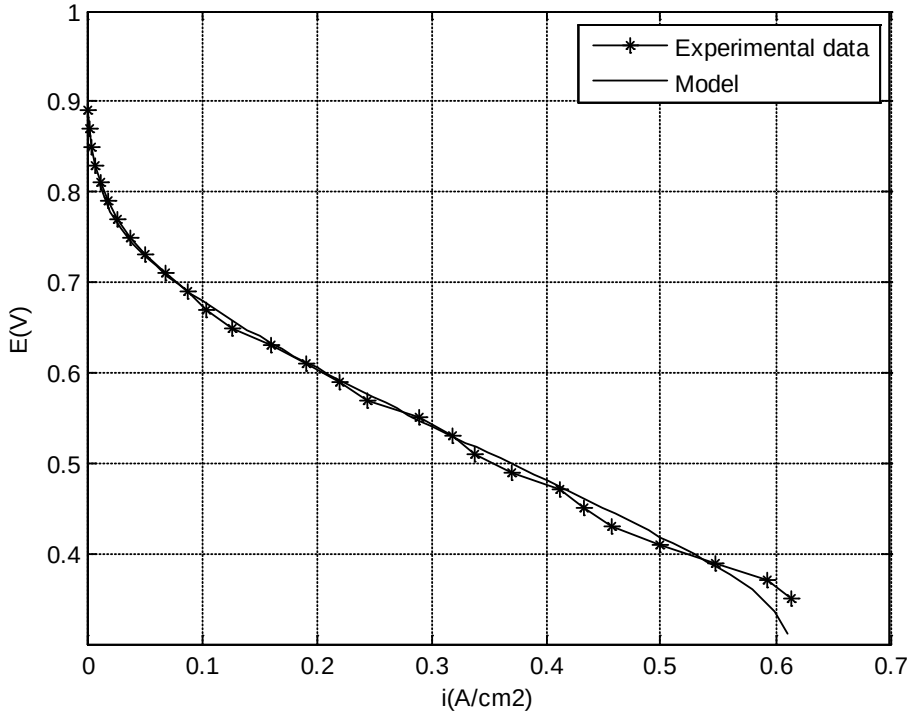

Figure B.12 Comparison of the model with the experimental polarization data obtained at 80 °C, 100 % RH air, 100 % RH H_2

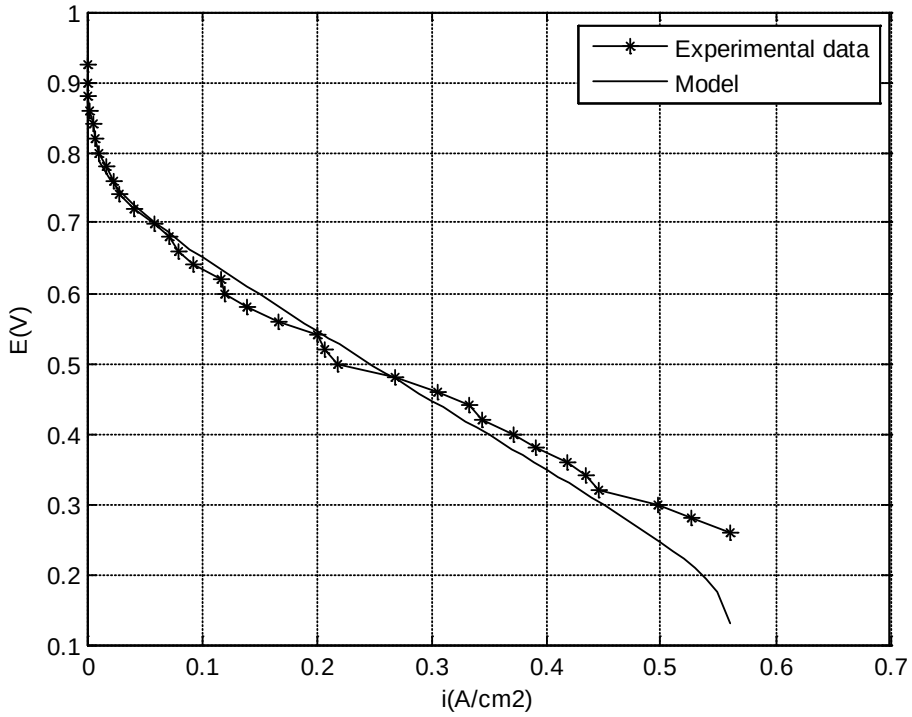

Figure B.13 Comparison of the model with the experimental polarization data obtained at 70 °C, 70 % RH air, 50 % RH H_2

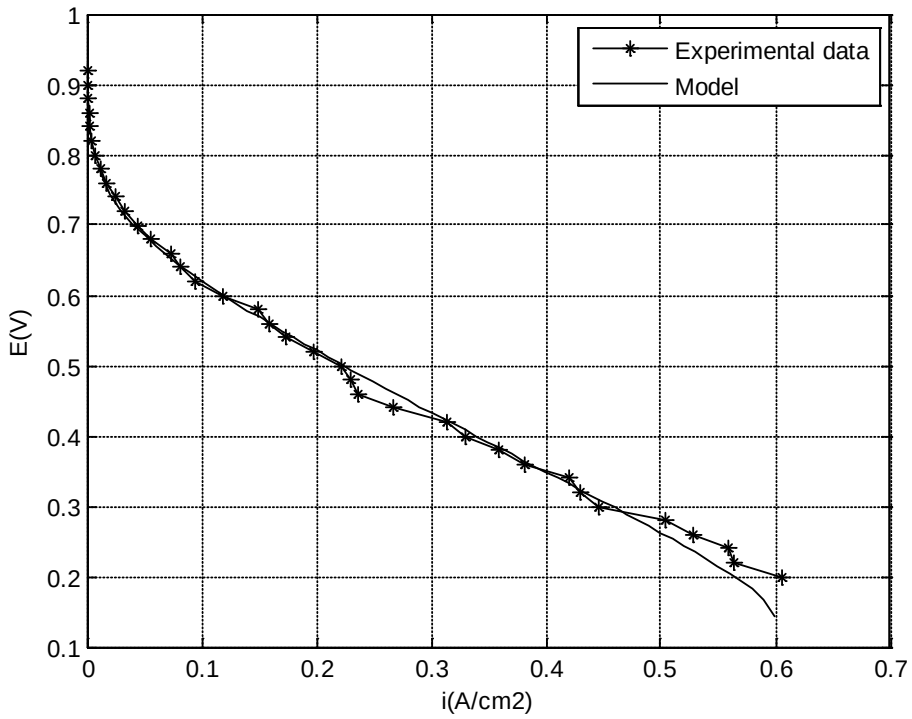

Figure B.14 Comparison of the model with the experimental polarization data obtained at 80 °C, 100 % RH air, 50 % RH H_2

APPENDIX C

SAMPLE CALCULATIONS

Standardization Values

It is often convenient to assume an ideal gas when specifying flows of gases, then covert the volumetric flows into standardized flow. There are many different standardization temperatures (i.e. 25 °C, 15 °C, 0 °C, etc.).

At 15 °C standard temperature:
Ideal Gas Constant (R): 8.31411 J / (mole K)
Standard Pressure: 101325 Pa

Water Constants

Density of Liquid Water: 1 g / ml
The atomic mass of water = 18.015 g / mole

Using the standardization values calculated above, and the atomic weight of water, the density of water vapor at the specified standard conditions can be calculated.

The density of water vapor at 15 °C : 18.02 / 22413: $8x10^{-4}$ g/sml
1/ The density of water vapor at 15 °C: 1 / $8x10^{-4}$: 1244.1 sml / g H_2O

Calculation of A Dew Point to Achieve a Desired Relative Humidity

Relative humidity is the actual water vapor pressure within a system divided by the water vapor pressure of the system at its dew point. The saturation vapor pressure is only a function of temperature. This means we can ignore pressure when calculating relative humidity. Thus if a gas being saturated to a given dew point, and then heated up, we can calculate the relative humidity as follows:

As an example, for 60 °C cell temperature, in order to supply air at 30 % relative humidity, required dew point was calculated.

ASHRAE Fundamentals (1981), provides Antoine equation that allows us to calculate the saturation pressure (in Pa) for any given temperature between 0 ^{o}C and 100 ^{o}C:

$$P_{vs} = e^{aT^{-1}+b+cT+dT^2+eT^3+f\ln(T)}$$

The coefficients are:

$$a = -5800.22$$
$$b = 1.39$$
$$c = -0.05$$
$$d = 0.42$$
$$e = -0.14$$
$$f = 6.55$$

For 60 °C= 333.15 K;

$$P_{vs} = e^{(-5800.22)\left(333.15^{-1}\right)+(1.39)+(-0.05)(333.15)+(0.42)333.15^2+(-0.14)333.15^3+(6.55)\ln(333.15)}$$

$$P_{vs} = 19.94 \text{ kPa}$$

$$\text{Water Partial Pressure} = \text{Saturation Vapor Pressure} * \text{Relative Humidity}$$

$$P_v = P_{vs} * \varphi$$

For 30 % RH;

$$P_v = 19.94 * 0.3$$

$$P_v = 5.98\ \text{kPa}$$

For a system at 60 °C and 30 % relative humidity requires a dew point temperature T_s of:

Using the backward equation of x, this can be converted into a dew point Ts :

$$\text{Ts} = 51.94 + \frac{\text{D}}{2} - \text{SQRT}(0.25 * \text{D}^2 - 325.09 * \text{D} + 105682)$$

$$\text{D} = 2 * \frac{\text{G}}{(-\text{F} - \text{SQRT}(\text{F}^2 - 4 * \text{E} * \text{G}))}$$

$$\text{E} = 0.0316 * \text{Pvs}^{0.5} - 3.036 * \text{Pvs}^{0.25} + 14.92$$

$$\text{F} = 36.9 * \text{Pvs}^{0.5} + 2137.8 * \text{Pvs}^{0.25} - 4823.3$$

$$\text{G} = -22901 * \text{Pvs}^{0.5} - 574881 * \text{Pvs}^{0.25} + 405113$$

For P_{vs}=5.98 kPa

$$\text{E} = 0.0316 * (5.98)^{0.25} - 3.036 * (5.98)^{0.25} + 14.92$$

$$\text{E} = 10.24$$

$$\text{F} = 36.9 * (5.98)^{0.5} + 2137.8 * (5.98)^{0.25} - 4823.3$$

$$\text{F} = -1390.02$$

$$\text{G} = -22901 * (5.98)^{0.5} - 574881 * (5.98)^{0.25} + 405113$$

$$G = -549875.9$$

$$D = 2 * \frac{-549875.9}{(-(-1390.02) - SQRT((-1390.02)^2 - 4 * (10.24) * (-549875.9))}$$

$$D = 309.34$$

$$Ts = 51.94 + \frac{309.34}{2} - SQRT(0.25 * (309.34)^2 - 325.09 * (309.34) + 105682)$$

$$Ts = 36.1\ ℃$$

All other dew point calculation was done by equations above by EXCEL.

Flow rate calculation of reactant gases

At the beginning of the tests, polarization curve data for commercial PEM MEA was obtained from Paxitech. According to polarization curve data obtained from Paxitech, at 0.6 V and 0.7 V, current density is changing from 1000 to 1500 mA/cm^2. Therefore, 1400 mA/cm^2 was determined for optimal value for flow rate calculation. The rates at which hydrogen and air are consumed and water is generated are determined by Faraday's Law. It is known that the reactants flow rate at the inlet of the fuel cell must be equal to or higher than the rate at which those reactants are being consumed in the fuel cell. In general, higher flow rates results in better fuel cell performance. If pure hydrogen is used, 1.1 to1.2 stoichiometry may be used for hydrogen. Similarly, when air is used, typical stoichiometry is 2 or higher for air (Barbir, 2005). It was also suggested by Paxitech that 1.2 and 2 stoichiometry for hydrogen and air can be used in the tests, respectively.

The volumetric flow rates of reactants consumption (in standard liters per minute or slpm) are calculated as:

$$V_{H2} = 23.65x60x\frac{I}{2F}$$

$$V_{Air} = \frac{1}{r_{O2}}23.65x60x\frac{I}{4F}$$

For 25 cm^2 PEM MEA, current is calculated at a current density of 1400 mA/cm^2 as:

$$\frac{1400mA}{cm^2}x\frac{1A}{1000mA}x25cm^2 = 35A$$

$$V_{H2} = 23.65x60\ x\ \frac{35}{2x96485}$$

$$V_{H2} = 0.257\ slpm$$

With a stoichiometry of 1.2 for hydrogen, inlet hydrogen flow rate to the fuel cell calculated as:

$$V_{H2} = 1.2\ x\ 0.257\ slpm$$

$$V_{H2} = 0.3\ slpm$$

Same calculations can be done for air:

$$r_{O2} = \text{oxygen volume fraction at fuel cell inlet}$$

So, oxygen volume fraction in air is 0.21

$$V_{Air} = \frac{1}{0.21}x23.65x60x\frac{35}{4x96485}$$

$$V_{Air} = 0.5\ slpm$$

With a stoichiometry of 2 for air, inlet air flow rate to the fuel cell calculated as:

$$V_{Air} = 2x0.5 \text{ slpm}$$

$$V_{Air} = 1 \text{ slpm}$$

Water Balance Calculations

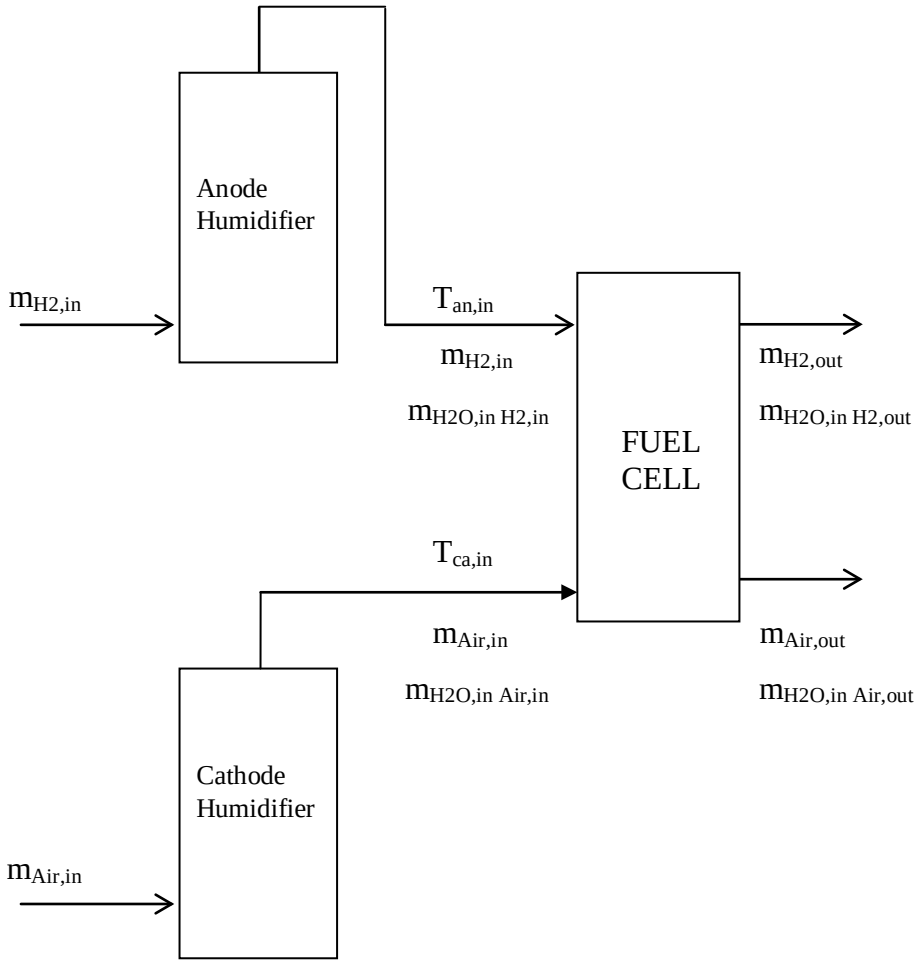

Assumptions:

1) The inlet gases are humidified to the assigned relative humidity in the humidifiers.
2) Humidifiers are operated at dew point temperature.
3) Gases leaving the humidifiers are in thermal equilibrium with the liquid at dew point temperature.
4) Gases are saturated with water vapor at humidifier temperature.
5) Gas inlet temperatures are equal to humidifier outlet temperatures. (Gas lines are heated to eliminate any condensation of vapor).
6) Gases outlet temperatures are equal to fuel cell operating temperature.
7) Both anode and cathode inlet and outlet pressures are taken as 1 atm.
8) Pressure drop between humidifiers and fuel cell connections are negligible.
9) Water transfer from anode to cathode by electro osmotic drag is considered as each proton accompanied by 1 water molecule.
10) Net electro osmotic drag coefficient is assumed as 0.93.

Calculations are done by Faraday's Law:

Water vapor in hydrogen inlet to the fuel cell in $gmin^{-1}$

$$m_{H_2O,in\ H_2,in} = S_{H_2} \frac{M_{H_2O}}{2F} \frac{\varphi_{an} P_{vs}(T_{an,in})}{P_{an} - \varphi_{an} P_{vs}(T_{an,in})} I * n_{cell} * 60$$

n_{cell} = 1 (single cell PEM fuel cell). It will be taken as 1 for the following calculations

Water vapor in air inlet to the fuel cell in $gmin^{-1}$

$$m_{H_2O,\text{in Air,in}} = \frac{S_{O_2}}{r_{O_2}} \frac{M_{H_2O}}{4F} \frac{\varphi_{ca} P_{vs}(T_{ca,in})}{P_{ca} - \varphi_{ca} P_{vs}(T_{ca,in})} I * n_{cell} * 60$$

Water content in hydrogen exhaust in $gmin^{-1}$

$$m_{H_2O,\text{in } H_2,out} = m_{H_2O,\text{in } H_2,in} - m_{H_2O,ED} + m_{H_2O,BD}$$

Electro osmotic drag was calculated as:

$$m_{H_2O,ED} = \xi \frac{M_{H_2O}}{F} I * n_{cell}$$

Where $\xi = 1$ (each proton is accompanied by 1 water molecule) (Barbir, 2005)

Yan et al. (2006) obtained the net electro osmotic drag coefficient ranged from − 0.02 to 0.93, and was dependent on the operating conditions, the current load and the level of humidification.

It is assumed that the net drag coeffcient is 0.93. Then

Net electro osmotic drag = Electro osmotic drag coefficient (EOD) – back diffusion coefficient (BD)

NDC = ξ- β

$$0.93 = 1 - \beta \quad \Rightarrow \quad \beta = 0.07$$

$$m_{H_2O,BD} = \beta m_{H_2O,ED} = \beta\xi \frac{M_{H_2O}}{F} I * n_{cell}$$

Water vapor at anode exhaust calculated as:

$$m_{H_2O,inH_2,out\,V} = \min\left[(S_{O2}-1)\frac{M_{H_2O}}{2F}\frac{P_{vs}(T_{out,an})}{P_{an}-\Delta P_{an}-P_{vs}(T_{out,an})}I * n_{cell}\,,\; m_{H_2O,in\,H_2,out}\right]$$

Liquid water at anode exhaust calculated as:

$$m_{H_2O,inH_2,out\,L} = m_{H_2O,inH_2,out} - m_{H_2O,in\,H_2,out\,V}$$

Water content in the cathode exhaust in $gmin^{-1}$

$$m_{H_2O,in\,Air,out} = m_{H_2O,in\,Air,in} + m_{H_2O,qen} + m_{H_2O,ED} - m_{H_2O,BD}$$

$$m_{H_2O,in\,Air,out\,V} = \min\left[\frac{S_{O_2}-r_{O_2,in}}{r_{O_2,in}}\frac{M_{H_2O}}{4F}\frac{P_{vs}(T_{out,ca})}{P_{ca}-\Delta P_{ca}-P_{vs}(T_{out,ca})}I * n_{cell}\,, m_{H_2O,in\,Air,out}\right]$$

$$m_{H_2O,in\,Air,out\,L} = m_{H_2O,in\,Air,out} - m_{H_2O,in\,Air,out\,V}$$

Sample Calculation of Water Balance

For 60 ^oC fuel cell temperature 30 % RH of air with 100 % RH of H_2, it is determined from its polarization curve that at 0.4 V current density of 580 mA/cm^2 was obtained.

The current is:

$$\frac{580\ mA}{cm^2}\ x\frac{1A}{1000mA}x25cm^2 = 14.5A$$

Water vapor in Hydrogen inlet ($gmin^{-1}$)

$$m_{H_2O,in\,H_2,in} = 1.2 * \frac{18\ g/mol}{2*96485\ Cmol^{-1}} * \frac{1*19.94\ kPa}{101.325kPa-(1*19.94kPa)} * 14.5\ A*60$$

$$m_{H_2O,\text{in } H_2,\text{in}} = 0.024 \text{ gmin}^{-1}$$

Water content in hydrogen exhaust in min^{-1}

It is assumed that $\xi = 1$

Then

NDC = ξ- β

$$0.93 = 1 - \beta \quad \Rightarrow \quad \beta = 0.07$$

$$m_{H_2O,ED} = 1\frac{18 \text{ g/mol}}{46485}14.5A * 60$$

$$m_{H_2O,ED} = 0.162 \text{ g/min}$$

$$m_{H_2O,BD} = \beta m_{H_2O,ED} = \beta\xi\frac{M_{H_2O}}{F} I * n_{cell}$$

$$m_{H_2O,BD} = 0.07\ (0.162) = 0.011 \text{ g/min}$$

$$m_{H_2O,\text{in } H_2\text{out}} = m_{H_2O,\text{in } H_2,\text{in}} - m_{H_2O,ED} + m_{H_2O,BD}$$

Then;

$$m_{H_2O,\text{in } H_2\text{out}} = 0.024 - 0.162 + 0.011$$

$$m_{H_2O,\text{in } H_2\text{out}} = -0.127 \text{ g/min}$$

Depending on the flow rate, that is, stoichiometry and conditions at the outlet, water at hydrogen exhaust may be present as vapor only, or liquid water may be present after the gas is saturated with water vapor. The water vapor content at anode outlet is the smaller of total water flux at anode outlet and the maximum amount the exhaust gas can carry (saturation) (Barbir, 2005):

$$m_{H_2O,inH_2,out\,V} = \min\left[(S_{H2} - 1)\frac{M_{H_2O}}{2F}\frac{P_{vs}(T_{out,an})}{P_{an} - \Delta P_{an} - P_{vs}(T_{out,an})}I * n_{cell}\,,\; m_{H_2O,in\,H_2,out}\right]$$

$$m_{H_2O,inH_2,out\,V} =$$

$$\min\left[(1.2 - 1)\frac{18\frac{g}{mol}}{2(96485)}\frac{19.94\text{ kPa}}{101.325\text{kPa} - 0 - 19.94\text{ kPa}}14.5\text{ A}\,,\; -0.127\frac{g}{min}\right]$$

$$m_{H_2O,inH_2,out\,V} = \min\left[0.004\frac{g}{min}, -0.127\text{ g/min}\right]$$

The water vapor content at anode outlet is the smaller of total water flux at anode outlet and the maximum amount the exhaust gas can carry;

$$m_{H_2O,inH_2,out\,V} = -0.127\text{ g/min}$$

$$m_{H_2O,inH_2,out\,L} = m_{H_2O,inH_2,out} - m_{H_2O,in\,H_2,out\,V}$$

$$m_{H_2O,inH_2,out\,L} = -\frac{0.127g}{min} - (-0.127)g/min$$

$$m_{H_2O,inH_2,out\,L} = 0\text{ g/min}$$

Water vapor in air inlet (min^{-1})

$$m_{H_2O,in\,Air,in} = \frac{2}{0.21} * \frac{18g/mol}{4 * 96485Cmol^{-1}} * \frac{0.3 * 5.98\,kPa}{101.325kPa - 0.3 * 5.98kPa} * 14.5\,A * 60$$

$$m_{H_2O,in\,Air,in} = 0.007\text{ gmin}^{-1}$$

Water content in the cathode exhaust in $gmin^{-1}$

$$m_{H_2O,\text{in Air,out}} = m_{H_2O,\text{in Air,in}} + m_{H_2O,qen} + m_{H_2O,ED} - m_{H_2O,BD}$$

Water generation at cathode side in $gmin^{-1}$

$$m_{H_2O,qen} = \frac{I}{2F} M_{H2O} * 60$$

$$m_{H_2O,qen} = \frac{14.5\ A}{2(96485)} 18 \frac{g}{s} * 60$$

$$m_{H_2O,qen} = 0.081\ gmin^{-1}$$

Then

$$m_{H_2O,\text{in Air,out}} = 0.007 \frac{g}{min} + 0.081 g/min + 0.162\ g/min - 0.011\ g/min$$

$$m_{H_2O,\text{in Air,out}} = 0.239\ g/min$$

$$m_{H_2O,\text{in Air,out V}} =$$

$$\min\left[\frac{2-0.21}{0.21} \frac{18 g/mol}{4(96485)} \frac{19.94\ kPa}{101.325\ kPa - 0 - 19.94\ kPa} 14.5A\ , m_{H_2O,\text{in Air,out}}\right]$$

$$m_{H_2O,\text{in Air,out V}} = \min\left[0.085 \frac{g}{min}, 0.239 g/min\right]$$

$$m_{H_2O,\text{in Air,out V}} = 0.085\ g/min$$

$$m_{H_2O,\text{in Air,out L}} = m_{H_2O,\text{in Air,out}} - m_{H_2O,\text{in Air,out V}}$$

$$m_{H_2O,\text{in Air,out L}} = 0.239 \frac{g}{min} - 0.085 g/min$$

$$m_{H_2O,\text{in Air,out L}} = 0.154\ g/min$$

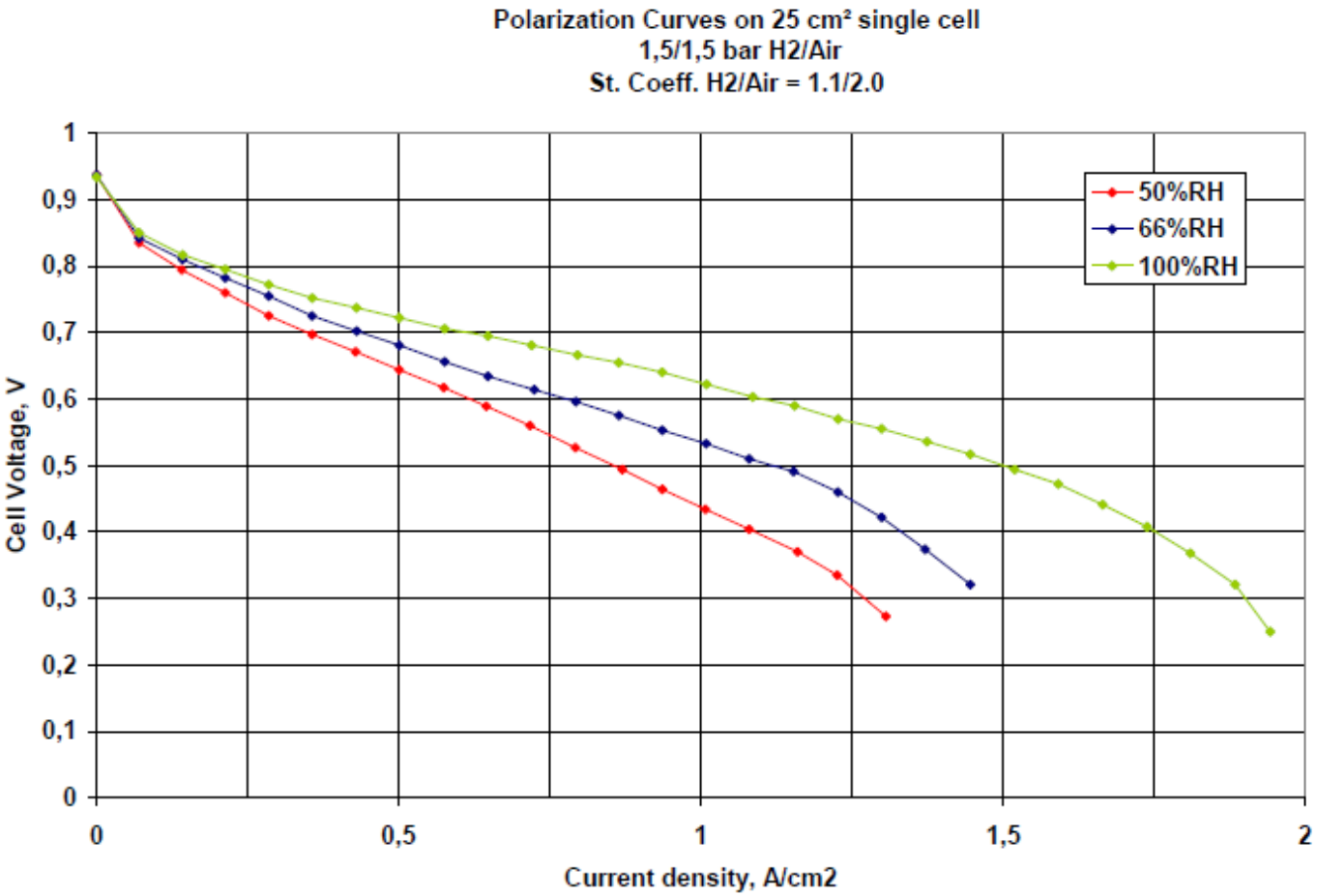

Figure C.1 Polarization curve obtained from PaxiTech